MHD waves driven by small-scale motion and implications for the Earth's core

N Ghanesh

Centre for Earth Sciences

Indian Institute of Science

This dissertation is submitted for the degree of

Master of Science (Engineering)

March 2017

This dissertation is dedicated to my family . . .

Acknowledgements

I owe my deepest gratitude to my advisor Prof. Binod Sreenivasan for the continuous support of my research, for his patience, motivation, and immense knowledge. His guidance helped me in all the time of research and writing of this thesis. I would like to thank Prof. Gaurav Tomar for the insightful comments on the thesis which were useful and led to an overall improvement in the quality of the thesis.

I am thankful to my labmates Swarandeep Sahoo, Venkatesh Gopinath and Subhajit Kar who were always there for the stimulating discussions that often cleared my doubts and led me in the right direction to conduct my research. I sincerely thank the Chairman, SERC for providing the Cray XC40 computational facility for the parallel runs without which solving the problem would have been more difficult.

It is a pleasure to thank my friends Jagannath, Kaushik, Keerthana, Subramanian, Shriram and Shankar for making my stay in IISc memorable and also for their continuous support and encouragement.

Finally, I owe my deep and sincere gratitude to my parents and brother for their unparalleled love and support. They always encouraged and inspired me to explore new directions in life and seek my own destiny. This journey would not have been possible if not for them, and I dedicate this milestone to them.

Abstract

Rotating convection in the Earth's core produces columnar vortices of radius ~ 10 km or less near the inner core boundary. Small-scale motions in the core can travel as Alfvén waves in the face of Ohmic diffusion, provided the ratio of the magnetic diffusion time t_η to the Alfvén wave travel time t_A (measured by the Lundquist number S_0) is much greater than unity. These motions transfer angular momentum from the core to the mantle, a process that can help explain variations in length of day. Vortices subject to the combined influence of a magnetic field and background rotation give rise to fast and slow Magneto-Coriolis (MC) waves whose damping is not well-understood. This thesis investigates the long-time evolution of magnetohydrodynamic (MHD) waves generated by an isolated, small-scale motion in an otherwise quiescent, electrically conducting fluid. The first part of the study focuses on the damping of small-scale Alfvén waves, which is independent of rotation. For a plausible magnetic field strength in the Earth's core, it is shown that flows of lengthscale ~ 5 km or larger can propagate across the core as damped Alfvén waves on sub-decadal timescales. The second part of the study looks at MC waves generated from an isolated blob under rotation and a uniform axial magnetic field. New timescales are derived for the onset of damping and the onset of the diffusion-dominated quasi-static (qs) state. This study shows for the first time that MC waves originating from small-scale vortices of magnetic Reynolds number $R_m \sim 1$ can be long-lived. The results of this study are extendible to small-scale MHD turbulence under rotation, whose damped wave phase has not been adequately addressed in the literature.

Table of contents

List of figures

List of tables

Chapter 1

Introduction

The magnetic field of Earth is generated by convection occurring in the planet's fluid core. Rapid rotation of a fluid layer heated from below is known to produce convective columns whose radius decreases progressively with increasing speed of rotation (Chandrasekhar, 1961; Busse, 1970). It is therefore reasonable to suppose that fluid motion in the Earth's outer core is made up of small-scale columns aligned with the rotation axis. In present-day Earth's core, convection is predominantly driven by blobs of light elements continuously released from the boundary of inner core as iron crystallizes (Moffatt and Loper, 1994) while rapid rotation elongates these three-dimensional structures into geostrophic cylinders. Each of these columns is likely to be in approximate balance between the magnetic (Lorentz), Coriolis, buoyancy and pressure forces. It is, however, not an easy matter to enforce this "magnetostrophic" balance on isolated columnar vortices in numerical simulations of the geodynamo because the viscous and Reynolds stresses are often not negligible in the force balance at small scales. The ratio of viscous to Coriolis forces (Ekman number Ek) in dynamo simulations is several orders of magnitude higher than the value for the outer core ($Ek \sim 10^{-15}$), while the actual ratio of nonlinear inertia to Coriolis forces increases quadratically with decreasing lengthscale $l_\perp$ perpendicular to the rotation axis (Sreenivasan and Jones, 2006). Consequently, it is apparent that idealized magnetohydrodynamic (MHD)

models of isolated vortices in electrically conducting liquids are necessary to gain insight into processes that are otherwise not realizable in fully nonlinear dynamo simulations. In particular, the fact that small-scale motions can support wave motion in the presence of magnetic diffusion needs to be understood from simplified MHD models rather than three-dimensional dynamo simulations. The aim of this thesis is to understand damped wave motion driven by isolated small-scale flows. To this end, the long-time evolution of a blob of fluid subject to rotation and a magnetic field is investigated. The study is performed in two parts. The first part consists of an approximate and exact analysis of the evolution of the blob in the presence of an axial magnetic field. The second part treats the evolution under the combined effects of magnetic field and rotation. In both these studies, the transitions from the MHD wave regime to the diffusion-dominated regime is studied in detail.

This chapter presents an overview of the basic elements of MHD, the role of rotation and magnetic fields in wave motion in fluids and some implications of these ideas for the Earth's liquid iron core.

1.1 Elements of magnetohydrodynamics

The subject of magnetohydrodynamics (MHD) deals with the interaction of fluid flows and magnetic fields. The interaction of fluid velocity $\boldsymbol{u}$ and magnetic field $\boldsymbol{B}$ is governed by the coupled equations of electromagnetism and fluid momentum (the Navier–Stokes equation). Maxwell's electrodynamic equations govern the behavior of the electric field and the magnetic field. These equations in differential form are given by,

$$\begin{aligned}
\nabla \cdot \boldsymbol{E} &= \rho_e/\varepsilon_0, && \text{(Gauss's law)} \\
\nabla \cdot \boldsymbol{B} &= 0, && \text{(divergence constraint on } \boldsymbol{B}\text{)} \\
\nabla \times \boldsymbol{E} &= -\frac{\partial \boldsymbol{B}}{\partial t}, && \text{(Faraday's law)} \\
\nabla \times \boldsymbol{B} &= \mu \left(\boldsymbol{j} + \varepsilon_0 \frac{\partial \boldsymbol{E}}{\partial t} \right). && \text{(Ampère-Maxwell equation)}
\end{aligned}$$

In addition, the charge conservation equation is given by

$$\nabla \cdot \boldsymbol{j} = -\frac{\partial \rho_e}{\partial t}. \tag{1.1}$$

In an electrically conducting fluid, the charge density ρ_e is negligible and hence plays no significant role. Furthermore, the displacement current term in the Ampère-Maxwell equation is less significant. Hence, the electrodynamic equations for MHD are governed by the pre-Maxwell form of equations,

1. Ampère's law with charge conservation:

$$\nabla \times \boldsymbol{B} = \mu \boldsymbol{j}, \tag{1.2}$$

$$\nabla \cdot \boldsymbol{j} = 0. \tag{1.3}$$

2. Faraday's law and divergence constraint on magnetic field $\boldsymbol{B}$:

$$\nabla \times \boldsymbol{E} = -\frac{\partial \boldsymbol{B}}{\partial t}, \tag{1.4}$$

$$\nabla \cdot \boldsymbol{B} = 0. \tag{1.5}$$

3. Ohm's law and the Lorentz force:

$$\boldsymbol{j} = \sigma(\boldsymbol{E} + \boldsymbol{u} \times \boldsymbol{B}), \tag{1.6}$$

$$\boldsymbol{F} = \boldsymbol{j} \times \boldsymbol{B}. \tag{1.7}$$

Combining the equations from Ampère's law, Faraday's law and Ohm's law, an equation relating $\boldsymbol{B}$ and $\boldsymbol{u}$, the magnetic induction equation is obtained (Roberts, 1967),

$$\frac{\partial \boldsymbol{B}}{\partial t} = \nabla \times (\boldsymbol{u} \times \boldsymbol{B}) + \eta \nabla^2 \boldsymbol{B}. \tag{1.8}$$

The Navier–Stokes equation governs the dynamics of the fluid flow. In the presence of a magnetic field acting on an incompressible fluid, we obtain

$$\frac{\partial \boldsymbol{u}}{\partial t} + \boldsymbol{u} \cdot \nabla \boldsymbol{u} = -\frac{\nabla p}{\rho} + \frac{\boldsymbol{j} \times \boldsymbol{B}}{\rho} + \nu \nabla^2 \boldsymbol{u}, \tag{1.9}$$

where p is the fluid pressure and ν is the kinematic viscosity. The momentum equation (1.9) and magnetic induction equation (1.8) govern the dynamics of fluid motion under a magnetic field. In the following section, the effects of rotation and magnetic field on the velocity are discussed.

1.2 Effect of rotation and magnetic field

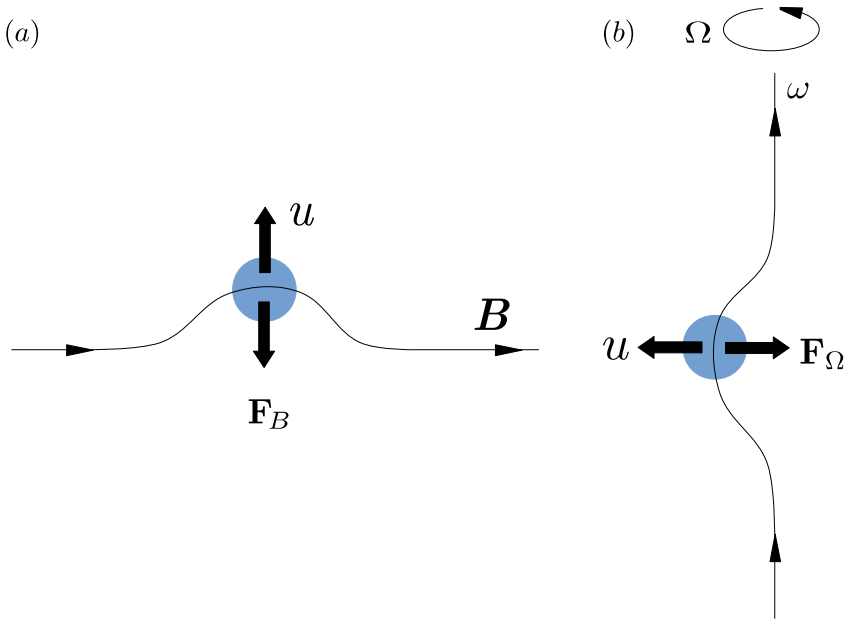

Fig. 1.1 Representation of the mechanism of formation of (a) Alfvén wave (b) Inertial wave

1.2.1 Alfvén waves

The possibility of wave propagation in an electrically conducting fluid was first proposed theoretically by Alfvén (1942). In a fluid with infinite electrical conductivity, an isolated

fluid parcel moving perpendicular to an external magnetic field $\boldsymbol{B}$ bends the field lines (fig. 1.1a). Consequently, the magnetic restoring force $\boldsymbol{F}_B$ opposes the fluid motion in the same way as tension in a plucked string. The action of this restoring Lorentz force leads to oscillations that propagate along the magnetic field lines which are called the *Alfvén waves*. These waves travel with a characteristic velocity called the Alfvén velocity given by $V_A = B_0/\sqrt{\mu\rho}$ and satisfy the wave equation (Davidson, 2001)

$$\frac{\partial^2 \nabla^2 \boldsymbol{u}}{\partial t^2} = V_A^2 \frac{\partial^2 \nabla^2 \boldsymbol{u}}{\partial z^2}. \tag{1.10}$$

The propagation of these waves is a linear system as the magnitude of non-linear inertia $\|\boldsymbol{u}\cdot\nabla\boldsymbol{u}\|$ is much less than the magnitude of Lorentz force $\|\boldsymbol{j}\times\boldsymbol{B}\|$ measured by the *magnetic interaction parameter* (N_0)

$$N_0 = \frac{\|\boldsymbol{j}\times\boldsymbol{B}\|}{\|\boldsymbol{u}\cdot\nabla\boldsymbol{u}\|}. \tag{1.11}$$

1.2.2 Inertial waves

In 1868, Lord Kelvin observed that dragging a sphere placed in a rotating fluid takes with it a column of fluid as if there was a rigid mass of water above and below the sphere (Fuentes, 2009). Thirty years later, Hough (1897) showed analytically that slow, steady motion in a rotating fluid is two-dimensional which was subsequently rediscovered in studies on the movement of rigid bodies in a rotating fluid (Proudman, 1916; Taylor, 1917). These studies led to the Taylor-Proudman theorem which states that slow, steady motions in an inviscid rotating fluid would become two-dimensional. The early studies on rotating flows are also reported in Greenspan (1968).

The formation and propagation of inertial waves could be attributed to the restoring action of Coriolis force on vortex streamlines. Consider a small parcel of fluid with vorticity ω as shown in fig. 1.1b. The line represents the vortex streamline whose instantaneous tangent gives the direction of vorticity of the fluid parcel. When this fluid parcel moves with velocity

$\boldsymbol{u}$ in a perpendicular direction to the vortex streamline, the Coriolis force $2\boldsymbol{u} \times \boldsymbol{\Omega}$ owing to the movement opposes the fluid motion which would bring back the fluid to its original position. The fluid parcel would overshoot from its equilibrium position due to inertia, and the Coriolis force would again try to restore the equilibrium. This oscillatory motion of the fluid parcel can support wave motion along the streamlines called the *inertial waves*. The perturbation velocity field $\boldsymbol{u}$ that propagates as inertial waves under rapid rotation satisfies the wave equation (Davidson, 2001)

$$\frac{\partial^2 \nabla^2 \boldsymbol{u}}{\partial t^2} = -4\Omega^2 \frac{\partial^2 \boldsymbol{u}}{\partial z^2}. \tag{1.12}$$

Equation (1.12) predicts wave motion with a characteristic frequency 2Ω. The propagation of the inertial waves is a linear system as the magnitude of non-linear inertia $\|\boldsymbol{u} \cdot \nabla \boldsymbol{u}\|$ is much less than the magnitude of Coriolis force $\|2\boldsymbol{\Omega} \times \boldsymbol{u}\|$ measured by the *Rossby number* (Ro)

$$Ro = \frac{\|2\boldsymbol{\Omega} \times \boldsymbol{u}\|}{\|\boldsymbol{u} \cdot \nabla \boldsymbol{u}\|}. \tag{1.13}$$

When both the rotation and magnetic field act on a fluid parcel, it leads to the formation of a different class of waves called as *Magneto-Coriolis* (MC) waves discussed in the following section.

1.2.3 Magneto-Coriolis waves

Magneto-Coriolis (MC) waves are excited in an electrically conducting incompressible fluid when it is subjected to both the magnetic field and rotation. Earlier studies (Acheson and Hide, 1973; Lehnert, 1955b; Moffatt, 1978) suggest that under rapid rotation, two classes of MC waves would exist under the combined action of rotation and magnetic field. These waves are the fast inertial wave modified weakly by magnetic field and slow magnetostrophic wave often called as the fast and slow MC waves respectively. The phase

velocities of the fast and slow MC waves are higher and lower than the corresponding non-rotating Alfvén wave's velocity.

For an inviscid, incompressible and electrically conducting fluid under rapid rotation, the wave equation for the velocity perturbation is given by (Davidson, 2001)

$$\left(\frac{\partial^2}{\partial t^2} - \frac{(\boldsymbol{B}\cdot\nabla)^2}{\mu\rho}\right)^2 \nabla^2\boldsymbol{u} = -4(\boldsymbol{\Omega}\cdot\nabla)^2\frac{\partial^2\boldsymbol{u}}{\partial t^2}. \tag{1.14}$$

The above equation (1.14) is fourth order in time which implies that there are four modes of wave propagation: a pair of slow and fast MC waves.

The relative strength of the Coriolis and Lorentz forces is measured by *Lehnert number* (*Le*) first introduced in Lehnert (1954a). It is defined as

$$Le = \frac{\|(\nabla\times\boldsymbol{B})\times\boldsymbol{B}/\mu\rho\|}{\|2\boldsymbol{u}\times\boldsymbol{\Omega}\|} = \frac{t_\Omega}{t_A} = \frac{V_A}{2\Omega l}. \tag{1.15}$$

In a rapidly rotating system Lehnert number $Le \ll 1$, implying that the Coriolis force is much stronger than the Lorentz force. It also means that the inertial time is much less than the Alfvén travel time. When $Le \gg 1$, Lorentz force is stronger than the Coriolis force and the Alfvén travel time is lesser than the inertial time. Lehnert number being greater or lesser than one affects the relative amplitudes of the slow and fast MC wave propagation.

It is clear that different classes of waves exist when an electrically conducting fluid is subjected to rotation, magnetic field, or both. In the following section, the geophysical significance of these waves is discussed.

1.3 Waves in the Earth's outer core

1.3.1 Secular variation

The Earth's surface magnetic field has been mapped for several hundred years (Jackson et al., 2000). These maps show that the magnetic field undergoes changes on various

timescales ranging from few days to several decades. This temporal change in the magnetic field is called the *secular variation*. One of the main features of the secular variation is the westward drift of the magnetic field, which may be due to zonal flows (Bullard et al., 1950) or hydromagnetic waves in the presence of rotation (Hide, 1966). Holme and Whaler (2001) and Jackson (2003) suggest that wave motion is a possible and also an important mechanism to explain the geomagnetic secular variation.

1.3.2 Torsional oscillations

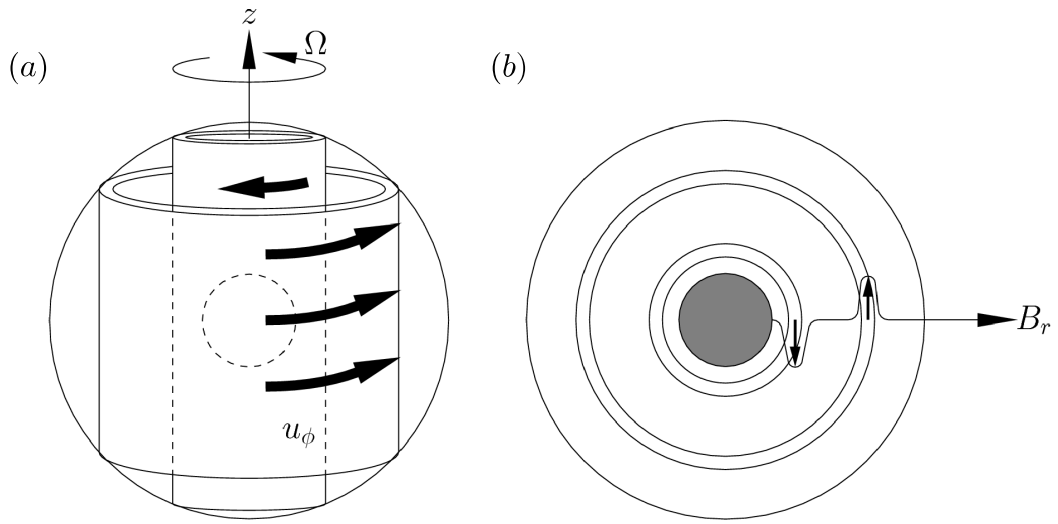

Fig. 1.2 Schematic representation of torsional waves. (a) Front view. (b) Top view seen through the z axis.

Braginsky (1970) proposed that the Earth's outer core fluid motions could exist as torsional oscillations that might explain the observed length of day (LOD) variations. It is thought that the large-scale geostrophic azimuthal cylindrical flows exist inside the Earth's core which are threaded by the radial magnetic field. When this radial field is perturbed by the azimuthal flow, the disturbances travel along the field line as Alfvén waves.

The schematic representation of the torsional oscillation is shown in the figure 1.2. In (a), the outermost sphere is the core-mantle boundary, and the inner dashed sphere is the inner

core boundary. The schematic drawing also shows the large-scale geostrophic cylinders with azimuthal velocity u_ϕ. In (b), the propagation of geostrophic cylinders as Alfvén waves due to the restoring action from radial magnetic field B_r is shown as seen along the rotation axis.

1.4 Large and small-scale motions in the Earth's core

Fluid motion in the outer core comprise flows of different lengthscales. The thickness of the outer core is approximately 2200 km. Lengthscales of the order of 1000 km which are of the order of the core thickness are considered to be large-scale motions. Present-day dynamo simulations often study the dynamics of these large-scale convective flows. Torsional oscillations and secular variation are also thought to be caused by the large-scale fluid motions. Lengthscales $\sim 1-10$ km constitute the small-scale motions. The outer core fluid has a finite magnetic diffusivity. Hence, these motions are thought to be diffusion dominated flows because the *magnetic Reynolds number* (R_m) which measures the ratio of the magnitude of convection to diffusion term of the magnetic induction equation (1.8) is of order unity. R_m is defined as (Roberts, 1967)

$$R_m = \frac{\|\nabla \times (\boldsymbol{u} \times \boldsymbol{B})\|}{\|\eta \nabla^2 \boldsymbol{B}\|} = \frac{t_\eta}{t_o} = \frac{ul}{\eta}, \tag{1.16}$$

where the characteristic length scale and velocity of a flow are l and u respectively, the mangetic diffusion time is $t_\eta = l^2/\eta$ and eddy turn-over time is $t_o = l/u$. When $R_m \ll 1$, the diffusion timescale is shorter than the eddy turn-over timescale. If $R_m \gg 1$, the flow does not diffuse easily as the diffusion time is much greater than the eddy turn-over time.

1.5 Small-scale flows and wave motion

Small-scale flows can propagate as Alfvén waves provided the wave propagation time t_A is significantly shorter than the magnetic diffusion time t_η. The ratio t_η/t_A is termed the

Lundquist number (Lundquist, 1949)

$$S_0 = \frac{t_\eta}{t_A} = \frac{V_A l}{\eta}. \tag{1.17}$$

Alfvén waves can exist even at low magnetic Reynolds number R_m if the Lundquist number (S_0) is greater than one. High Lundquist number regimes can exist irrespective of whether R_m is low or high. However, the survival time of these damped wave propagation against magnetic diffusion is not clear. One of the objectives of this thesis is to understand the wave–diffusion transition of low-R_m small-scale flows.

1.6 Quasi-static (*qs*) approximation

The fact that the eddy turn-over time t_o is sufficiently larger than the diffusion time t_η in low-R_m essentially translates to the inequality (Roberts, 1967)

$$\|\partial \boldsymbol{B}/\partial t\| \ll \|\eta \nabla^2 \boldsymbol{B}\|,$$

because of which an approximately steady state ensues where the convection term is balanced by the diffusion term in the induction equation. This is the quasi-static (*qs*) approximation.

The quasi-static regime is well addressed in the literature. The kinetic energy (E_k), magnetic energy (E_m) and length scale parallel to the magnetic field lines $(l_\parallel)$ of a quasi-static diffused velocity field along the direction of magnetic field decays as (Davidson, 1995; Moffatt, 1967; Sommeria and Moreau, 1982)

$$E_k \sim (t/\tau)^{-1/2},\ E_m \sim (t/\tau)^{-3/2},\ l_\parallel \sim l_\perp (t/\tau)^{1/2}, \tag{1.18}$$

where $l_\perp$ is the characteristic length scale perpendicular to the external magnetic field.

1.7 An outline of the objective and structure of the thesis

The main objective of the thesis is to understand small-scale MHD waves in the Earth's outer core by studying the evolution of an isolated blob in the presence of magnetic field and rotation. In Chapter 2, a review of the literature on MHD waves, torsional oscillations, secular variation and small-scale turbulence is presented. In Chapter 3, the problem of evolution of small-scale motions in the presence of a uniform magnetic field is considered. This chapter focuses on estimating the survival time of waves driven by small-scale motion under finite magnetic diffusion. To this end, the transition timescale from the damped Alfvén wave phase to a purely diffusive, quasi-static (qs) phase is examined. The possibility of such small-scale disturbances propagating as Alfvén waves across the outer core on sub-decadal timescales is also discussed. In chapter 4, the dynamics of small-scale vortices in the presence of both magnetic field and rotation is investigated, where both the field and rotation are co-axial. The damping timescales of the slow and fast Magneto-Coriolis (MC) waves are studied theoretically. The relative strengths of the slow and fast waves is understood by varying the magnetic field strength in the problem. This study is a first step in understanding the evolution of damped MC waves in the Earth's core. In chapter 5, the main conclusions are summarized and the scope for future work is discussed.

Chapter 2

An overview of small-scale motions and MHD waves in Earth's core

The problem of hydromagnetic waves and small-scale motions inside the Earth's core has been addressed previously. In this chapter, a review of these studies is presented in three sections. The first section discusses the studies on hydromagnetic waves, torsional oscillations and secular variation. Secondly, studies on small-scale motions in the Earth's core are presented. Finally, some studies on low R_m MHD turbulence are reviewed.

2.1 Studies on hydromagnetic waves, torsional oscillations and secular variation

The existence of waves in hydromagnetic fluids was first proposed in Alfvén (1942). Alfvén showed that the induced magnetic field in a liquid permeated by an external uniform magnetic field satisfies a wave equation that represents wave propagation along the magnetic field line. Many experimental studies were attempted to see these waves in the laboratory. Much of the earlier experimental works studied the harmonic response of the waves. Lundquist (1949) did the first experiment using mercury to find evidence of these waves. Lehnert (1954b) used liquid sodium instead of mercury as the working fluid due to

the former's lower magnetic diffusivity. Lehnert used a cylindrical container to excite waves by oscillating a disc along the axis of symmetry made of copper. The disk's frequency of oscillation was fixed to 30 cm/s, and the field strength was varied between 0.3-1 T to change the resonant frequency of the system. The potential difference induced by fluid motion between two probes placed on the surface of the liquid was measured. The maximum potential difference obtained was only 1.15 times the potential difference at an infinite field intensity at the resonance point. The lower value of the potential difference at the resonant location is attributed to Ohmic diffusion and losses in the copper disc implying that the waves were strongly damped.

Jameson (1961) performed experiments to obtain Alfvén waves in a torus with rectangular cross section. In the first part of the study, Jameson demonstrated the generation of standing Alfvén waves using vertical magnetic field whose strength was varied between 0.65 - 1 T. Only the magnetic field was measured in this experiment. Standing Alfvén waves were obtained using sinusoidal input current. The induced field measurements showed a strong resonance at the fundamental frequency and a weak resonance at three times this frequency. Also, at the resonant frequency, the magnitude of the induced magnetic field was nine times greater than the magnitude of the field that would have been generated in free space by the exciting current. This experiment showed a stronger evidence for the existence of Alfvén waves in a laboratory setup.

In a recent experiment (Alboussière et al., 2011), unlike previous experiments that measured only the harmonic response, velocity measurements were also performed that showed a clear evidence for the propagation of Alfvén waves. A cylindrical container was filled with Gallium alloy and an axial magnetic field was imposed. The field strength was varied between 0-13 T. The maximum field strength corresponded to a Lundquist number $S_0 \approx 60$. Numerical simulations were performed at a given Lundquist number and the experimental result matched the numerical values within agreeable limits. A clear evidence of Alfvén waves was obtained in this experiment. The Lundquist number of the system was varied

by changing the magnetic field strength. The amplitude of the Alfvén wave corresponding to the largest field strength was greater than the amplitude of the waves generated from a relatively weak field strength. The velocity measurements indicated that the waves were traveling with Alfvén travel velocity.

All these experiments were performed using liquid metals in laboratory conditions. In almost all the experiments, the waves obtained were damped due to the low R_m of the setup. Alboussière et al. (2011) were still able to clearly identify the Alfvén waves due to larger field strength. Since small-scale motions are low R_m flows, these experiments suggest that small-scale flows can support wave motion.

Lehnert (1954a, 1955a) studied the effects of rotation on hydromagnetic waves. It was shown that the disturbance in an electrically conducting fluid under rapid rotation splits into two circularly polarized waves. As discussed earlier in the previous chapter, these waves are called Magneto-Coriolis (MC) waves. The fast MC wave has its period similar to the inertial wave and the slow MC wave has a longer period.

Braginsky (1964, 1967) studied the effects of buoyancy on the hydromagnetic waves. It was shown that the presence of buoyancy would still give rise to the propagation of fast and slow waves but with their frequency modified by buoyancy. These waves are termed as Magneto-Archimedean-Coriolis (MAC) waves as the interaction between Lorentz, buoyancy, and Coriolis forces causes these waves. Hide (1966) was the first to study these rotating hydromagnetic waves in a spherical geometry. A linearly varying Coriolis force was assumed across the latitude similar to the β-plane approximation used in Rossby (1939). Fluid in a spherical shell under rapid rotation and an azimuthal magnetic field was considered. Hide showed that such a hydromagnetic system would give rise to the propagation of Rossby and MC-Rossby waves. Rossby waves are caused due to the latitudinal variation of Coriolis force while the MC-Rossby waves are caused due to the balance between Lorentz and latitudinal variation of the Coriolis force. The MC-Rossby waves are similar to the slow

MC waves that has longer periods and hence Hide suggested that these waves could be attributed to the long time features of the geomagnetic secular variation.

Braginsky (1970) suggested that Alfvén waves exist inside the Earth's core in the form of Torsional Oscillations (TOs) where large-scale coaxial cylinders undergo oscillations due to the restoring action of the radial magnetic field. Braginsky suggested that the momentum transfer from these large-scale TOs could cause the variations in the length of day. Braginsky (1984) suggested that the short-time secular variation (SSV) features and LOD variation, where both had 60 year period could be explained by TOs with the same period. Jault et al. (1988) suggested that TOs occur at decadal period which was also supported by a good correlation between the estimated angular momentum transfer from the core to the mantle and the LOD variation between 1970-1985.

Mound and Buffet (2005, 2006) proposed that the TOs along with the gravitational coupling between the inner core and the mantle has a 6-7 year period of oscillation and showed a good correlation with the LOD variation signal that spanned around 42 years. Gillet et al. (2010) showed that TOs inside Earth's core has a time period of 4-6 years. A good match between the angular momentum transfer and the LOD variations was observed between 1960-1980.

TOs were also obtained in numerical dynamo simulations (Teed et al., 2014; Wicht and Christensen, 2010). Plausible excitation mechanisms were discussed in the numerical studies (Teed et al., 2014, 2015), where they proposed that the ageostrophic part of Lorentz force acting at the inner-core boundary might excite these waves inside the Earth's core. Hori et al. (2015) obtained MC-Rossby waves in their magnetoconvection simulations and proposed that the secular variation near the equator is dominated by the zonal flow while at higher latitudes, the variation might be primarily due to the MC-Rossby waves.

All the above studies proposed different mechanisms to explain LOD and secular variation using torsional oscillations and MC-Rossby waves. In all the above-mentioned studies, the

wave motions are associated with large-scale flows. Some previous studies on small-scale flows in the Earth's core are discussed in the following section.

2.2 Studies on small-scale motions in Earth's core

Braginsky and Meytlis (1990) proposed that small-scale flows in the core are produced by the release of light elements from the inner core boundary. The formation of plate-like structures along the direction of rotation and magnetic field was predicted analytically. Contrary to the idea of elongated structures, Moffatt and Loper (1994) showed analytically for the same governing equations that a buoyant blob would travel across the entire outer core without any change in its shape. It was proposed that the case of elongated structures is not applicable in a regime where the Coriolis and Lorentz forces are of same magnitude. In order to ascertain whether the Braginsky-Meytlis model or the Moffatt-Loper model is correct, St Pierre (1996) performed a numerical study on the rise of a buoyant parcel. He showed that the parcel would form plate-like structures which elongated along the direction of magnetic field and rotation and supported the Braginsky-Meytlis model. Davidson and Siso-Nadal (2002) gave a physical explanation to the formation of plate-like structures. It was proposed that these structures are formed as a result of conservation of angular momentum of the fluid parcel placed under rotation and magnetic field.

Loper and Shimizu (1997) studied theoretically the length and timescales of buoyancy driven small-scale flows and identified four types of primary flows depending upon the relative strengths of the Coriolis, Lorentz, and viscous forces. In all these four types, the flow would be elongated either along the rotation or magnetic field direction depending on the relative strength of the forces. For Earth, the structures would correspond to two of the primary modes where either the Coriolis or Lorentz force is the strongest. In all these modes, there would be an initial period where wave propagation is dominant before the transition to the *qs* state. Similar to the Earth's core, viscous diffusion was considered to be

negligible when compared to Ohmic diffusion. The transition time to the *qs* state was found to be several times greater than magnetic diffusion timescale.

The simulations of Matsushima et al. (1999) also showed that the small-scale flows would form elongated structures along the plane spanned by rotation and magnetic field. This study showed that the anisotropic diffusion of small-scale flows would play a significant role in the diffusion of large-scale fields. A turbulent diffusivity for the fluid was proposed to parameterize the diffusive effects of the small-scale flows on the large-scale structures.

Jault (2008) proposed an alternative mechanism for the excitation and propagation of torsional oscillations. Localized small-scale motion excited from inner core jerks would form a geostrophic column; this columnar structure would then propagate as an Alfvén wave along the radial magnetic field lines. This study proposed an alternative mechanism for torsional oscillations but did not show any evidence for a correlation between the angular momentum transfer and LOD variation. On similar arguments, buoyant parcels released from the inner core boundary could also form geostrophic columns and propagate as Alfvén waves, a possibility which is considered in the Chapter 3.

2.3 Studies on low R_m MHD turbulence

Both the laboratory MHD flows as well as small-scale motions inside the Earth's core have low magnetic Reynolds number (R_m). In this section, previous studies on low R_m MHD turbulence are briefly discussed.

Lehnert (1955b) studied the final phase of decay of low R_m MHD turbulence in the presence of magnetic field and rotation. In the first part of the study, the effect of magnetic field alone was considered. In the second part of the study, the combined effect of rotation and magnetic field was considered. In the presence of the magnetic field, Lehnert proposed that all periodic (wave-like) and aperiodic (diffusive) solutions are damped rapidly. At large times, Lehnert envisaged that the decaying turbulent flow would become approximately

two-dimensional along the field lines. With rotation and magnetic field, Lehnert showed that the decaying modes perpendicular to the rotation vector would split into four solutions.

Moffatt (1967) studied the evolution of low R_m homogeneous MHD turbulence. In this study the interaction parameter $N_0 \gg 1$, hydrodynamic Reynolds number $Re \gg 1$ and magnetic Reynolds number $R_m \ll 1$. For Lundquist numbers $S_0 \ll 1$, the kinetic and magnetic energies (E_k, E_m) decay asymptotically as $t^{-1/2}$ and $t^{-3/2}$ respectively. For $S_0 \gg 1$, E_k and E_m decay in equipartition as $t^{-5/2}$. In this regime, E_k and E_m tend to their quasi-static values on timescales $t \sim \sqrt{S_0} t_\eta$ and $t \sim S_0 t_\eta$ respectively.

Sommeria and Moreau (1982) and Davidson (1995) independently investigated the evolution of low R_m MHD turbulence using the linearized momentum and induction equations. These studies used the *qs* approximation (Roberts, 1967) where the growth rate of the induced field is negligible compared to the other frequencies of the system. These studies predict that the lengthscale parallel to the magnetic field evolves as $\sim t^{1/2}$ whereas the perpendicular lengthscale remains approximately invariant. Furthermore, the kinetic energy of the system decays as $\sim t^{-1/2}$.

This study examines the wave phase that *precedes* the purely diffusive *qs* phase, for which one must reinstate the growth rate of the induced field $\partial \boldsymbol{b}/\partial t$ in the induction equation. This provides the timescales for transition from the wave-dominated regime to the diffusion-dominated regime.

Chapter 3

Evolution of small-scale motions in the presence of a magnetic field

This chapter investigates small-scale convective motions of low R_m that have Lundquist numbers S_0 large enough to cause the propagation of Alfvén waves across the outer core on sub-decadal timescales. To this end, the long-time evolution of an isolated small-scale flow in a uniform magnetic field is investigated. The approximate solution of this problem is along the lines of Moffatt (1967) for turbulence, and gives estimates of the kinetic and magnetic energies and the wave–diffusion transition times. The exact solution of this problem gives the structure of the flow in the damped wave phase, with the *qs* solution provided for comparison. The energies and Ohmic dissipation in the damped wave phase are shown to evolve very differently from that in the *qs* solution. The exact solution also gives the rate at which the true value of the Lundquist number decreases in time, essential to the understanding of how Alfvén waves degenerate into diffusion, and how the timescales of wave propagation and the action of nonlinear inertial forces are vastly different. Finally, the possibility of small-scale motion travelling as damped Alfvén waves across the outer core is examined. The knowledge of core travel times obtained from length of day variation data can help place a lower bound on the lengthscale of convection in the core.

As background rotation does not influence the timescale of damping of Alfvén waves, rotation is not included in the equation of motion. Nevertheless, the role of rotation is forming cylindrical columns from three-dimensional structures is apparent from the relative magnitudes of the inertial wave and Alfvén wave timescales.

The problem is approached by considering a localized disturbance in a quiescent, incompressible fluid of finite magnetic diffusivity and small viscosity. The fluid is threaded by a uniform magnetic field $\boldsymbol{B}_0 = B_0\hat{\boldsymbol{e}}_z$. Although here the mean magnetic field is aligned with the axis z for mathematical simplicity, the laws of evolution derived for this configuration are extendible without loss of generality to the outer core where wave motion occurs along the mean field lines in the radial (s) direction.

The condition of $R_m \ll 1$ and $N_0 \gg 1$ apply to the system (Moffatt, 1967). The condition of $N_0 \gg 1$ implies that the magnitude of nonlinear inertial force is much smaller than the Lorentz force ($|\boldsymbol{u}\cdot\nabla\boldsymbol{u}| \ll |\boldsymbol{j}\times\boldsymbol{B}_0|$). Hence, the velocity field $\boldsymbol{u}$ is determined by the linearized equation of motion

$$\frac{\partial \boldsymbol{u}}{\partial t} = -\frac{\nabla p'}{\rho} + \frac{1}{\mu\rho}(\boldsymbol{B}_0\cdot\nabla)\boldsymbol{b} + \nu\nabla^2\boldsymbol{u}, \tag{3.1}$$

where μ, ρ, ν are the magnetic permeability, density and kinematic viscosity of the fluid. p' is the modified pressure which gives the sum of mechanical (p) and magnetic pressure $(\boldsymbol{b}^2/2\mu)$ of the fluid

$$p' = p + \frac{\boldsymbol{b}^2}{2\mu}.$$

When $R_m \ll 1$, the induced magnetic field $\boldsymbol{b}$ is of order $R_m\boldsymbol{B}_0$ and therefore satisfies the following linearized induction equation (Lehnert, 1955b)

$$\frac{\partial \boldsymbol{b}}{\partial t} = \nabla\times(\boldsymbol{u}\times\boldsymbol{B}_0) + \eta\nabla^2\boldsymbol{b}. \tag{3.2}$$

In the following section, the wave equation for Alfvén waves at low R_m and the corresponding dispersion relation is obtained.

3.1 Dispersion relation for Alfvén waves at low R_m

Considering $\boldsymbol{B}_0 = B_0\hat{\boldsymbol{e}}_z$ and seeking solutions to $\boldsymbol{u}$ and $\boldsymbol{b}$ from (3.1) and (3.2) of the form $e^{i\boldsymbol{k}\cdot\boldsymbol{x}+i\lambda t}$ gives the following dispersion relation (Chandrasekhar, 1961, p157):

$$\lambda_{\pm} = \pm\sqrt{V_A^2 k_z^2 - \frac{(\nu-\eta)^2 k^4}{4}} + i\frac{(\nu+\eta)k^2}{2}, \tag{3.3}$$

where $V_A = B_0/\sqrt{\mu\rho}$ is the Alfvén velocity.

In the *qs* limit ($\partial\boldsymbol{b}/\partial t = 0$), following a similar procedure yields a purely imaginary frequency that implies pure magnetic damping (no wave motion) (Roberts, 1967, p136):

$$\lambda = \lambda_{qs} = i\left(\frac{k_z^2}{\tau k^2} + \nu k^2\right), \tag{3.4}$$

where $\tau = \eta/V_A^2$ is the timescale of magnetic damping called the Joule time.

3.2 Approximate form of frequencies with damping

In this section, the approximate form of frequencies $\lambda_{\pm}$ are obtained for different regimes which are characterized by the parameter ζ introduced by Lehnert (1955b):

$$\zeta = \frac{2V_A k_z}{|\eta-\nu|k^2}.$$

The ratio $|\zeta| \gg 1$ and $|\zeta| \ll 1$ correspond to wave and diffusion-dominated regimes respectively.

The magnetic Prandtl number $P_m = \nu/\eta$ for the Earth's core is $P_m \sim 10^{-6}$ based on the molecular diffusivities. $P_m = 10^{-6}$ also means that the viscous diffusion affects the dynamics of the flow only at $t \sim 10^6 t_\eta$ where $t_\eta = \delta^2/\eta$ is the magnetic diffusion time. In the inviscid ($\nu \to 0$) limit, ζ would represent the ratio

$$(\zeta)_{\nu=0} = S_t = \frac{2V_A k_z}{\eta k^2}, \tag{3.5}$$

where S_t is called the *true Lundquist number* because (3.5) gives the actual ratio of magnetic diffusion timescale $(\eta k^2)^{-1}$ and Alfvén travel timescale $(V_A k_z)^{-1}$. Therefore, in the inviscid limit, the wave and diffusion dominated regimes are characterized by $S_t \gg 1$ and $S_t \ll 1$ respectively. The approximate form of frequencies obtained in the following section are used to obtain the kinetic and magnetic energy estimates in wave and diffusion-dominated regimes.

3.2.1 Wave-dominated regime $(S_t \gg 1)$

In the inviscid limit, $\lambda_\pm$ modes from (3.3) are,

$$\lambda_\pm = \pm\sqrt{V_A^2 k_z^2 - \left(\frac{\eta k^2}{2}\right)^2} + i\frac{\eta k^2}{2}.$$

Since $V_A k_z \gg \eta k^2/2$,the frequencies $\lambda_\pm$ can be written as

$$\lambda_\pm = \pm V_A k_z \sqrt{1 - \left(\frac{\eta k^2}{2V_A k_z}\right)^2} + i\frac{\eta k^2}{2}.$$

Since $\eta k^2/(2V_A k_z) \ll 1$, the Taylor series expansion of $\lambda_\pm$ gives

$$\begin{aligned}
\lambda_\pm &\approx \pm V_A k_z \left[1 - \frac{1}{2}\left(\frac{\eta k^2}{2V_A k_z}\right)^2\right] + i\frac{\eta k^2}{2}, \\
\lambda_\pm &\approx \pm V_A k_z + i\frac{\eta k^2}{2}.
\end{aligned} \tag{3.6}$$

3.2.2 Diffusion-dominated regime ($S_t \ll 1$)

In the inviscid limit, λ_+ mode is

$$\lambda_+ = \sqrt{V_A^2 k_z^2 - \left(\frac{\eta k^2}{2}\right)^2} + i\frac{\eta k^2}{2}.$$

Since $\eta k^2/2 \gg V_A k_z$, λ_+ can be written as

$$\lambda_+ = \frac{\eta k^2}{2}\sqrt{\left(\frac{2V_A k_z}{\eta k^2}\right)^2 - 1} + i\frac{\eta k^2}{2}.$$

Since $2V_A k_z/\eta k^2 \ll 1$, the Taylor series expansion of λ_+ is

$$\begin{aligned}\lambda_+ &\approx i\frac{\eta k^2}{2}\left[1-\frac{1}{2}\left(\frac{2V_A k_z}{\eta k^2}\right)^2\right]+i\frac{\eta k^2}{2},\\ &\approx i\eta k^2 - i\frac{V_A^2 k_z^2}{\eta k^2},\\ \lambda_+ &\approx i\eta k^2.\end{aligned}$$

Now, consider λ_- mode

$$\begin{aligned}\lambda_- &= -\sqrt{V_A^2 k_z^2 - \left(\frac{\eta k^2}{2}\right)^2}+i\frac{\eta k^2}{2},\\ &= -\frac{\eta k^2}{2}\sqrt{\left(\frac{2V_A k_z}{\eta k^2}\right)^2 - 1}+i\frac{\eta k^2}{2}.\end{aligned} \tag{3.7}$$

Using Taylor series expansion, λ_- becomes

$$\begin{aligned}\lambda_- &\approx -i\frac{\eta k^2}{2}\left[1-\frac{1}{2}\left(\frac{2V_A k_z}{\eta k^2}\right)^2\right]+i\frac{\eta k^2}{2},\\ \lambda_- &\approx i\frac{V_A^2 k_z^2}{\eta k^2} = i\frac{k_z^2}{\tau k^2}.\end{aligned} \tag{3.8}$$

From (3.7) and (3.8), it is clear that λ_- is same as the *qs* frequency in (3.4), suggesting that this diffusion dominated phase is same as *qs* regime. Since only one mode can physically exist in this regime, $\lambda_- = \dfrac{ik_z^2}{\tau k^2}$ is the relevant mode of the system.

3.3 Problem definition and general solutions

In cylindrical polar coordinates (s,ϕ,z), the initial velocity field perturbation is taken to be axisymmetric about its own axis (independent of ϕ) and of the form $\boldsymbol{u} = (0, u_{\phi 0}, 0)$, where

$$u_{\phi 0} = As\exp\left[-(s^2+z^2)/\delta^2\right]. \tag{3.9}$$

Here A is a constant and δ is the lengthscale of the flow. Figure 3.1 is the schematic representation of this initial blob in presence of the external magnetic field $\boldsymbol{B}_0 = B_0\hat{\boldsymbol{e}}_z$.

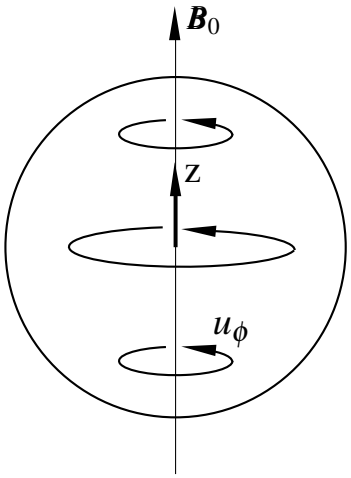

Fig. 3.1 A localized flow perturbation of the initial form given by (3.9) in an otherwise quiescent electrically conducting fluid permeated by an axial (z) magnetic field.

This initial vortex subsequently evolves in time obeying the following MHD equations:

$$\frac{\partial u_\phi}{\partial t} = \frac{B_0}{\mu\rho}\frac{\partial b_\phi}{\partial z} + \nu\left(\frac{1}{s}\frac{\partial}{\partial s}\left(s\frac{\partial u_\phi}{\partial s}\right) + \frac{\partial^2 u_\phi}{\partial z^2} - \frac{u_\phi}{s^2}\right), \tag{3.10}$$

$$\frac{\partial b_\phi}{\partial t} = B_0\frac{\partial u_\phi}{\partial z} + \eta\left(\frac{1}{s}\frac{\partial}{\partial s}\left(s\frac{\partial b_\phi}{\partial s}\right) + \frac{\partial^2 b_\phi}{\partial z^2} - \frac{b_\phi}{s^2}\right). \tag{3.11}$$

The following Hankel-Fourier transform pair is considered,

$$\hat{\boldsymbol{f}}(k_s,k_z) = \frac{1}{2\pi^2}\int_0^\infty\int_0^\infty \boldsymbol{f}(s,z)\, J_1(k_s s)\, e^{-ik_z z}\, s\, ds\, dz, \tag{3.12}$$

$$\boldsymbol{f}(s,z) = 4\pi\int_0^\infty\int_0^\infty \hat{\boldsymbol{f}}(k_s,k_z) J_1(k_s s)\, e^{ik_z z}\, k_s\, dk_s\, dk_z. \tag{3.13}$$

Applying (3.12) to (3.10) and (3.11) gives

$$\frac{\partial \hat{u}_\phi}{\partial t} = \frac{B_0 i k_z}{\mu\rho}\hat{b}_\phi - \nu k^2\hat{u}_\phi, \tag{3.14}$$

$$\frac{\partial \hat{b}_\phi}{\partial t} = B_0 i k_z \hat{u}_\phi - \eta k^2\hat{b}_\phi, \tag{3.15}$$

where $k^2 = k_s^2 + k_z^2$, k_s and k_z being the wavenumbers in the s and z directions. Eqs. (3.14) and (3.15) must be solved subject to the initial conditions for $\hat{u}_\phi$, $\hat{b}_\phi$ and their time derivatives. If the background (mean) magnetic field $\boldsymbol{B}_0$ is taken to be switched on at the instant $t = 0$, the magnetic field perturbation $\boldsymbol{b}$ takes finite time to develop by induction (Moffatt, 1967); therefore the condition $\hat{\boldsymbol{b}} = 0$ is appropriate at $t = 0$. The initial conditions are (Abramowitz and Stegun, 1964),

$$\hat{u}_{\phi 0} = \frac{k_s \delta^5}{16\pi^{3/2}} e^{-k^2\delta^2/4}, \tag{3.16}$$

$$\hat{b}_{\phi 0} = 0, \tag{3.17}$$

$$\left.\frac{\partial \hat{u}_\phi}{\partial t}\right|_{t=0} = -\nu k^2 \hat{u}_{\phi 0}, \tag{3.18}$$

$$\left.\frac{\partial \hat{b}_\phi}{\partial t}\right|_{t=0} = B_0 i k_z \hat{u}_{\phi 0}. \tag{3.19}$$

The general solution for eqs. (3.14) and (3.15) subject to the conditions (3.16)–(3.19) are therefore,

$$\hat{u}_\phi = \left[-\frac{\hat{u}_{\phi 0}(\lambda_- - i\nu k^2)}{\lambda_+ - \lambda_-}\right] e^{i\lambda_+ t} + \left[\frac{\hat{u}_{\phi 0}(\lambda_+ - i\nu k^2)}{\lambda_+ - \lambda_-}\right] e^{i\lambda_- t}, \tag{3.20}$$

$$\hat{b}_\phi = \frac{B_0 k_z \hat{u}_{\phi 0}}{\lambda_+ - \lambda_-}(e^{i\lambda_+ t} - e^{i\lambda_- t}), \tag{3.21}$$

which gives damped Alfvén waves propagating along lines of $\boldsymbol{B}_0$. Here λ_+ and λ_- are the two frequencies arising from the characteristic equation (3.3), representing waves travelling in opposite directions.

In the quasi-static (qs) approximation, the frequency λ_{qs} is purely imaginary (3.4), which gives the following decaying solution:

$$\hat{u}_{\phi,qs} = \hat{u}_{\phi 0} \exp\left[-\left(\frac{k_z^2}{\tau k^2} + \nu k^2\right) t\right], \tag{3.22}$$

$$\hat{b}_{\phi,qs} = \frac{B_0 i k_z \hat{u}_{\phi,qs}}{\eta k^2}. \tag{3.23}$$

For a given time, the velocity and magnetic field perturbations in real space (u_ϕ, b_ϕ) may now be recovered from (3.20), (3.21) & (3.22), (3.23) by the inverse Hankel-Fourier transform (3.13).

3.4 Approximate energies and their wave–diffusion transitions

3.4.1 Kinetic energy (E_k)

Wave-dominated regime $(S_t \gg 1)$

From (3.6), the frequencies in this regime are:

$$\lambda_\pm \approx \pm V_A k_z + i\frac{\eta k^2}{2}.$$

Let $\alpha = V_A k_z$ and $\beta = \eta k^2/2$ such that $\lambda_\pm = \pm\alpha + i\beta$. The inviscid form of u_ϕ general solution (3.20) is considered,

$$\hat{u}_\phi = \left[-\frac{\hat{u}_{\phi 0}\lambda_-}{\lambda_+ - \lambda_-}\right] e^{i\lambda_+ t} + \left[\frac{\hat{u}_{\phi 0}\lambda_+}{\lambda_+ - \lambda_-}\right] e^{i\lambda_- t}. \tag{3.24}$$

Using $\lambda_\pm = \pm\alpha + i\beta$ in (3.24), the general solution $\hat{u}_\phi$ simplifies to the following form:

$$\hat{u}_\phi = \hat{u}_{\phi 0} e^{-\beta t}\left[\cos(\alpha t) + \frac{\beta}{\alpha}\sin(\alpha t)\right]. \tag{3.25}$$

Now, since the total kinetic energy E_k is given by Parseval's theorem as (Appendix B.3)

$$E_k = 16\pi^4 \int_0^\infty \int_0^\infty |\hat{u}_\phi|^2 \, k_s \, dk_s \, dk_z. \tag{3.26}$$

for $S_t \gg 1$, E_k is approximated by

$$E_k \approx 16\pi^4 \int_0^\infty \int_0^\infty |\hat{u}_{\phi 0}|^2 \, e^{-\eta k^2 t} \, k_s \, dk_s \, dk_z.$$

For $t \ll t_\eta$, the exponential decay is small and the kinetic energy (E_k) is

$$\begin{aligned}
E_k &\approx 16\pi^4 \int_0^\infty \int_0^\infty |\hat{u}_{\phi 0}|^2 \, k_s \, dk_s \, dk_z, \\
&\approx \frac{\pi\delta^{10}}{16} \int_0^\infty \int_0^\infty k_s^3 \exp\left(-\frac{\delta^2 k^2}{2}\right) \, dk_s \, dk_z, \\
&\approx \frac{\pi\delta^{10}}{16} \int_0^\infty k_s^3 \exp\left(-\frac{\delta^2 k_s^2}{2}\right) \, dk_s \int_0^\infty \exp\left(-\frac{\delta^2 k_z^2}{2}\right) \, dk_z, \\
\text{Using } I_0(a) &= \frac{1}{2}\sqrt{\frac{\pi}{a}} \text{ and } I_3(a) = \frac{1}{2a^2} \text{ (Appendix A.1)}, \\
E_k &\approx \frac{\sqrt{2}\pi^{3/2}\delta^5}{16}.
\end{aligned}$$

Therefore, for $t \ll t_\eta$, the kinetic energy is

$$E_k \approx \frac{\sqrt{2}\pi^{3/2}\delta^5}{16} = E_0. \tag{3.27}$$

For $t \gtrsim O(t_\eta)$, the exponential decay term becomes significant and hence E_k is

$$\begin{aligned}
E_k &\approx \frac{\pi\delta^{10}}{16} \int_0^\infty \int_0^\infty k_s^3 \exp\left[-\left(\frac{k^2\delta^2}{2} + \eta k^2 t\right)\right] \, dk_s \, dk_z, \\
&\approx \frac{\pi\delta^{10}}{16} \int_0^\infty k_s^3 \exp\left[-k_s^2\left(\frac{\delta^2}{2} + \eta t\right)\right] \, dk_s, \\
&\qquad \times \int_0^\infty \exp\left[-k_z^2\left(\frac{\delta^2}{2} + \eta t\right)\right] \, dk_z, \\
\text{Using } I_0(a) &= \frac{1}{2}\sqrt{\frac{\pi}{a}} \text{ and } I_3(a) = \frac{1}{2a^2} \text{ from (Appendix A.1)}, \\
&\approx \frac{\pi\delta^{10}}{16} \times \frac{1}{2\left((\delta^2/2) + \eta t\right)^2} \times \frac{1}{2}\sqrt{\frac{\pi}{(\delta^2/2) + \eta t}}, \\
&\approx \frac{\pi^{3/2}\delta^{10}}{64\left((\delta^2/2) + \eta t\right)^{5/2}}, \\
&\approx \frac{2^{5/2}\pi^{3/2}\delta^5}{64} \times \frac{1}{(1 + 2(t/t_\eta))^{5/2}},
\end{aligned}$$

For $t \gg t_\eta$, E_k becomes

$$E_k \approx \frac{\pi^{3/2}\delta^5}{64}\left(\frac{t}{t_\eta}\right)^{-5/2}. \tag{3.28}$$

Quasi-static regime $(S_t \ll 1)$

The inviscid solution of *qs* velocity field (3.22) is considered,

$$\hat{u}_{\phi,qs} = \hat{u}_{\phi 0} \exp\left(-\frac{k_z^2 t}{\tau k^2}\right). \tag{3.29}$$

The quasi-static kinetic energy $E_{k,qs}$ is

$$\begin{aligned} E_{k,qs} &= 16\pi^4 \int_0^\infty \int_0^\infty |\hat{u}_{\phi,qs}|^2 \, k_s \, dk_s \, dk_z, \\ E_{k,qs} &= \frac{\pi\delta^{10}}{16} \int_0^\infty \int_0^\infty k_s^3 \exp\left[-\left(\frac{k^2\delta^2}{2} + \frac{2k_z^2 t}{\tau k^2}\right)\right] dk_s \, dk_z. \end{aligned}$$

For $t \ll \tau$, the exponential decay is small and the kinetic energy is

$$E_{k,qs} \approx 16\pi^4 \int_0^\infty \int_0^\infty |\hat{u}_{\phi 0}|^2 \, k_s \, dk_s \, dk_z = E_0.$$

Therefore, for $t \ll \tau$, the $E_{k,qs}$ is the initial kinetic energy of the blob.

For large time $t \gg \tau$, $k_z \ll k_s$ (so that $k \approx k_s$). Therefore, $E_{k,qs}$ is

$$\begin{aligned} E_{k,qs} &\approx \frac{\pi\delta^{10}}{16} \int_0^\infty \int_0^\infty k_s^3 \exp\left[-\left(\frac{k_s^2\delta^2}{2} + \frac{2k_z^2 t}{\tau k_s^2}\right)\right] dk_s \, dk_z, \\ &\approx \frac{\pi\delta^{10}}{16} \int_0^\infty k_s^3 \exp\left(-\frac{k_s^2\delta^2}{2}\right) dk_s \int_0^\infty \exp\left(-\frac{2k_z^2 t}{\tau k_s^2}\right) dk_z, \\ \text{Using } I_0(a) = \frac{1}{2}\sqrt{\frac{\pi}{a}} &\text{ and } I_4(a) = \frac{3}{8a^2}\sqrt{\frac{\pi}{a}} \text{ from (Appendix A.1)}, \\ &\approx \frac{\pi\delta^{10}}{16} \int_0^\infty k_s^3 \exp\left(-\frac{k_s^2\delta^2}{2}\right) dk_s \times \frac{k_s}{2}\sqrt{\frac{\pi\tau}{2t}}, \\ &\approx \left(\frac{t}{\tau}\right)^{-1/2} \times \frac{\delta^{10}\pi^{3/2}}{32\sqrt{2}} \int_0^\infty k_s^4 \exp\left(-\frac{k_s^2\delta^2}{2}\right) dk_s, \\ &\approx \left(\frac{t}{\tau}\right)^{-1/2} \times \frac{\delta^{10}\pi^{3/2}}{32\sqrt{2}} \times \frac{3\sqrt{\pi}}{\delta^5\sqrt{2}}, \\ E_{k,qs} &\approx \frac{3\delta^5\pi^2}{64}\left(\frac{t}{\tau}\right)^{-1/2}. \end{aligned} \tag{3.30}$$

Hence, the energy estimate (3.30) is the quasi-static kinetic energy of a swirling vortex blob.

Kinetic energy's transition time to the *qs* state

From (3.28) and (3.30),

$$E_k \sim \left(\frac{t}{t_\eta}\right)^{-5/2},\ E_{k,qs} \sim \left(\frac{t}{\tau}\right)^{-1/2}.$$

It is found that the kinetic energy E_k tends to its quasi-static value $E_{k,qs}$ when

$$\begin{aligned} E_k &\sim E_{k,qs}, \\ \left(\frac{t}{t_\eta}\right)^{-5/2} &\sim \left(\frac{t}{\tau}\right)^{-1/2}, \end{aligned}$$

Using $S_0^2 = t_\eta/\tau$, replacing τ by t_η/S_0^2 in the above relation,

$$\begin{aligned} \left(\frac{t}{t_\eta}\right)^{-5/2} &\sim \left(\frac{S_0^2 t}{t_\eta}\right)^{-1/2}, \\ t &\sim \sqrt{S_0} t_\eta, \end{aligned} \tag{3.31}$$

which is same as the wave–diffusion transition time for the kinetic energy in MHD turbulence of known initial energy spectrum (Moffatt, 1967).

3.4.2 Magnetic energy (E_m)

Wave-dominated regime $(S_t \gg 1)$

The $\hat{b}_\phi$ solution from (3.21) is considered,

$$\hat{b}_\phi = \frac{B_0 k_z \hat{u}_{\phi 0}}{\lambda_+ - \lambda_-}(e^{i\lambda_+ t} - e^{i\lambda_- t}).$$

Using $\lambda_\pm \approx \alpha + i\beta$ where $\alpha = V_A k_z$ and $\beta = \eta k^2/2$. In the inviscid limit, the $\hat{b}_\phi$ magnetic field solution is

$$\hat{b}_\phi \approx \frac{iB_0 k_z \hat{u}_{\phi 0}}{\alpha} e^{-\beta t} \sin(\alpha t) = i\sqrt{\mu\rho}\ \hat{u}_{\phi 0}\ e^{-\eta k^2 t/2}\ \sin(V_A k_z t). \tag{3.32}$$

From Appendix (B.4), the total magnetic energy E_m is given by

$$E_m = \frac{16\pi^4}{\mu\rho}\int_0^\infty\int_0^\infty |\hat{b}_\phi|^2 k_s\, dk_s\, dk_z, \tag{3.33}$$
$$E_m \approx 16\pi^4\int_0^\infty\int_0^\infty |\hat{u}_{\phi 0}|^2\, e^{-\eta k^2 t}\, \sin(V_A k_z t)\, k_s\, dk_s\, dk_z.$$

Since $S_t \gg 1$, the diffusion time (t_η) is much greater than the Alfvén travel time (t_A). For $t \ll t_A$, the magnitude of $\sin(V_A k_z t)$ term is small such that $E_m \sim 0$. For $t_A \ll t \ll t_\eta$, the $|\hat{u}_{\phi 0}|^2$ is dominant and $E_m \approx E_0$ as obtained in (3.27) signifying an equipartition between kinetic and magnetic energies.

For $t \gtrsim t_\eta$, E_m is approximated by

$$E_m \approx 16\pi^4\int_0^\infty\int_0^\infty |\hat{u}_{\phi 0}|^2 e^{-\eta k^2 t}\, k_s\, dk_s\, dk_z,$$

which in turn results in (3.28), the approximate value of E_k. Therefore for $t \gtrsim t_\eta$, the magnetic energy decays as

$$E_m \approx \frac{\pi^{3/2}\delta^5}{64}\left(\frac{t}{t_\eta}\right)^{-5/2}. \tag{3.34}$$

Quasi-static regime $(S_t \ll 1)$

The inviscid $\hat{b}_{\phi,qs}$ solution from (3.23) is considered,

$$\hat{b}_{\phi,qs} = \frac{iB_0 k_z \hat{u}_{\phi 0}}{\eta k^2}\exp\left(-\frac{k_z^2 t}{\tau k^2}\right). \tag{3.35}$$

The magnetic energy associated with the above field is

$$E_{m,qs} = \frac{16\pi^4}{\mu\rho}\int_0^\infty\int_0^\infty |\hat{b}_{\phi,qs}|^2\, k_s\, dk_s\, dk_z,$$
$$= \frac{16\pi^4 B_0^2}{\mu\rho\eta^2}\int_0^\infty\int_0^\infty \frac{k_z^2}{k^4}\, |\hat{u}_{\phi 0}|^2 \exp\left(-\frac{2k_z^2 t}{\tau k^2}\right)\, k_s\, dk_s\, dk_z.$$

For $t \ll \tau$, the exponential decay term is small and the magnetic energy is approximated by

$$E_{m,qs} \approx \frac{16\pi^4 B_0^2}{\mu\rho\eta^2} \int_0^\infty \int_0^\infty \frac{k_z^2}{k^4} |\hat{u}_{\phi 0}|^2 \, k_s \, dk_s \, dk_z.$$

Using $k_s = k\cos\theta$ and $k_z = k\sin\theta$, $E_{m,qs}$ becomes

$$\begin{aligned}
E_{m,qs} &\approx \frac{\pi V_A^2 \delta^{10}}{16\eta^2} \int_0^\infty k^2 \exp\left(-\frac{k^2\delta^2}{2}\right) dk \int_0^{\pi/2} \sin^2\theta \cos^3\theta \, d\theta, \\
\text{Using } I_2(a) &= \frac{1}{4a}\sqrt{\frac{\pi}{a}} \text{ (Appendix A.1)}, \\
&\approx \frac{\pi V_A^2 \delta^{10}}{16\eta^2} \times \frac{1}{\delta^3}\sqrt{\frac{\pi}{2}} \times \frac{2}{15}, \\
E_{m,qs} &\approx S_0^2 \, E_0
\end{aligned}$$

For $t \gg \tau$, $k_z \ll k_s$ (so that $k \approx k_s$) and the magnetic energy is

$$\begin{aligned}
E_{m,qs} &\approx \frac{\pi B_0^2 \delta^{10}}{16\mu\rho\eta^2} \int_0^\infty \int_0^\infty \frac{k_z^2}{k_s} \exp\left[-\left(\frac{k_s^2\delta^2}{2} + \frac{2k_z^2 t}{\tau k_s^2}\right)\right] dk_s \, dk_z, \\
&\approx \frac{\pi B_0^2 \delta^{10}}{16\mu\rho\eta^2} \int_0^\infty \frac{1}{k_s} \exp\left(-\frac{k_s^2\delta^2}{2}\right) dk_s \int_0^\infty k_z^2 \exp\left(-\frac{2k_z^2 t}{\tau k_s^2}\right) dk_z, \\
\text{Using } I_2(a) &= \frac{1}{4a}\sqrt{\frac{\pi}{a}} \text{ (Appendix A.1)}, \\
&\approx \frac{\pi B_0^2 \delta^{10}}{16\mu\rho\eta^2} \int_0^\infty \frac{1}{k_s} \exp\left(-\frac{k_s^2\delta^2}{2}\right) dk_s \times \left(\frac{2t}{\tau k_s^2}\right)^{-3/2} \frac{\sqrt{\pi}}{4}, \\
&\approx \left(\frac{t}{\tau}\right)^{-3/2} \times \frac{\pi^{3/2}\delta^{10}}{128\sqrt{2}} \times \frac{B_0^2}{\mu\rho\eta^2} \times \int_0^\infty k_s^2 \exp\left(-\frac{k_s^2\delta^2}{2}\right) dk_s, \\
&\approx \left(\frac{t}{\tau}\right)^{-3/2} \times \frac{\pi^{3/2}\delta^{10}}{128\sqrt{2}} \times \frac{B_0^2}{\mu\rho\eta^2} \times \left(\frac{\delta^2}{2}\right)^{-3/2} \frac{\sqrt{\pi}}{4}, \\
&\approx \left(\frac{t}{\tau}\right)^{-3/2} \times \frac{\pi^2\delta^5}{256} \times \frac{B_0^2\delta^2}{\mu\rho\eta^2}, \\
E_{m,qs} &\approx \frac{\pi^2\delta^5 S_0^2}{256}\left(\frac{t}{\tau}\right)^{-3/2}.
\end{aligned}$$

Therefore quasi-static magnetic energy evolves as

$$E_{m,qs} \approx \frac{\pi^2\delta^5 S_0^2}{256}\left(\frac{t}{\tau}\right)^{-3/2}. \tag{3.36}$$

Magnetic energy's transition time to the *qs* state

The E_m transition time is found in this section by equating the energy estimates in the wave-dominated and *qs* regimes. From (3.34) and (3.36), we have

$$E_m \sim \left(\frac{t}{t_\eta}\right)^{-5/2},\ E_{m,qs} \sim S_0^2 \left(\frac{t}{\tau}\right)^{-3/2}.$$

Now, equating the two estimates

$$\begin{aligned} E_m &\sim E_{m,qs}, \\ \left(\frac{t}{t_\eta}\right)^{-5/2} &\sim S_0^2 \left(\frac{t}{\tau}\right)^{-3/2}, \\ \frac{t}{t_\eta} &\sim S_0. \end{aligned} \tag{3.37}$$

Therefore the magnetic energy E_m tends to the quasi-static magnetic energy at $t \sim S_0 t_\eta$.

In summary, for an isolated flow structure situated in a uniform magnetic field, the following decay laws for the kinetic and magnetic energy are obtained in the limit of $S_0 \gg 1$ and $P_m \to 0$:

$$\frac{E_k(t)}{E_0} \approx \begin{cases} 1 & (t \ll t_\eta), \\ (t/t_\eta)^{-5/2} & (t_\eta \ll t \ll \sqrt{S_0} t_\eta), \\ (t/\tau)^{-1/2} & (t \gg \sqrt{S_0} t_\eta), \end{cases} \tag{3.38}$$

$$\frac{E_m(t)}{E_0} \approx \begin{cases} 1 & (t_A \ll t \ll t_\eta), \\ (t/t_\eta)^{-5/2} & (t_\eta \ll t \ll S_0 t_\eta), \\ S_0^2 (t/\tau)^{-3/2} & (t \gg S_0 t_\eta). \end{cases} \tag{3.39}$$

When the initial Lundquist number $S_0 \ll 1$, the evolution is always in *qs* phase and the energies decay as

$$\frac{E_k(t)}{E_0} \approx \begin{cases} 1 & (t \ll \tau), \\ (t/\tau)^{-1/2} & (t \gg \tau), \end{cases} \tag{3.40}$$

$$\frac{E_m(t)}{E_0} \approx \begin{cases} S_0^2 & (t_\eta \ll t \ll \tau), \\ S_0^2 (t/\tau)^{-3/2} & (t \gg \tau). \end{cases} \tag{3.41}$$

The laws of evolution of E_k and E_m and their qs-transition times are essentially the same for the case of an isolated flow structure considered in this section and for a sea of turbulence made up of a large number of such eddies (Moffatt, 1967). However, the choice of an initial structure of finite lengthscale δ motivates the idea of damped Alfvén waves driven by isolated blobs of $R_m \sim 1$ near the Earth's inner core boundary. In particular, the timescale $t \sim \sqrt{S_0}\, t_\eta$ is relevant to the outer core because it represents the time during which a damped wave can traverse the depth of the core before undergoing pure diffusion. Before discussing the propagation of damped Alfvén waves in the core, it is instructive to look at the exact solutions for the evolution of such waves at low R_m. This study is presented in the following section. For $S_0 \gg 1$, it is shown that the estimates of E_k and E_m obtained above are not merely of the correct order of magnitude, but are very good approximations of the exact energies. However, the exact time at which wave motion gives way to pure diffusion can differ considerably from the approximate transition timescales. The exact analysis also gives the rate at which the true value of the Lundquist number decreases in time, essential to the understanding of how purely diffusive flows evolve from Alfvén waves.

3.5 Exact solutions for the evolution of a localized flow in a magnetic field

In this section, exact solutions for the long-time evolution of the initial localized flow given by eq. (3.9) are obtained from the general solution (3.20) and (3.21). The solutions in the qs approximation, obtained from (3.22) and (3.23), are provided for comparison. The peak value of the initial velocity U_0 and the flow lengthscale δ are chosen such that the magnetic Reynolds number $R_m = 0.01$. The Lundquist number S_0, fixed by the mean magnetic

field strength B_0, is an input parameter. The ratio of viscous to magnetic diffusivities, $P_m = \nu/\eta = 10^{-6}$, so that viscous forces are negligible until very long times of evolution.

3.5.1 Evolution of the velocity and the induced magnetic field

In this section, a qualitative understanding of the wave–diffusion transition is described by studying the evolution of the velocity and induced magnetic field structure both in spectral and physical space. A domain spanning across the (k_s, k_z) wavenumber space is used to resolve the velocity and magnetic field spectral solutions. The grid resolution required and other properties of this domain are discussed in the following section.

Spectral domain and its grid independence

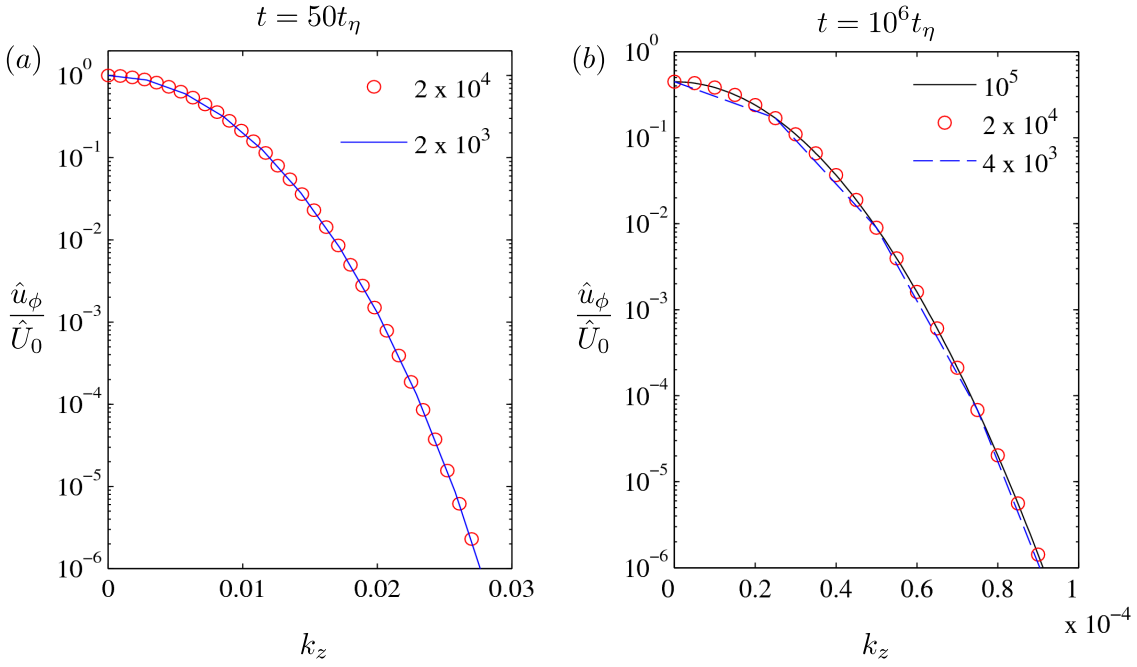

Fig. 3.2 Variation of the velocity transform $\hat{u}_\phi$ (normalized by the maximum value of the initial velocity transform $\hat{U}_0$) with the axial wavenumber k_z at two times (in units of magnetic diffusion time t_η) for different grid resolutions. The truncation values of k_z for the two times are 5.73 ($t = 50t_\eta$) and 0.1 ($t = 10^6 t_\eta$). The Lundquist number $S_0 = 100$.

The $\hat{u}_\phi$ and $\hat{b}_\phi$ spectral solutions are used to find the exact energy estimates. The spectral solutions should be resolved throughout the evolution of the vortex in order to achieve correct energy estimates. Hence, the grid independence of the $\hat{u}_\phi$ spectra is discussed first. Figure 3.2 gives the velocity spectrum, showing grid independence at two times during the evolution of the vortex. At $t = 10^6 t_\eta$, the truncation value of the axial wavenumber k_z can be set to a much smaller value than for $t = 50t_\eta$ because of the strong anisotropy of the flow arising from diffusion along the mean field lines. While 2×10^3 points in k_z adequately resolve the flow at $t = 50t_\eta$, at least 2×10^4 points are required to resolve the flow at $t = 10^6 t_\eta$. A grid of $10^5 \times 10^5$ points is used to resolve the (k_z, k_s) space throughout a calculation, which ensures that progressively larger number of points in k_z are available to resolve the flow as time advances.

A large memory was required to store such huge arrays of velocity and magnetic field spectral solutions. A parallel python script using MPI was developed to divide the spectral contours into many smaller chunks of data and distribute them to specified number of processors. This method enabled to resolve the spectra using large number of points. Once the velocity and magnetic field spectral solutions at a given time are obtained, the energy estimates and other diagnostics characterizing the wave–diffusion transition are computed.

Spectral contours and the concept of Joule cone

Fig. 3.3 shows the normalized velocity and induced magnetic field spectra at different times for Lundquist number $S_0 = 100$. The initial velocity spectrum (fig 3.3a) has weak anisotropy that arises purely from the choice of our initial condition (3.9), for which $k_{z0}/k_0 = 0.447$, k_{z0} and k_0 being the axial and resultant wavenumbers at $t = 0$. For $t \sim t_\eta$ the spectrum shows alternating patches of opposite sign along k_z (fig. 3.3b), which is indicative of wave motion in the z-direction. For the plot at $t = 10^3 t_\eta$ (fig 3.3c), the k_z-axis range is substantially reduced, which reveals the formation of a distinct conical section where all the energy is concentrated in the neighbourhood of the k_s-axis.

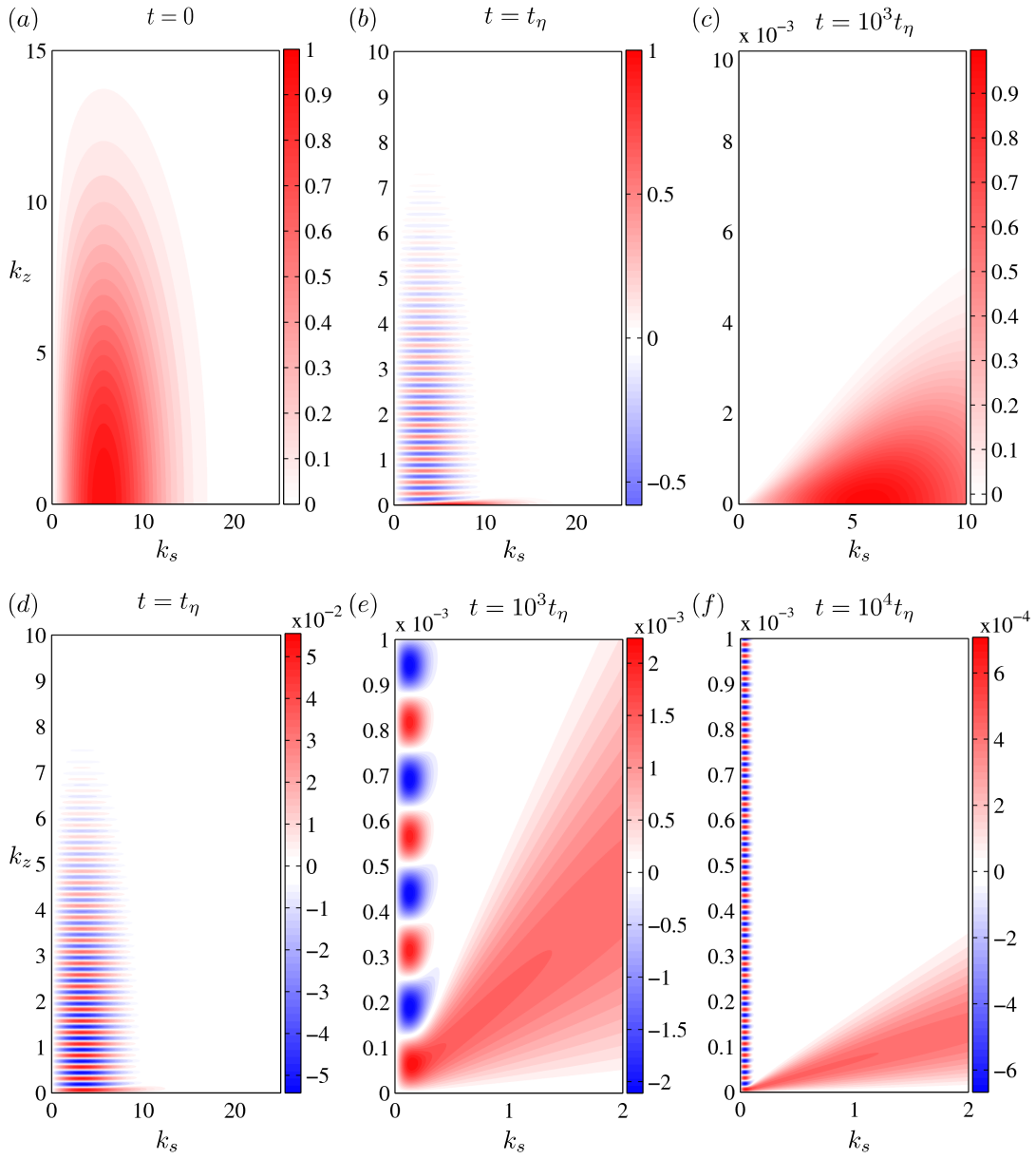

Fig. 3.3 Contour plots for $S_0 = 100$ at different times (in units of the magnetic diffusion time t_η) of the velocity spectrum $\hat{u}_\phi$ (*a-c*) and the induced magnetic field spectrum $\hat{b}_\phi$ (*d-f*), both normalized with respect to the initial velocity spectrum $\hat{u}_{\phi 0}$. Here k_s and k_z are the radial and axial wavenumbers.

The cone represents the energy distribution in the quasi-static (qs) regime in spectral space (Alemany et al., 1979). From equation (3.22) in the inviscid limit , $\hat{u}_{\phi,qs}$ can be written as

$$\hat{u}_{\phi,qs} = \hat{u}_{\phi 0}\, e^{-\cos^2\theta\,(t/\tau)}, \tag{3.42}$$

where $\cos\theta = k_z/k$ is the degree of anisotropy.

In the cone whose axis is aligned with k_z (fig. 3.4), region A contains the energy-containing modes and region B contains the modes that are damped by Ohmic dissipation. The half-angle of the cone θ widens with time owing to continual angular energy transfer from A to B, an effect that is visible in two snapshots of the magnetic field spectra shown on the same k_z axis range (figs. 3.3e and f). In the quasi-static regime, k_z/k is interpreted in physical space as the ratio of the lengthscales perpendicular and parallel to the mean magnetic field, $l_\perp/l_\parallel$, which has been shown to evolve as $(t/\tau)^{1/2}$ (Davidson, 1995; Sommeria and Moreau, 1982).

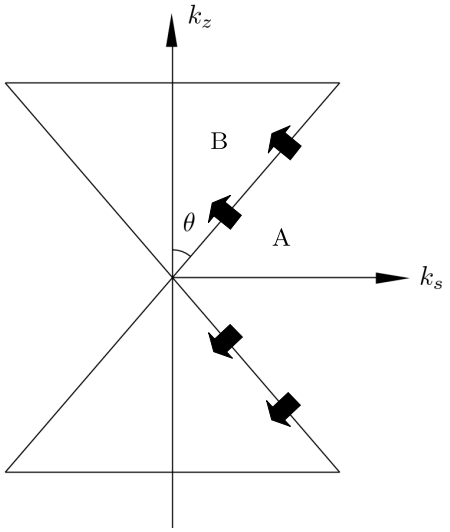

Fig. 3.4 Schematic representation of Joule cone showing the energy containing modes in region A and the Joule dissipation region B. The black arrows represent the angular energy transfer from region A to B.

A comparison of the velocity and induced magnetic field spectra for $S_0 = 100$ reveals that their wave–diffusion transitions do not coincide in time. At time $t = t_\eta$, $\hat{u}_\phi$ and $\hat{b}_\phi$

have similar structures indicating Alfvén waves (figs. 3.3b and d), although the magnitude of $\hat{b}_\phi$ is much smaller than that of $\hat{u}_\phi$. At $t = 10^3 t_\eta$, $\hat{u}_\phi$ has entered the purely diffusive quasi-static regime, as the signature of wave motion along the mean field direction has disappeared (fig. 3.3c). However, $\hat{b}_\phi$ shows thin alternating patches of opposite sign along k_z as well as a conical section (fig. 3.3e), indicative of a *mixed* wave-diffusion regime. At $t = 10^4 t_\eta$, wave motion is negligible whereas the energy containing region has narrowed considerably at the expense of the dissipative region (fig. 3.3f). These results indicate that the induced magnetic field supports wave motions at large times, when the velocity field undergoes pure diffusion.

Velocity and magnetic field contours

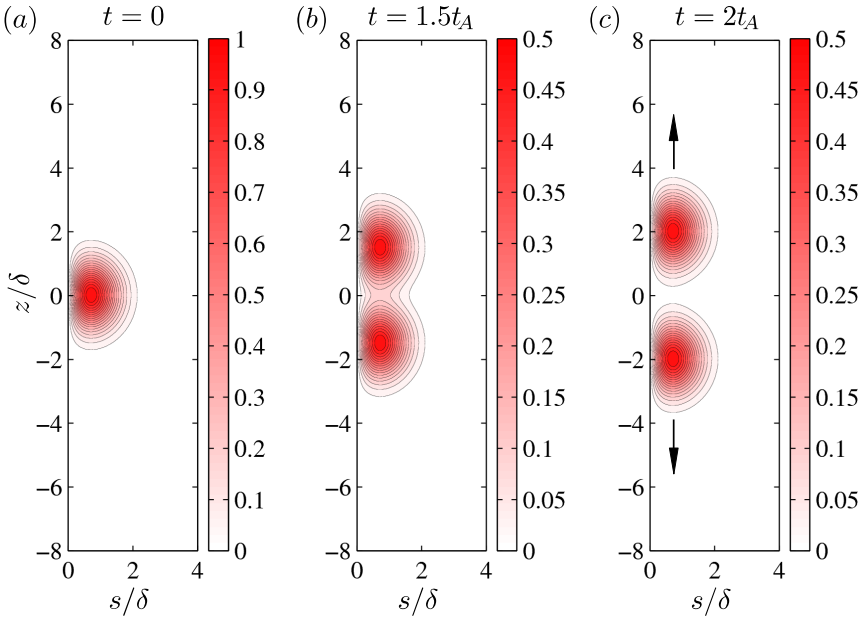

Fig. 3.5 The initial evolution of an isolated disturbance in a quiescent fluid subject to an axial (z) magnetic field for $S_0 = 2000$. The times shown are in units of the Alfvén wave travel time t_A with the velocities normalized with respect to initial maximum velocity (U_0).

The axisymmetric velocity u_ϕ and the induced magnetic field b_ϕ at different times are recovered from the general solutions for $\hat{u}_\phi$ (3.20) and $\hat{b}_\phi$ (3.21) via the inverse Hankel-

Fourier transform (3.13). Fig. 3.5 shows the initial evolution of the velocity perturbation for $S_0 = 2000$ with time in units of the Alfvén wave travel time $t_A = \delta/V_A$. As the blob splits in two, its peak velocity is halved, following which the wave packets propagate along the field lines in opposite directions.

Fig. 3.6 compares the evolution of the flow at two times with its quasi-static (*qs*) counterpart obtained by taking the inverse transform of the *qs* solution (3.22). The region $z \geq 0$ is shown in focus. In the full (wave) calculations shown in figs. 3.6(a) & (c) ($S_0 = 100$) and 3.6(e) & (g) ($S_0 = 10$), the location of the peak velocity at the wave front is $z/\delta = t/t_A$, so that $z = V_A t$. The diffusion strands that trail the wave front are weak for $S_0 = 100$, but comparable in strength to the wave front itself for $S_0 = 10$ (fig. 3.6e).

At $t = 80t_A$, the peak velocity appears to have shifted back to the origin from the wave front (fig. 3.6g), a process that will be investigated in section 3.5.2. For the *qs* calculations, the blob undergoes pure diffusion from the start, as understood from figs. 3.6 (b) & (d). The weak counterflow patch around the primary flow originates from the interaction of the closing electric current loops with the mean magnetic field (e.g. Davidson, 1995), an effect also observed in experiments of diffusive, low R_m MHD (Sreenivasan, 2003). This counterflow is also noted for the full calculation at the relatively low Lundquist number $S_0 = 10$ (fig. 3.6e,g), where diffusion is stronger than at $S_0 = 100$ for the same Alfvén times.

For the *qs* calculations given in fig. 3.6, the diffusion of the flow is much weaker at $S_0 = 10$ than at $S_0 = 100$ because the characteristic timescale in this regime is the Joule time $\tau = \eta/V_A^2$. Since the lengthscale parallel to the mean field direction evolves as $\sim (t/\tau)^{1/2}$ (e.g. Sommeria and Moreau, 1982), it is clear why the flow at $t = 100\tau$ ($S_0 = 10$) has diffused only a third of the distance diffused by the flow at $t = 1000\tau$ ($S_0 = 100$).

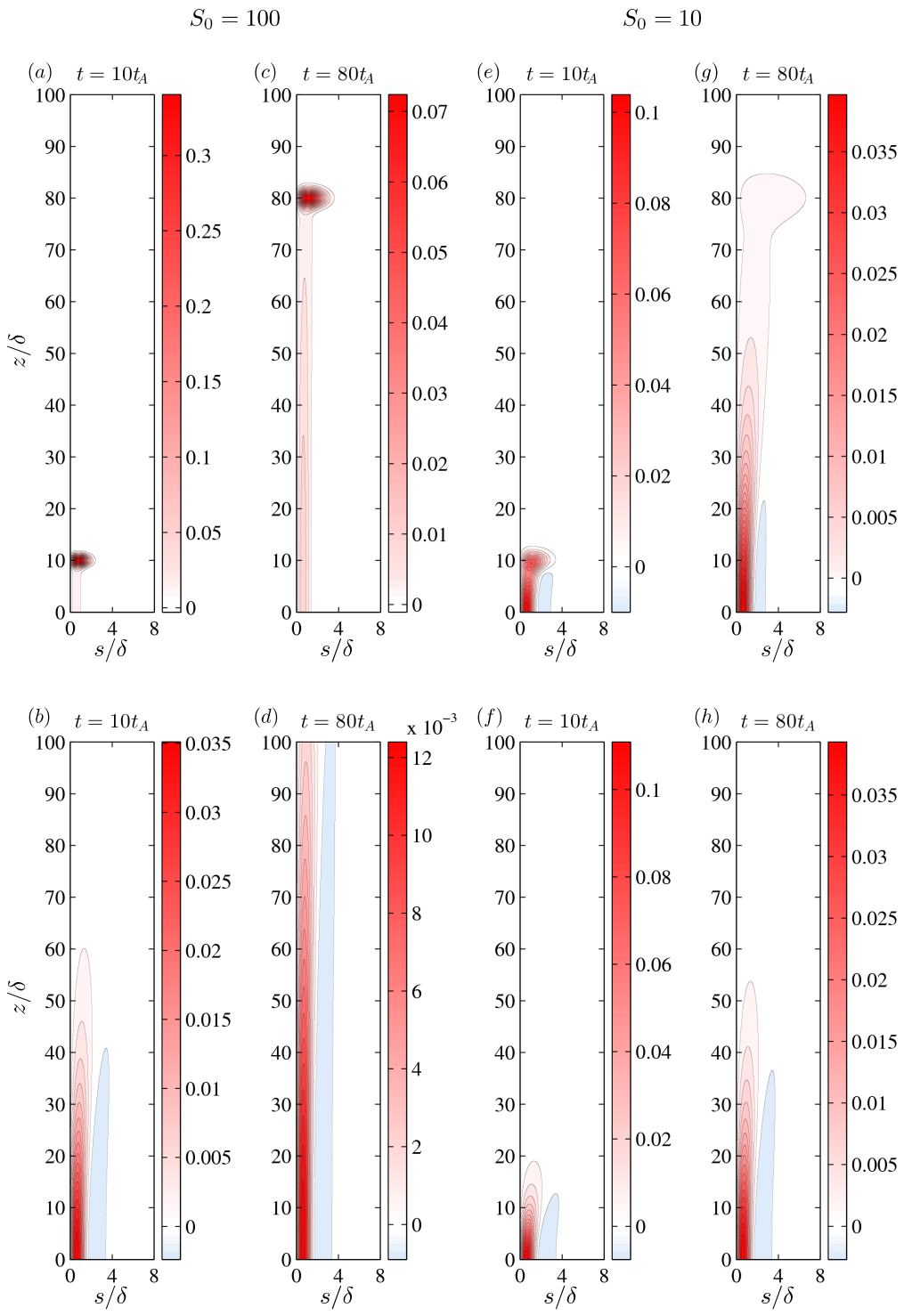

Fig. 3.6 Comparison of the evolution of an isolated blob in an axial magnetic field (upper panels) with the equivalent quasi-static (*qs*) evolution (lower panels). Two Lundquist numbers are investigated, $S_0 = 100$ and 10. The times shown are in units of the Alfvén wave travel time t_A. The respective times in units of the Joule time are $t = 1000\tau$ & $t = 8000\tau$ ($S_0 = 100$), and $t = 100\tau$ & $t = 800\tau$ ($S_0 = 10$). In units of the magnetic diffusion time, these times are $t = 0.1t_\eta$ & $t = 0.8t_\eta$ ($S_0 = 100$), and $t = t_\eta$ & $t = 8t_\eta$ ($S_0 = 10$).

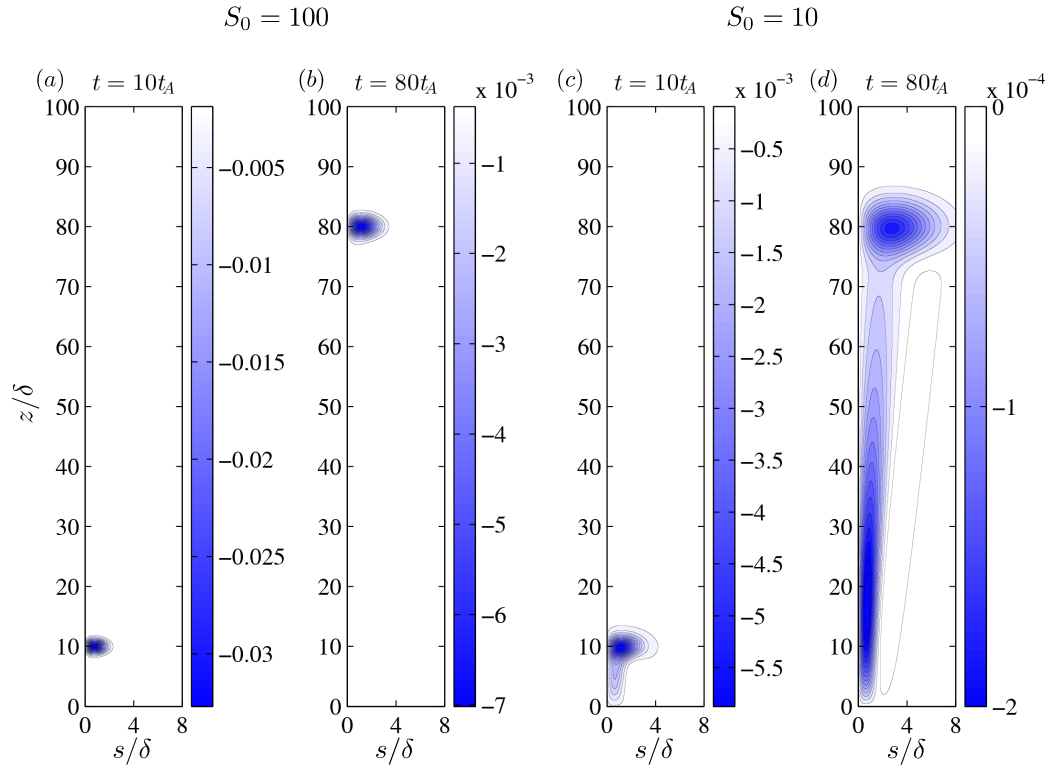

Fig. 3.7 Contour plots showing the evolution of the induced magnetic field b_ϕ for $S_0 = 100$ and 10. The times are in units of the Alfvén wave travel time t_A. The equivalent times in units of the Joule time τ and the magnetic diffusion time t_η are as given in fig. 3.6.

Fig. 3.7 shows the evolution in time of the induced magnetic field. As the sole component of this field b_ϕ is generated via $B_0\,\partial u_\phi/\partial z$, it is negatively signed for $z > 0$ and also antisymmetric about the mid-plane ($z = 0$). For $S_0 = 100$, the location of the wave fronts confirm that the waves propagate at the Alfvén speed. In contrast to the velocity u_ϕ at the same time, b_ϕ does not develop diffusion strands, implying that b_ϕ would cross over to the *qs* state much later than u_ϕ. (For $S_0 = 10$, however, diffusion makes its appearance within ~ 10 Alfvén times). Although plot (d) appears to touch the boundary, it is neither a physical nor a numerical boundary that affects the blob's evolution. This is because the contour is obtained from the inverse transform of magnetic field spectra. The delayed onset of diffusion for $\boldsymbol{b}$ is consistent with the predicted timescale for its transition to the *qs* state ($t \sim S_0 t_\eta$), which is much larger than that for $\boldsymbol{u}$ ($t \sim \sqrt{S_0}\,t_\eta$) if $S_0 \gg 1$.

From a comparison of the contour plots for $S_0 = 10$ at $t = 10t_A$ ($t = t_\eta$) and $t = 80t_A$ ($t = 8t_\eta$) in fig. 3.7, it is apparent that the decay of the wave front is essentially isotropic for times $t \gtrsim t_\eta$. This behaviour, notably absent for times $t \ll t_\eta$, is because the decay factor $e^{-\eta k^2 t}$ (see eq. 3.25) is independent of the angle θ between k_z and k. By contrast, the *qs* decay is strongly anisotropic because the decay factor is a function of θ.

3.5.2 Identification of the wave–diffusion transition

While the timescales for the wave–diffusion transition for the $\boldsymbol{u}$ and $\boldsymbol{b}$ perturbation fields are obtained from the approximate solutions for the kinetic and magnetic energies (Section 3.4), more precise transitions may be derived from the exact solutions. To this end, the frequency (λ), phase (c_p) and the group (c_g) velocities are computed. Frequency is computed from eq. (3.3). The phase and group velocities along the direction of magnetic field are:

$$c_p = \frac{\lambda_\pm}{k_z} = \pm\frac{1}{k_z}\left(\sqrt{V_A^2 k_z^2 - \frac{(\nu-\eta)^2 k^4}{4}}\right), \tag{3.43}$$

$$c_g = \frac{\partial \lambda_\pm}{\partial k_z} = \pm\frac{1}{\sqrt{X}}\left(V_A^2 k_z - \frac{(\nu-\eta)^2 k^2 k_z}{2}\right), \tag{3.44}$$

where $X = V_A^2 k_z^2 - \dfrac{(\nu-\eta)^2 k^4}{4}$. These equations use mean values of the wavenumbers k_z and k for the velocity and magnetic fields taken through the L^2 norm:

$$k_{z,\boldsymbol{f}} = \frac{\|k_z \hat{\boldsymbol{f}}\|}{\|\hat{\boldsymbol{f}}\|}, \;\; k_{\boldsymbol{f}} = \frac{\|k \hat{\boldsymbol{f}}\|}{\|\hat{\boldsymbol{f}}\|}, \tag{3.45}$$

where $\boldsymbol{f} = (\boldsymbol{u}, \boldsymbol{b})$.

Figs. 3.8 (a) & (b) compare the actual axial displacement of the $\boldsymbol{u}$ and $\boldsymbol{b}$ fields obtained by tracking their peak values with that computed from the group velocity c_g of the respective fields. The values agree very well until the point when c_p and c_g depart from each other (note that $c_p = c_g$ for undamped Alfvén waves). This transition time is different for the two fields, $\sim \sqrt{S_0}\, t_\eta$ for $\boldsymbol{u}$ and $\sim S_0 t_\eta$ for $\boldsymbol{b}$, indicating that the onset of magnetic diffusion is

delayed for $\boldsymbol{b}$. Interestingly, these times mark a spontaneous shift in the peak values of the fields to their starting points (fig. 3.8 c & d).

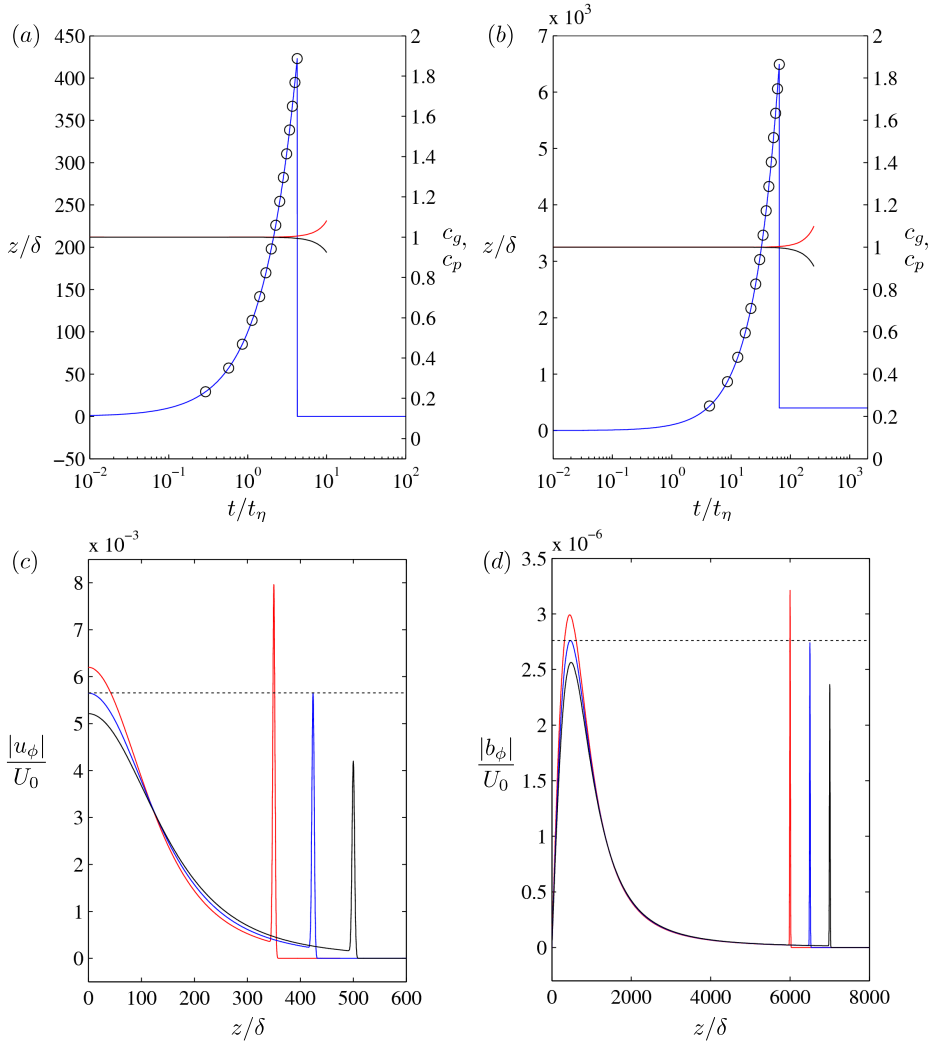

Fig. 3.8 (a) Location of the peak value of the velocity u_ϕ (blue line) compared with the product of the group velocity and time (black circles). The group velocity c_g (red line) and phase velocity c_p (black line) are normalized with respect to the Alfvén velocity. (b) Same plots and line styles as (a), but for the induced magnetic field b_ϕ. (c) u_ϕ as a function of z at times $t = 3.5t_\eta$ (red), $t = 4.24t_\eta$ (blue) and $t = 5t_\eta$ (black). (d) b_ϕ as a function of z at times $t = 60t_\eta$ (red), $t = 65t_\eta$ (blue) and $t = 70t_\eta$ (black). The Lundquist number $S_0 = 100$.

For $S_0 = 100$, the peak value of u_ϕ at $t = 3.5t_\eta$ is located within the propagating wave front. At $t = 4.24t_\eta$, u_ϕ at the wave front and the origin ($z = 0$) are exactly equal, whereas

at $t = 5t_\eta$, the maximum value of u_ϕ has shifted to $z = 0$. The peak value of b_ϕ shifts to $z = 0$ after $t = 65t_\eta$. The c_p and c_g of b_ϕ are equal till this time. After separating from each other, c_p and c_g eventually go to zero when the real part of the frequency vanishes, signifying complete cessation of wave motion.

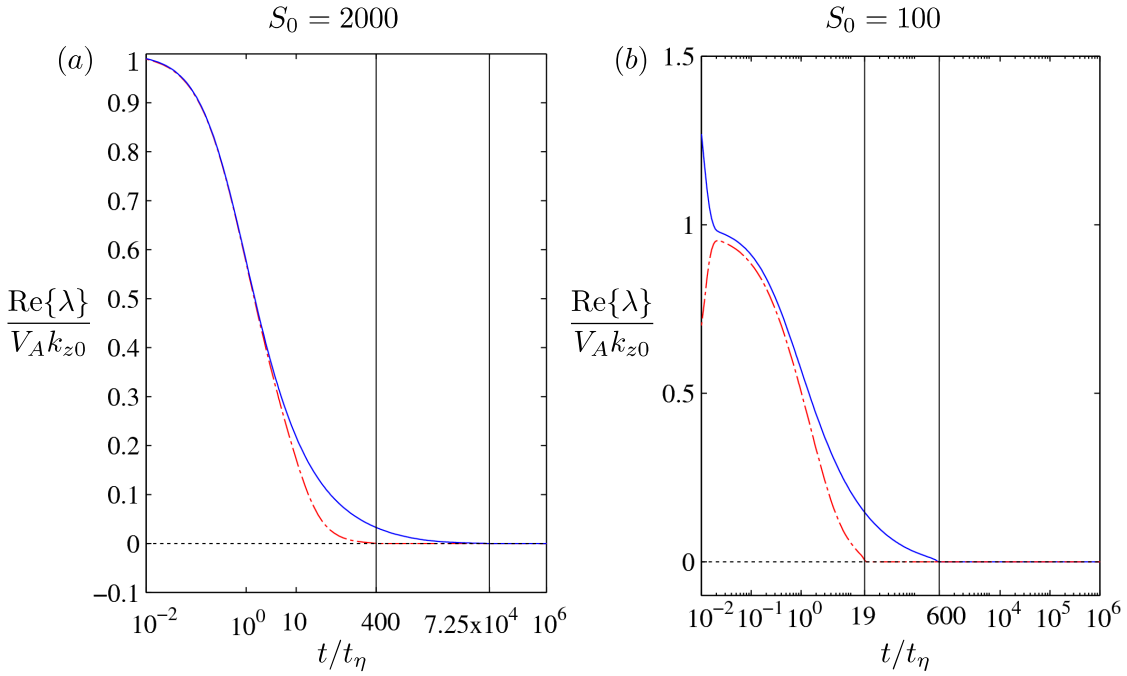

Fig. 3.9 Normalized real part of the frequency (λ) of the velocity field (red dashed line) and the induced magnetic field (blue line) for two Lundquist numbers. The vertical lines show the exact times at which $\mathrm{Re}\{\lambda\} = 0$.

Figure 3.9 shows $\mathrm{Re}\{\lambda\}$ normalized by the initial frequency $V_A k_{z0}$, calculated separately for $\boldsymbol{u}$ and $\boldsymbol{b}$ using their respective mean wavenumbers. For $S_0 = 2000$, oscillations in $\boldsymbol{u}$ cease at $t = 400t_\eta$, whereas oscillations in $\boldsymbol{b}$ cease at $t = 7.25 \times 10^4 t_\eta$. For $S_0 = 100$, the respective times are $t = 19t_\eta$ and $t = 600t_\eta$. The exact wave–diffusion transition times for $S_0 \gg 1$ can therefore be significantly larger than the transition timescales ($\sim \sqrt{S_0}\,t_\eta$ for $\boldsymbol{u}$ and $\sim S_0 t_\eta$ for $\boldsymbol{b}$) predicted by the approximate solutions. In the following section, the time at which $\mathrm{Re}\{\lambda\}$ goes to zero is used to interpret the transitions in the kinetic and magnetic energies.

3.5.3 Exact energies and their transitions

Energy transitions

Figures 3.10 and 3.11 present the exact kinetic and magnetic energies calculated in spectral space via eqs. (3.26) and (3.33) from the general solutions for velocity and magnetic fields, (eqs. 3.20 and 3.21). The upper limits of the k_z and k_s integrals are not infinity, but fixed by values that adequately resolve $\hat{\boldsymbol{u}}$ and $\hat{\boldsymbol{b}}$ (Section 3.5.1). The energies in the quasi-static approximation, calculated from the respective solutions for $\hat{\boldsymbol{u}}_{qs}$ and $\hat{\boldsymbol{b}}_{qs}$ (eqs. 3.22 and 3.23) provide the reference against which the actual energies can be compared.

For $S_0 = 2000$ (fig. 3.10a), E_k and E_m evolve in approximate equipartition in a damped wave phase as $\sim t^{-5/2}$ until time $t \sim 10t_\eta$. Subsequently, E_k enters its *qs* decay phase, $\sim t^{-1/2}$ whereas E_m continues to decay as $\sim t^{-5/2}$ until $t \approx 7.25 \times 10^4 t_\eta$ where it begins its *qs* phase. As P_m for this study is set to 10^{-6}, viscous diffusion is experienced at $t \sim 10^6 t_\eta$ because of which the *qs* phase of E_m is short. For $S_0 = 100$ (fig. 3.10b), the $\sim t^{-5/2}$ wave phase of E_k is too short to be visible, but the $\sim t^{-1/2}$ *qs* phase begins at $t \approx 19t_\eta$ and lasts for several decades in time until viscous diffusion takes over. For E_m, however, there is a $\sim t^{-5/2}$ damped wave phase until $t \approx 600t_\eta$, after which a well-defined $\sim t^{-3/2}$ *qs* phase exists for a few decades in time. The *qs*-transition times for E_k and E_m agree closely with the times at which the real part of the frequency for the $\boldsymbol{u}$ and $\boldsymbol{b}$ fields goes to zero (marked by the two vertical lines). For $S_0 = 10$ (figs 3.11a), the $\sim t^{-5/2}$ damped wave phase is nearly absent, but the *qs* phases $E_k \sim t^{-1/2}$ and $E_m \sim t^{-3/2}$ span several decades. The *qs*-transition times, $t = 1.6t_\eta$ for E_k and $t = 20.5t_\eta$ for E_m, agree closely with the respective frequency transition times for the two fields. For the lowest Lundquist number $S_0 = 1$ (figs 3.11b), E_k and E_m are far from equipartition even at the start, and the evolution is entirely in the *qs* phase. Table 1 gives the energy ratios $E_k/E_{k,qs}$ and $E_m/E_{m,qs}$ at different times, including the *qs*-transition times predicted by approximate theory and the times when the real part of the frequencies λ_u and λ_b go to zero.

Table 3.1 **Energies, frequencies and their *qs* transition timescales**.

S_0	t/t_η	$E_k/E_{k,qs}$	$E_m/E_{m,qs}$	$\mathrm{Re}\{\lambda_u\}/\{V_A k_{z0}\}$	$\mathrm{Re}\{\lambda_b\}/\{V_A k_{z0}\}$
	0.2	1.927	2.749	0.602	0.843
	0.25	1.890	3.244	0.575	0.791
	0.6	1.612	5.012	0.374	0.626
	1	1.376	5.084	0.224	0.521
10	1.3	1.295	5.065	0.128	0.468
	1.6	1.240	4.581	0	0.427
	3.16^*	1.098	3.818	0	0.311
	$10^\dagger$	1.013	2.086	0	0.132
	20.5	1.004	1.510	0	0
	0.025	7.857	2.243	0.951	0.975
	0.4	8.603	35.792	0.701	0.739
	1	4.450	41.951	0.506	0.570
	4	1.479	23.536	0.182	0.325
100	8	1.136	13.362	0.078	0.232
	10^*	1.088	11.078	0.056	0.207
	19	1.026	7.133	0	0.147
	$100^\dagger$	1.001	2.126	0	0.051
	600	1.000	1.186	0	0
	0.0025	53.237	1.576	0.996	0.998
	0.4	156.275	751.305	0.743	0.745
	1.5	40.05	745.238	0.494	0.510
	11	2.383	181.835	0.159	0.208
2000	25	1.302	90.800	0.066	0.139
	44.72^*	1.101	49.707	0.030	0.093
	400	1.001	6.710	0	0.033
	$2000^\dagger$	1.000	2.212	0	0.012
	7.25×10^4	1.000	1.0025	0	0

Table 3.1 Evolution in time (measured in units of magnetic diffusion time t_η) of energies and frequencies for an isolated blob given by the initial condition (3.9). Here S_0 is the initial Lundquist number, E_k and E_m are the kinetic and magnetic energies, λ_u and λ_b are the frequencies of the velocity and magnetic fields, V_A is the Alfvén velocity, k_{z0} is the z-wavenumber at time $t = 0$ and the subscript *qs* represents the quasi-static regime. The superscript symbols $*$ and † denote the timescales $\sqrt{S_0}t_\eta$ and $S_0 t_\eta$ at which the velocity and the magnetic field reach their *qs* values.

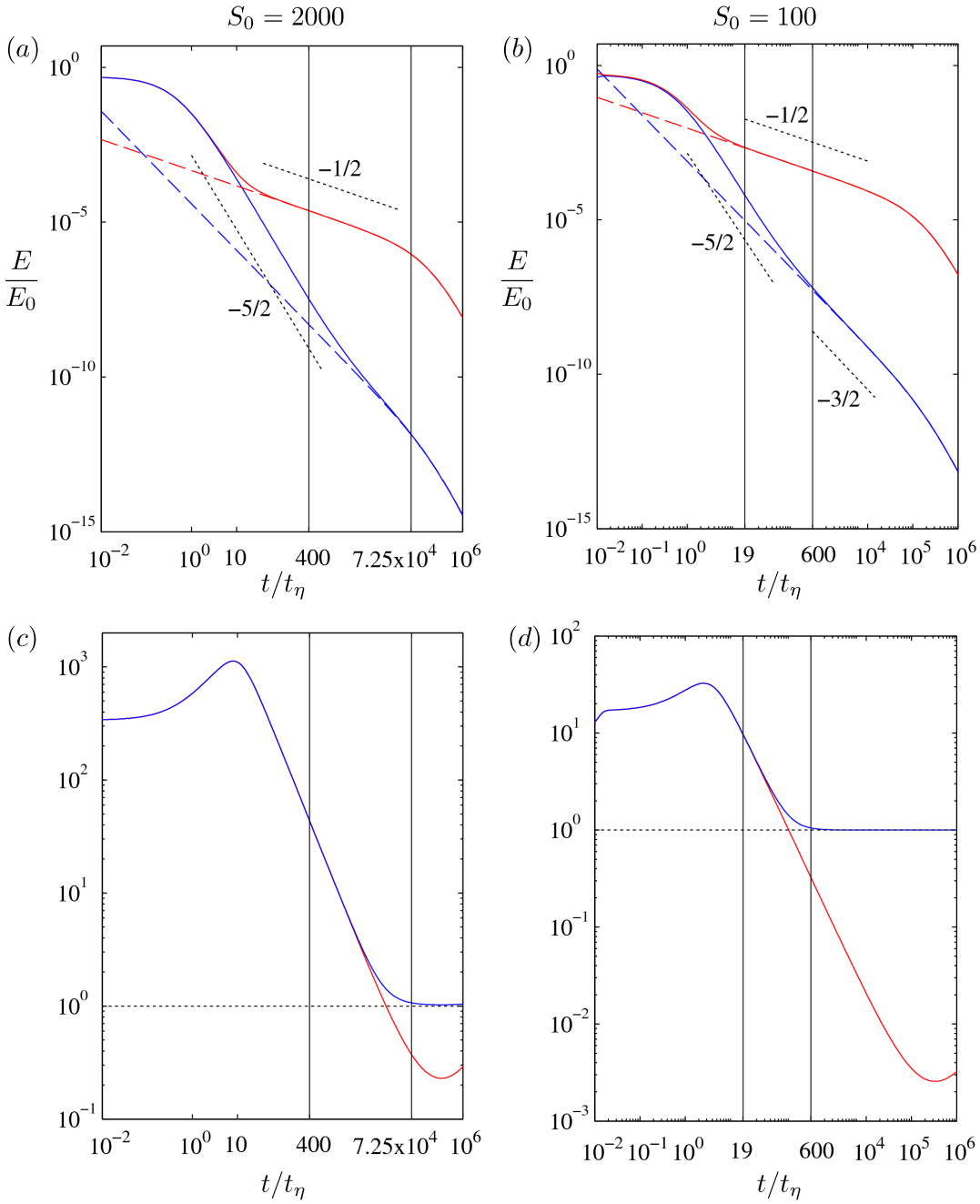

Fig. 3.10 (a) & (b): Kinetic (red line) and magnetic (blue line) energies normalized by the initial kinetic energy (E_0) plotted versus magnetic diffusion time. The quasi-static (qs) kinetic (dashed red line) and magnetic (dashed blue line) are given as the reference states. (c) & (d): Ratios of terms in the induction equation in spectral space, $(\partial\hat{\boldsymbol{b}}/\partial t)$ to $\eta k^2\hat{\boldsymbol{b}}$ (red line) and $B_0 ik_z\hat{\boldsymbol{u}}$ to $\eta k^2\hat{\boldsymbol{b}}$ (blue line). The vertical lines in the figures represent the times at which the real part of the frequency (λ) of $\boldsymbol{u}$ and $\boldsymbol{b}$ go to zero.

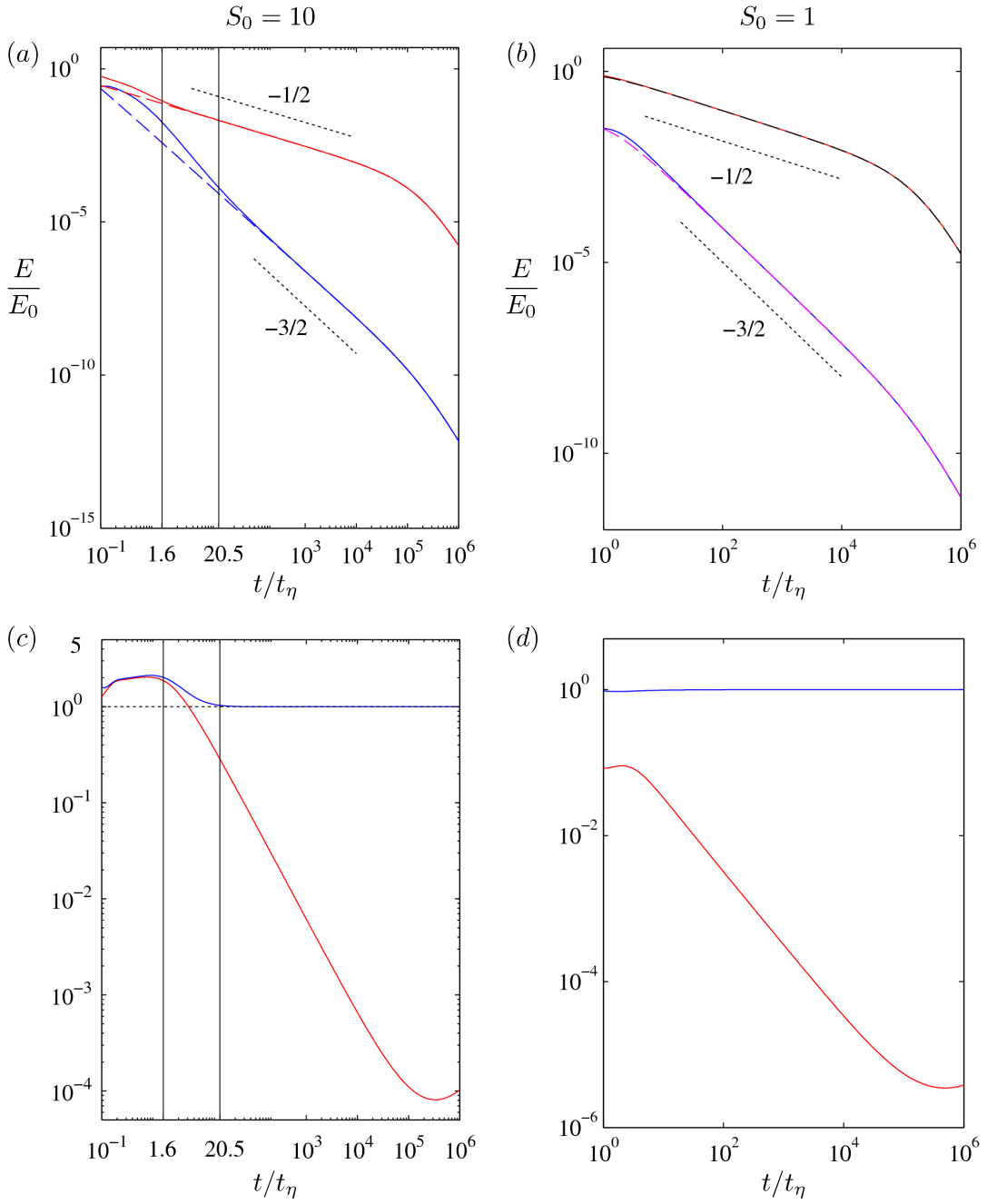

Fig. 3.11 (a) & (b): Kinetic (red line) and magnetic (blue line) energies normalized by the initial kinetic energy (E_0) plotted versus magnetic diffusion time. The quasi-static (qs) kinetic (dashed red line) and magnetic (dashed blue line) are given as the reference states. (c) & (d): Ratios of $(\partial\hat{\boldsymbol{b}}/\partial t)$ to $\eta k^2\hat{\boldsymbol{b}}$ (red line) and $B_0 ik_z\hat{\boldsymbol{u}}$ to $\eta k^2\hat{\boldsymbol{b}}$ (blue line). The vertical lines in the figures represent the times at which the real part of the frequency (λ) of $\boldsymbol{u}$ and $\boldsymbol{b}$ go to zero.

Transition of induction equation terms

The transitions in the energies are compared with the transitions in the ratio of terms in the induction equation:

$$\frac{\|\partial\hat{\boldsymbol{b}}/\partial t\|}{\|\eta k^2\hat{\boldsymbol{b}}\|},\quad \frac{\|B_0 ik_z\hat{\boldsymbol{u}}\|}{\|\eta k^2\hat{\boldsymbol{b}}\|}, \tag{3.46}$$

the magnitude of each term being evaluated by the L^2 norm. For $S_0 = 2000$ (fig. 3.10c), the two ratios closely follow each other indicating wave dominance, and at $t = 7.25\times10^4 t_\eta$ when the magnetic field enters its *qs* phase, the ratio of convection to diffusion terms tends to unity. Lower Lundquist numbers show the same trend (fig. 3.10d & fig. 3.11c), confirming that the system attains the *qs* regime only by the induced magnetic field reaching its *qs* value. For $S_0 = 1$, the convection and diffusion terms are approximately equal from the start so that $\partial\boldsymbol{b}/\partial t$ is small (fig. 3.11d). As the velocity perturbation reaches its *qs* value much earlier than the magnetic field, small-scale flows of $R_m \sim 1$ would not survive when the system attains its *qs* state.

Exact vs approximate energy estimates

Fig. 3.12 shows the comparison between the exact energies at $S_0 = 2000$ and the approximate solutions obtained for the damped wave and *qs* regimes:

$$\begin{aligned} E_m = E_k &\approx \frac{\pi^{3/2}\delta^5}{64}\left(\frac{t}{t_\eta}\right)^{-5/2}, \\ E_{k,qs} &\approx \frac{3\pi^2\delta^5}{64}\left(\frac{t}{\tau}\right)^{-1/2}, \\ E_{m,qs} &\approx \frac{\pi^2\delta^5}{256}S_0^2\left(\frac{t}{\tau}\right)^{-3/2}. \end{aligned}$$

The agreement between the approximate and exact solutions is very good in the two regimes, although if S_0 does not significantly exceed unity the damped wave regime itself would be too short or non-existent.

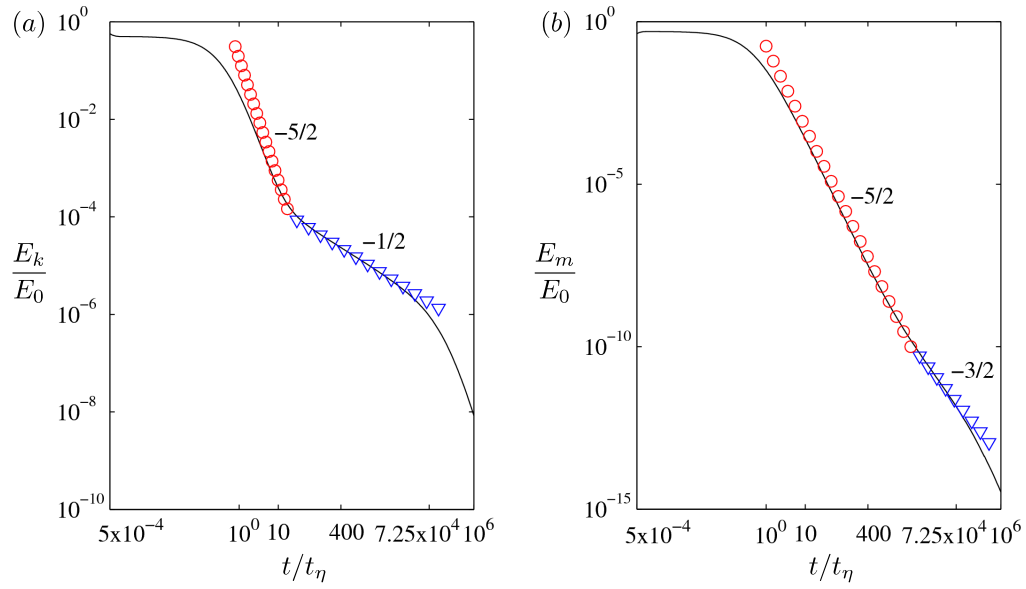

Fig. 3.12 Comparison of the exact kinetic energy E_k and magnetic energy E_m (black lines) with the approximate solutions (marker symbols). The damped wave regime is shown in red circles and the *qs* regime is shown in blue triangles. The Lundquist number $S_0 = 2000$.

3.5.4 Joule dissipation

In the limit of small magnetic Prandtl number, the rate of change of total energy of the system equals the Ohmic dissipation:

$$\frac{\partial E}{\partial t} = -\frac{1}{\mu\rho}\int j^2 dV, \tag{3.47}$$

where j is the induced electric current density, which in low-frequency MHD is related to the induced magnetic field via Ampère's law:

$$\boldsymbol{j} = \frac{1}{\mu}\nabla\times\boldsymbol{b}. \tag{3.48}$$

However, in the *qs* limit, the curl of Ohms's law gives

$$\nabla\times\boldsymbol{j} = \frac{1}{\mu\eta}(\boldsymbol{B}\cdot\nabla)\boldsymbol{u},$$

from which j is estimated by (Davidson, 1995)

$$j_{qs} \sim \frac{1}{\mu\eta} B_0 u \frac{l_\perp}{l_\parallel}, \tag{3.49}$$

where $l_\perp$ and $l_\parallel$ are the flow lengthscales perpendicular and parallel to the mean magnetic field lines. The qs estimate of Ohmic dissipation is therefore

$$\frac{\partial E}{\partial t} \sim -\frac{E}{\tau}\left(\frac{l_\perp}{l_\parallel}\right)^2. \tag{3.50}$$

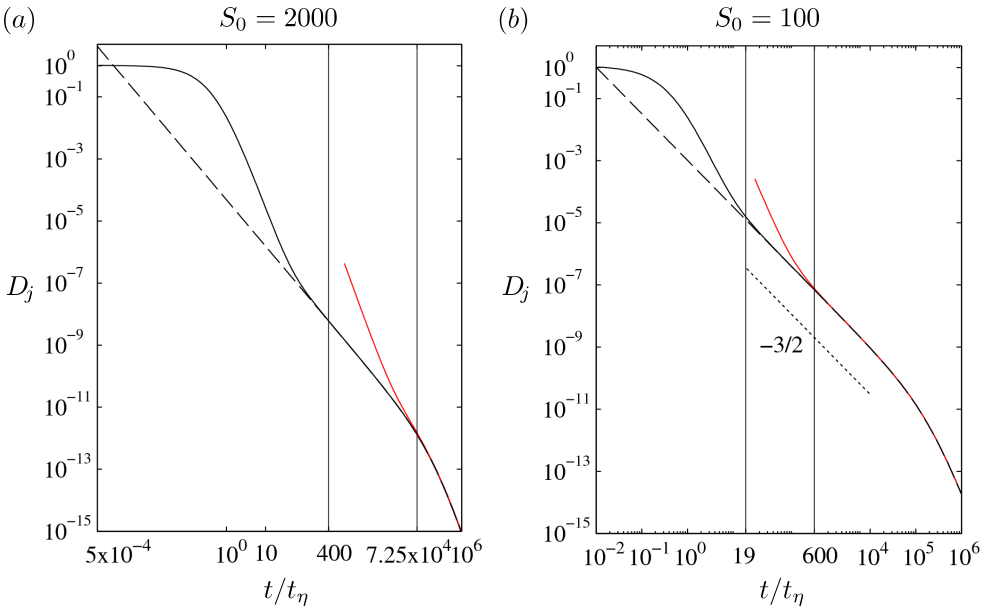

Fig. 3.13 Line plots of Joule dissipation (D_j) plotted as a function of number of magnetic diffusion times for (a) $S_0 = 2000$ (b) $S_0 = 100$. Black curve represents the actual joule dissipation without qs approximation. Dashed black curve is the qs Joule dissipation. Red curve represents the Joule dissipation estimate from Ohm's law. Both the plots (a,b) are normalized with respect to the D_j value at one Alfvén travel time. Vertical lines in both the plots mark the corresponding frequency transition time.

Fig. 3.13 gives the exact integral value of the Ohmic dissipation D_j calculated from the general solution (3.21) and the qs solution (3.23), shown in solid and dashed black lines respectively. As the qs kinetic energy decays as $t^{-1/2}$, the qs dissipation decays as $t^{-3/2}$.

For the estimate (3.50) shown in red lines, the lengthscale ratio $l_\perp/l_\parallel$ is approximated by k_z/k. For both $S_0 = 2000$ and $S_0 = 100$, it is evident that the inverse relation between the lengthscale and the wavenumber holds only when the frequency of the induced field $\hat{\boldsymbol{b}}$ goes to zero; that is, when the system is entirely in the *qs* regime. The solid and dashed black lines in fig. 3.13 do not coincide before the *qs* onset of $\boldsymbol{u}$, which shows that low R_m flows that support wave motion in the core must dissipate obeying Ampère's law rather than the quasi-static Ohm's law.

3.5.5 Anisotropy, true Lundquist number and the role of nonlinear inertia

The anisotropy of fields $\boldsymbol{u}$ and $\boldsymbol{b}$, measured by the ratio of the respective wavenumbers k_z/k, is obtained from (3.45) and shown in fig. 3.14. The relatively high Lundquist numbers $S_0 = 2000$ and $S_0 = 100$ (fig. 3.14 a & b) show the flow anisotropy evolving as $t^{-3/2}$ for many decades in magnetic diffusion time until the frequency of the induced field $\boldsymbol{b}$ goes to zero (which is when the convection and diffusion terms in the induction equation balance). At this point, k_z/k changes course and assumes the well-known *qs* scaling of the anisotropy, $t^{-1/2}$. (The anisotropy for the purely *qs* calculations is shown in dashed lines). It is notable that the $t^{-3/2}$ scaling for k_z/k persists long after the kinetic energy has switched over to the $t^{-1/2}$ decay phase (see fig. 3.10 a & b). The magnetic field anisotropy scales as t^{-1}, but at high S_0 does not reach its *qs* scaling before viscous diffusion takes over. As S_0 is decreased (fig. 3.14 c & d), the *qs* phase broadens at the expense of the damped wave phase. For $S_0 = 10$, the $t^{-3/2}$ phase of the velocity anisotropy has all but disappeared, whereas the t^{-1} phase of the magnetic field anisotropy is brief. For $S_0 = 1$, the anisotropy approximately follows the $t^{-1/2}$ *qs* scaling for both fields.

The evolution of the *true* Lundquist number S_t, defined in eq. (3.5), may be understood from the anisotropy of $\boldsymbol{u}$. The time variation of S_t/S_0 (fig. 3.15a) shows a steep $t^{-3/2}$ decrease consistent with the decrease of k_z/k (fig. 3.15), followed by a self-similar $t^{-1/2}$

range where the characteristic timescale is the Joule time τ. The entry to the self-similar range coincides with the entry of the induced field $\boldsymbol{b}$ to the *qs* phase, which is also when the convection and diffusion terms in the induction equation balance (fig. 3.10). Since the interaction parameter N_0 is related to the Lundquist number S_0 by $N_0 = S_0^2/R_m$, the *true* interaction parameter is given by

$$N_t = \frac{4}{\tau k u}\left(\frac{k_z}{k}\right)^2. \tag{3.51}$$

The evolution of N_t for small-scale flows with the initial conditions $S_0 \gg 1$ and $R_m \sim 1$ provides some insight into the role of inertia in such flows (fig. 3.15b). The decrease of N_t from its high ($\sim S_0^2$) value at $t \sim t_\eta$ to a low (~ 1) value at $t \sim S_0 t_\eta$ is due to the decrease in the magnitude of the Lorentz force, which in turn is caused by the fall in electric current density $\boldsymbol{j}$ as the flow develops anisotropy. (The electric current must flow through longer paths in z as diffusion strands develop. This also explains the fall in Ohmic dissipation in the damped wave regimes of fig. 3.13). The value of N_t merges with its *qs* value (shown in dashed lines in fig. 3.15b) when the induced field $\boldsymbol{b}$ crosses over to its *qs* value. It was noted earlier that the ratio of convection to diffusion terms in the induction equation becomes unity at this time. As this time is passed, the inverse relation between the wavenumber and lengthscale holds, and therefore $N_t \sim N_e(l_\perp/l_\parallel)^2$, where N_e is the the ratio of the instantaneous eddy turn-over time to the Joule time. The above estimate of N_t is essentially the ratio of the Lorentz to nonlinear inertial forces in the equation of motion (Sreenivasan and Alboussière, 2000, 2002). For the cases considered in fig. 3.15(b), N_t is of order unity when it merges with its *qs* value.

The particular case of $S_0 = 58$ and $R_m = 2.5$ in figure 3.15(b) applies to blobs of transverse lengthscale ≈ 5 km subject to a mean field of 1.3 mT (see section 3.6). Here the nonlinear inertial force becomes comparable to the Lorentz force at $t \sim 10^2 t_\eta$, which comes long after the wave phase of $\boldsymbol{u}$ has expired ($t \sim 10 t_\eta$). Therefore, nonlinear inertia is not likely to

affect the dynamics of these scales in the period that they travel across the core as Alfvén waves.

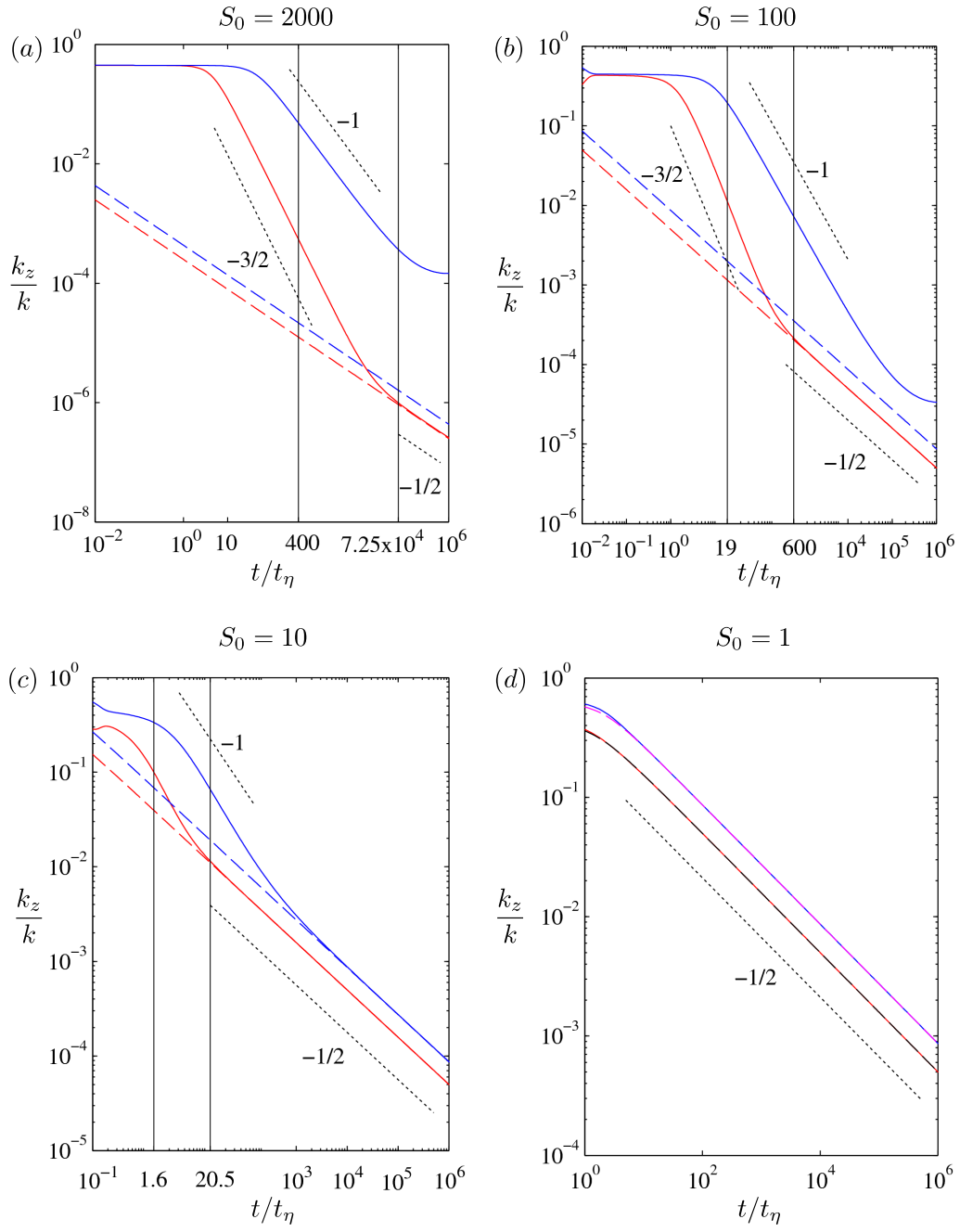

Fig. 3.14 Anisotropy (k_z/k) of the velocity field (red line) and the induced magnetic field (blue line) for four Lundquist numbers: 2000,100,10 and 1. The respective quasi-static (*qs*) values are shown in dashed red and dashed blue lines. The vertical lines in the figures represent the times at which the real part of the frequency (λ) of $\boldsymbol{u}$ and $\boldsymbol{b}$ go to zero.

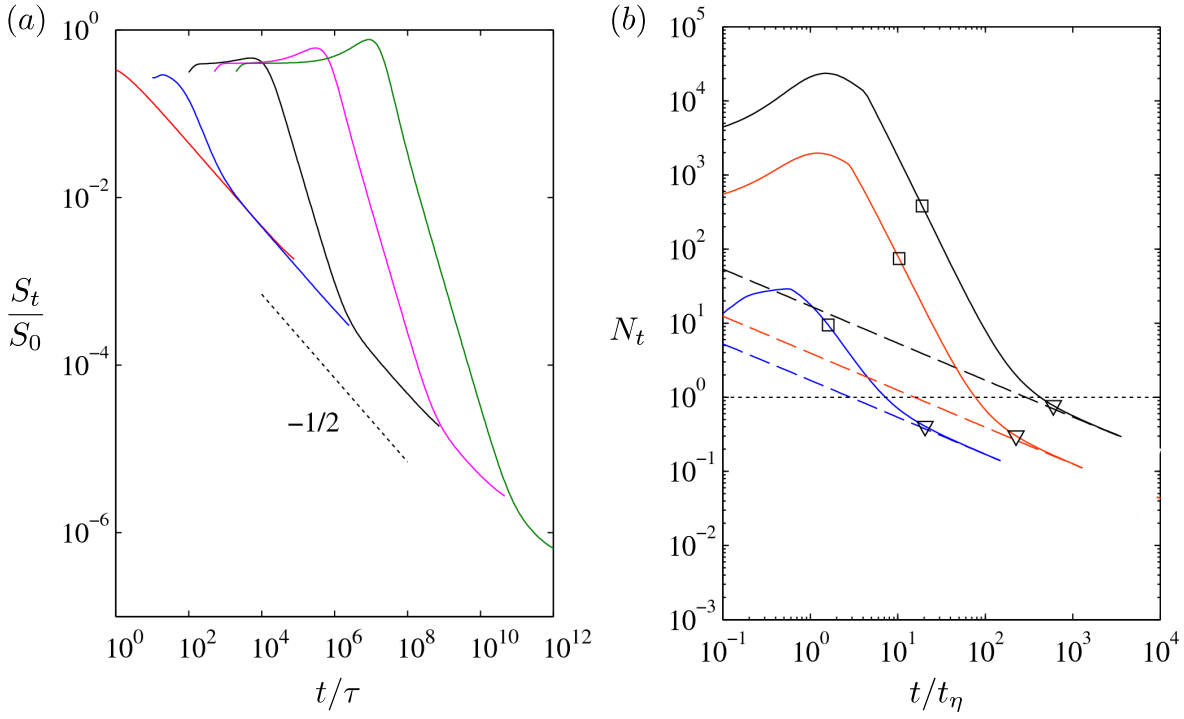

Fig. 3.15 (a) Evolution of the *true* Lundquist number S_t (normalized by S_0) in time measured in units of the Joule time τ. The cases presented are $S_0 = 1$ (red), $S_0 = 10$ (blue), $S_0 = 100$ (black), $S_0 = 500$ (magneta), $S_0 = 2000$ (green). (b) Evolution of the *true* interaction parameter N_t defined by eq.(3.51) in time measured in units of the diffusion time t_η. Three cases are presented: $S_0 = 10$, $R_m = 1$ (blue), $S_0 = 100$, $R_m = 1$ (black) and $S_0 = 58$, $R_m = 2.5$ (red). The dashed lines represent the quasi-static (*qs*) solutions of N_t for the same parameters. The square symbols give the wave–diffusion transition times of the velocity perturbation (when $\mathrm{Re}\{\lambda_u\} = 0$) and the triangular symbols give the transition times of the induced magnetic field (when $\mathrm{Re}\{\lambda_b\} = 0$).

3.6 Small-scale Alfvén waves in the core

Small-scale convective motions arising from rapid rotation of the fluid core perturb the radial magnetic field near the inner core boundary (ICB), setting off Alfvén waves. The survival time of these waves is determined by the timescale for onset of the purely diffusive *qs* phase, which has been a point of investigation in this chapter. Because the fluid velocity

in the *qs* phase is lower than the initial velocity by several orders of magnitude, any transfer of momentum across the core must take place via waves rather than by diffusion. To obtain the smallest lengthscale of convection that can support oscillations as far as the core–mantle boundary (CMB), it must be ascertained whether the timescale for the damping of Alfvén waves at that scale is sufficiently longer than the core travel time of the waves. It is also essential to know whether the perturbations that propagate as waves are approximately two-dimensional in the sense that they form tall columns aligned with the rotation axis along which the velocity variation is small.

Although the radial magnetic field in the outer core is not uniform, it is possible to constrain the mean field strength from the observed period of geostrophic oscillations (Gillet et al., 2010). For example, a mean radial field strength $B_s = 1.3$ mT corresponds to a core travel time of 6 years. Table 2 presents a comparative study of Alfvén wave propagation under three field strengths that correspond to core travel times of 4, 6 and 20 years. For each case, blob lengthscales in the range $\delta = 2$–10 km are considered. These lengthscales have R_m in the range 1–5, taking a root mean square (rms) core velocity $u = 5 \times 10^{-4}$ ms^{-1} (Starchenko and Jones, 2002) and magnetic diffusivity $\eta = 1$ m^2 s^{-1}. Since the Lundquist number S_0 for these lengthscales does not exceed $\sim 10^2$ (taking density $\rho = 10^4$ kg m^{-3}), the exact *qs*-phase cross-over times of $\boldsymbol{u}$ and $\boldsymbol{b}$ are of the same order of magnitude as the respective timescales $t \sim \sqrt{S_0}\, t_\eta$ and $t \sim S_0\, t_\eta$ (see table 3.2); hence these timescales are presented for each δ. As the problem addressed here is whether the waves generated at small scales can transport momentum across the outer core, the *qs*-phase cross-over time of $\boldsymbol{u}$ is of primary concern. Waves excited at lengthscale $\delta = 2$ km are magnetically damped on a timescale much shorter than core travel times of 4–6 years, whereas waves excited at $\delta = 5$ km can survive till they reach the CMB (table 3.2). Of course, waves at larger δ can comfortably reach the CMB with progressively lesser loss of energy. At smaller field strength ($B_s = 0.4$ mT) the waves would require a larger lengthscale $\delta > 10$ km to survive damping.

Fig. 3.16 shows a schematic of progressive stages of evolution of an ensemble of small-scale velocity perturbations in the core. For times $t_\eta < t < \sqrt{S_0}\,t_\eta$, a horizontal ($z$) section of the flow presents a picture consisting of dominant (high-energy) wave packets trailed by relatively weak diffusion strands (compare this picture with figs. 3.6 a & c). The question of whether the perturbations originating near the ICB form columns aligned with z is addressed by estimating the ratio of the inertial wave timescale to the Alfvén wave timescale (Lehnert, 1954a)

$$Le = \frac{V_A}{2\Omega\,\delta}. \tag{3.52}$$

Although the Lehnert number Le is $\sim 10^{-4}$ for flow perturbations of the size of the inner core (Jault, 2008), here we examine the values of Le for much smaller lengthscales δ that correspond to $R_m \sim 1$ (table 3.2). For isolated flow structures of $\delta = 5$ km subject to fields $B_s = 1.3-2$ mT, $Le \sim 10^{-2}$, indicating that three-dimensional perturbations near the ICB can form Taylor columns before they propagate radially outward. Furthermore, it is noted from nonlinear dynamo simulations that B_s near the ICB is much weaker than in the flow interior (fig. 3.17a); therefore the Alfvén velocity V_A near the ICB is lower than its mean core value (also see fig. 3 in Teed et al., 2015) and as a consequence Le is also lower than the value given in table 3.2. (By contrast, fig. 3.17b shows that the azimuthal magnetic field can be strong near the ICB, promoting slow Magneto-Coriolis waves). The essential idea that comes from this discussion is that velocity perturbations near the ICB need not be of the lengthscale of the inner core for the Lehnert number to be small. The propagating wave packets shown in fig. 3.16 may be seen as z-sections of thin cylinders on which the magnetostrophic balance holds, whereas the weak diffusion strands trailing these waves are plate-like structures on $\boldsymbol{B}$–$\boldsymbol{\Omega}$ planes.

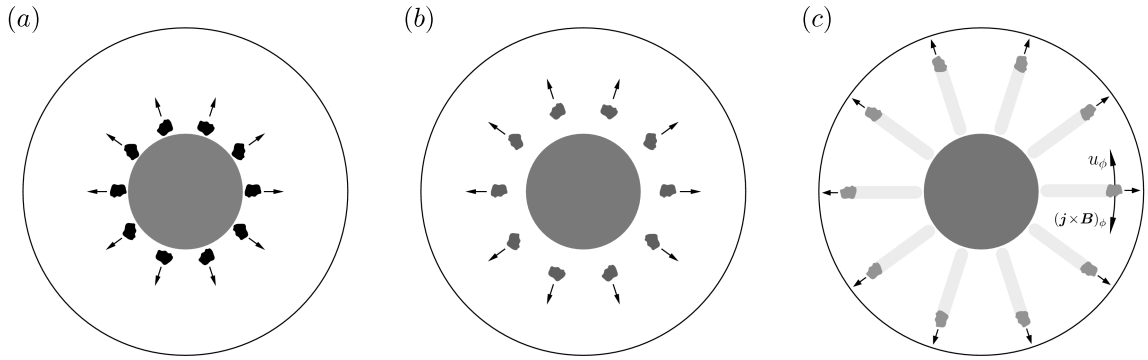

Fig. 3.16 Small-scale velocity perturbations originating near the inner core boundary propagate as diffused Alfvén waves across the outer core.

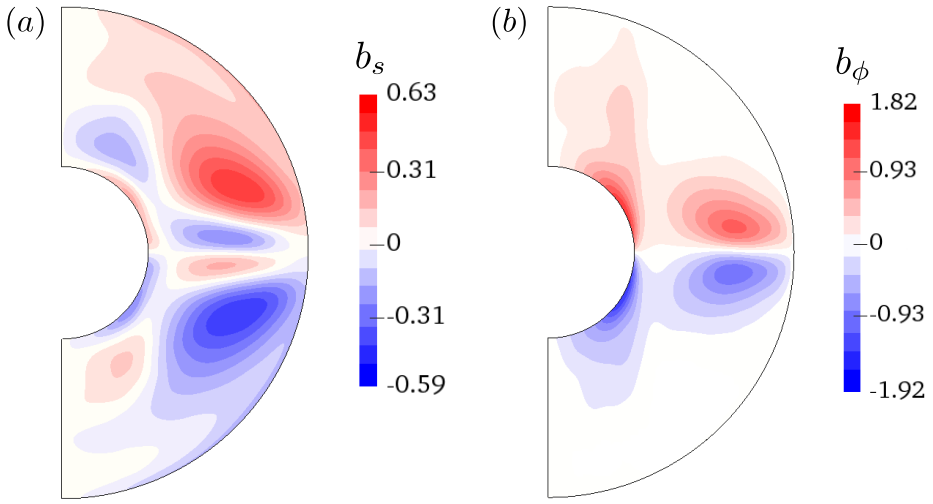

Fig. 3.17 Azimuthally averaged meridional section plots of (a) the radial magnetic field B_s and (b) azimuthal magnetic field B_ϕ from a nonlinear spherical shell dynamo simulation with the following parameters: Ekman number $E = \nu/2\Omega L^2 = 5\times10^{-6}$ (here L is the shell thickness), Prandtl number $Pr = 1$, magnetic Prandtl number $P_m = 3$, Rayleigh number $Ra = 3.3\times$ the critical value for non-magnetic convection. No-slip conditions are satisfied at both boundaries, the inner boundary is electrically conducting and the outer boundary is electrically insulating. Convection is driven by an imposed temperature difference across the fluid layer.

Table 3.2 **Wave–diffusion transition timescales for Earth-like parameters**

B_0(mT)	Le	δ(km)	R_m	Ek	S_0	$\sqrt{S_0}t_\eta$(yrs)	$S_0 t_\eta$(yrs)
	0.080	1	0.5	6.88×10^{-9}	11.60	0.11	0.37
	0.040	2	1	1.72×10^{-9}	23.20	0.61	3
1.3	0.016	5	2.5	2.75×10^{-10}	57.98	6	46
	0.010	8	4	1.07×10^{-10}	92.77	20	188
	0.008	10	5	6.88×10^{-11}	116	34	368
	0.123	1	0.5	6.88×10^{-9}	17.84	0.13	0.57
	0.061	2	1	1.72×10^{-9}	35.68	0.78	4.50
2	0.025	5	2.5	2.75×10^{-10}	89.21	7.50	71
	0.015	8	4	1.07×10^{-10}	143	24	290
	0.012	10	5	6.88×10^{-11}	178.41	42	566

Table 3.2 Earth-like regimes for 1.3 mT and 2 mT radial field strength are tabulated. The non-dimensional parameters and *qs* diffusion timescales for lengthscales between 1-10 km are shown. The core travel time (t_{IC}) for all the lengthscales for 1.3 mT and 2 mT field strength is 6 years and 4 years respectively.

3.7 Summary

Small-scale flows of magnetic Reynolds number $R_m \sim 1$ propagate as damped Alfvén waves if the ratio of the wave frequency to the diffusion frequency is greater than unity throughout the travel period. For core travel times of 4–6 years, the mean radial field strength is in the range 1.3–2 mT, which in turn gives Lundquist numbers $S_0 \sim 100$ that allow strong wave motions for flows of lengthscale ≈ 5 km or larger. An interesting aspect of damped waves at $S_0 \gg 1$ is that the velocity perturbation $\boldsymbol{u}$ and the induced magnetic field $\boldsymbol{b}$ cross over to the purely diffusive *qs* phase at different timescales, $\sqrt{S_0}t_\eta$ and $S_0 t_\eta$

respectively. The *qs*-transition timescale of $\boldsymbol{u}$ helps constrain the smallest lengthscale that would support Alfvén waves in the core. As background rotation does not affect the damping of Alfvén waves, the Coriolis force is not present in the equation of motion. Nevertheless, it is apparent from this study that the inertial wave timescale is sufficiently shorter than the Alfvén wave timescale so that three-dimensional structures near the ICB are rapidly elongated into columns before their radial propagation.

The importance of small scales in the dynamics of the core is not easily understood from nonlinear dynamo simulations because viscous and nonlinear inertial forces may be present in the force balance at small scales. The simplified model of an isolated blob in a mean magnetic field has the advantage that viscous effects can be kept small by the choice of a low, Earth-like magnetic Prandtl number. Furthermore, for Lundquist numbers $S_0 \sim 100$, the nonlinear inertial force is very small compared to the Lorentz force (and by extension, the Coriolis force) on the core travel timescale of Alfvén waves. Therefore, it is likely that these waves are generated from small-scale convection columns that exist in an approximate magnetostrophic balance.

Chapter 4

Evolution of small-scale motions in the presence of magnetic field and rotation

The previous chapter studied the effect of a uniform axial magnetic field on an isolated small-scale perturbation in an electrically conducting fluid. In an Earth-like planet with strong core convection, small-scale vortices are influenced by both the magnetic field and rotation. While it is anticipated that the strong rotation of the core gives rise to Taylor columns aligned with the rotation axis (Busse, 1970) via inertial wave propagation (Davidson et al., 2006), the addition of the magnetic field brings effects which have been studied only at asymptotically large times where magnetic diffusion controls the dynamics. The occurrence of damped Magneto-Coriolis (MC) waves and their diffusion timescales have not received attention. This chapter addresses the problem of the evolution of a localized small-scale perturbation under rotation and a uniform axial magnetic field. Solutions are derived for both fast and slow MC waves, their relative strengths being determined by the relative magnitudes of the rotation rate and the magnetic field intensity (measured by the Lehnert number *Le*). As with the non-rotating case presented in the previous chapter, the rotating MHD flow also experiences a transition from a wave-dominated phase to the diffusion-

dominated quasi-static (qs) phase due to finite magnetic diffusivity. The wave–diffusion cross-over timescales are derived for the same initial conditions as considered in Chapter 3.

The parameter regime of magnetic Reynolds number $R_m \ll 1$, magnetic interaction parameter $N_0 \gg 1$ and Rossby number $Ro \ll 1$ is considered. The governing momentum and magnetic induction equations are

$$\frac{\partial \boldsymbol{u}}{\partial t} = -\frac{\nabla p'}{\rho} + \frac{\boldsymbol{j}\times\boldsymbol{B}}{\rho} - 2\boldsymbol{\Omega}\times\boldsymbol{u} + \nu\nabla^2\boldsymbol{u}, \tag{4.1}$$

$$\frac{\partial \boldsymbol{b}}{\partial t} = \nabla\times(\boldsymbol{u}\times\boldsymbol{B}) + \eta\nabla^2\boldsymbol{b}, \tag{4.2}$$

where $p' = p - \frac{\rho}{2}|\boldsymbol{\Omega}\times\boldsymbol{x})|^2$. Equation (4.1) and (4.2) can be rewritten as

$$\frac{\partial \boldsymbol{u}}{\partial t} = -\frac{\nabla p^*}{\rho} + \frac{(\boldsymbol{B}.\nabla)\boldsymbol{b}}{\mu\rho} - 2\boldsymbol{\Omega}\times\boldsymbol{u} + \nu\nabla^2\boldsymbol{u}, \tag{4.3}$$

$$\frac{\partial \boldsymbol{b}}{\partial t} = (\boldsymbol{B}.\nabla)\boldsymbol{u} + \eta\nabla^2\boldsymbol{b}, \tag{4.4}$$

where $p^* = p - \frac{\rho}{2}|\boldsymbol{\Omega}\times\boldsymbol{x}|^2 + \frac{\boldsymbol{b}^2}{2\mu}$.

In the following section the dispersion relation for the damped MC wave is derived.

4.1 Dispersion relation for damped MC waves

Taking the curl of equations (4.3) and (4.4) gives

$$\frac{\partial \boldsymbol{\omega}}{\partial t} = \frac{(\boldsymbol{B}\cdot\nabla)\boldsymbol{j}}{\rho} + 2(\boldsymbol{\Omega}\cdot\nabla)\boldsymbol{u} + \nu\nabla^2\boldsymbol{\omega}, \tag{4.5}$$

$$\frac{\partial \boldsymbol{j}}{\partial t} = \frac{(\boldsymbol{B}\cdot\nabla)\boldsymbol{\omega}}{\mu} + \eta\nabla^2\boldsymbol{j}. \tag{4.6}$$

Eliminating $\boldsymbol{j}$ from (4.5) using (4.6) gives

$$\left[\left(\frac{\partial}{\partial t} - \nu\nabla^2\right)\left(\frac{\partial}{\partial t} - \eta\nabla^2\right) - \frac{(\boldsymbol{B}\cdot\nabla)^2}{\mu\rho}\right]\boldsymbol{\omega} = 2(\boldsymbol{\Omega}\cdot\nabla)\left(\frac{\partial}{\partial t} - \eta\nabla^2\right)\boldsymbol{u}. \tag{4.7}$$

Substituting $\nu = \eta = 0$ in (4.7) gives the undamped form of the characteristic equation (Acheson and Hide, 1973). Since $\nabla \times \boldsymbol{\omega} = -\nabla^2 \boldsymbol{u}$, the curl of equation (4.7) gives

$$\left[\left(\frac{\partial}{\partial t} - \nu\nabla^2\right)\left(\frac{\partial}{\partial t} - \eta\nabla^2\right) - \frac{(\boldsymbol{B}\cdot\nabla)^2}{\mu\rho}\right]\nabla^2\boldsymbol{u} = -2(\boldsymbol{\Omega}\cdot\nabla)\left(\frac{\partial}{\partial t} - \eta\nabla^2\right)\boldsymbol{\omega}. \tag{4.8}$$

Eliminating $\boldsymbol{\omega}$ from equation (4.8) using (4.7) gives

$$\left[\left(\frac{\partial}{\partial t} - \nu\nabla^2\right)\left(\frac{\partial}{\partial t} - \eta\nabla^2\right) - \frac{(\boldsymbol{B}\cdot\nabla)^2}{\mu\rho}\right]^2\nabla^2\boldsymbol{u} = -4(\boldsymbol{\Omega}\cdot\nabla)^2\left(\frac{\partial}{\partial t} - \eta\nabla^2\right)^2\boldsymbol{u}. \tag{4.9}$$

Equation (4.9) represents a wave equation for the velocity field $\boldsymbol{u}$. Now, the forward Hankel-Fourier transform of equation (4.9) gives

$$\left[\left(\frac{\partial}{\partial t} + \nu k^2\right)\left(\frac{\partial}{\partial t} + \eta k^2\right) + V_A^2 k_z^2\right]^2 \hat{\boldsymbol{u}} = -\frac{4\Omega^2 k_z^2}{k^2}\left(\frac{\partial}{\partial t} + \eta k^2\right)^2 \hat{\boldsymbol{u}}, \tag{4.10}$$

where $V_A = B_0/\sqrt{\mu\rho}$ is the Alfvén wave velocity. Now, considering $\hat{\boldsymbol{u}} \sim e^{i\lambda t}$, equation (4.10) becomes

$$\left[\left(i\lambda + \nu k^2\right)\left(i\lambda + \eta k^2\right) + V_A^2 k_z^2\right]^2 = -\frac{4\Omega^2 k_z^2}{k^2}\left(i\lambda + \eta k^2\right)^2.$$

This equation simplifies to

$$\left(i\lambda + \nu k^2\right)\left(i\lambda + \eta k^2\right) + V_A^2 k_z^2 = \pm i\left[\frac{2\Omega k_z}{k}\left(i\lambda + \eta k^2\right)\right].$$

Solving for λ, the following dispersion relation is obtained.

$$\lambda = \pm\frac{\Omega k_z}{k} + \frac{i(\nu+\eta)k^2}{2} \pm \sqrt{V_A^2 k_z^2 + \left(\frac{\Omega k_z}{k} \pm \frac{ik^2(\nu-\eta)}{2}\right)^2}, \tag{4.11}$$

which can be written as

$$\lambda = \pm\frac{1}{2}\left[\frac{2\Omega k_z}{k} + i(\nu+\eta)k^2 \pm \sqrt{4V_A^2 k_z^2 + \left(\frac{2\Omega k_z}{k} \pm ik^2(\nu-\eta)\right)^2}\right].$$

This expression for λ consists of four fundamental inverse timescales. These are inertial frequency $(2\Omega k_z/k)$, Alfvén frequency $(V_A k_z)$, inverse of magnetic diffusion (ηk^2) and

viscous diffusion (νk^2) timescales. Based on the relative magnitude of these fundamental frequencies, different regimes which are either dominated by wave propagation or diffusion are possible.

The four modes from the dispersion relation (4.11) are:

$$\lambda_1 = \frac{\Omega k_z}{k} + \frac{i(\nu+\eta)k^2}{2} + \sqrt{V_A^2 k_z^2 + \left(\frac{\Omega k_z}{k} + \frac{ik^2(\nu-\eta)}{2}\right)^2},$$
$$\lambda_2 = \frac{\Omega k_z}{k} + \frac{i(\nu+\eta)k^2}{2} - \sqrt{V_A^2 k_z^2 + \left(\frac{\Omega k_z}{k} + \frac{ik^2(\nu-\eta)}{2}\right)^2},$$
$$\lambda_3 = -\frac{\Omega k_z}{k} + \frac{i(\nu+\eta)k^2}{2} + \sqrt{V_A^2 k_z^2 + \left(\frac{\Omega k_z}{k} - \frac{ik^2(\nu-\eta)}{2}\right)^2},$$
$$\lambda_4 = -\frac{\Omega k_z}{k} + \frac{i(\nu+\eta)k^2}{2} - \sqrt{V_A^2 k_z^2 + \left(\frac{\Omega k_z}{k} - \frac{ik^2(\nu-\eta)}{2}\right)^2}.$$

In the limit of $\nu = \eta = 0$, $\lambda_1 - \lambda_4$ reduce to

$$\begin{aligned}\lambda_1 &= \frac{\Omega k_z}{k} + \sqrt{V_A^2 k_z^2 + \left(\frac{\Omega k_z}{k}\right)^2},\ \lambda_2 = \frac{\Omega k_z}{k} - \sqrt{V_A^2 k_z^2 + \left(\frac{\Omega k_z}{k}\right)^2},\\ \lambda_3 &= -\frac{\Omega k_z}{k} + \sqrt{V_A^2 k_z^2 + \left(\frac{\Omega k_z}{k}\right)^2},\ \lambda_4 = -\frac{\Omega k_z}{k} - \sqrt{V_A^2 k_z^2 + \left(\frac{\Omega k_z}{k}\right)^2}.\end{aligned} \tag{4.12}$$

In a strongly rotating system, the inertial and Alfvén frequencies satisfy $\Omega k_z/k \gg V_A k_z$. A Taylor series expansion of the modes in (4.12) in the limit of $V_A k/\Omega \ll 1$ gives

$$\lambda_{1,4} = \pm\frac{2\Omega k_z}{k}\left(1 + \frac{V_A^2 k^2}{4\Omega^2}\right),\ \ \lambda_{3,2} \ \ = \pm\frac{V_A^2 k_z k}{2\Omega}. \tag{4.13}$$

Here $\lambda_{1,4}$ represent fast inertial waves weakly modified by the magnetic field and $\lambda_{2,3}$ represent slow magnetostrophic waves (Acheson and Hide, 1973; Lehnert, 1954a; Moffatt, 1978). For simplicity, these waves are henceforth called fast and slow Magneto-Coriolis (MC) waves.

In the weakly rotating regime $V_A k_z \gg \Omega k_z/k$, the Taylor series expansion of the frequencies (4.12) in the limit of $\Omega/(V_A k) \ll 1$ gives

$$\lambda_{1,4} \approx \pm\left(V_A k_z + \frac{\Omega k_z}{k}\right), \;\; \lambda_{3,2} \approx \pm\left(V_A k_z - \frac{\Omega k_z}{k}\right). \tag{4.14}$$

Since $V_A k_z \gg \Omega k_z/k$, the waves given by (4.14) propagate as Aflvén waves weakly modified by rotation.

4.2 Quasi-static dispersion relation

In the *qs* limit $(\partial \boldsymbol{b}/\partial t) = 0$, following a similar procedure as in section 4.1, the *qs* dispersion relation is

$$\lambda = \lambda_{qs} = \pm\frac{2\Omega k_z}{k} + i\left(\frac{V_A^2 k_z^2}{\eta k^2} + \nu k^2\right). \tag{4.15}$$

Comparing the λ_{qs} relation (4.15) with the non-rotating case (3.4), it is evident that the inertial frequency $(2\Omega k_z/k)$ additionally contributes to the *qs* dispersion relation. This suggests that the *qs* phase in presence of rotation and magnetic field constitutes propagation of damped inertial waves. Let these *qs* modes be denoted as

$$\lambda_{1,2} = \pm\frac{2\Omega k_z}{k} + i\left(\frac{k_z^2}{\tau k^2} + \nu k^2\right). \tag{4.16}$$

In the following section, the approximate form of frequencies in strongly and weakly rotating regimes are derived.

4.3 Approximate form of frequencies with damping

In this section, the approximate form of the frequencies $(\lambda_1 - \lambda_4)$ are obtained in the limit of zero viscosity but with finite magnetic diffusivity. The regimes considered are:

1. Strongly rotating regime:

   1.a) Wave-dominated phase: $\quad \dfrac{\Omega k_z}{k} \gg V_A k_z \gg \dfrac{\eta k^2}{2}$

1.b) Diffusion-dominated phase: $\frac{\eta k^2}{2} \gg \frac{\Omega k_z}{k} \gg V_A k_z$

2. Weakly rotating regime:

2.a) Wave-dominated phase: $V_A k_z \gg \frac{\Omega k_z}{k} \gg \frac{\eta k^2}{2}$

2.b) Diffusion-dominated phase: $\frac{\eta k^2}{2} \gg V_A k_z \gg \frac{\Omega k_z}{k}$

These frequencies in different regimes are obtained in order to find the approximate solutions of velocity and magnetic field in those regimes which are discussed in later sections.

4.3.1 Strongly rotating, wave-dominated regime

$\lambda_{1,4}$ modes

The λ_1 frequency

$$\lambda_1 = \frac{\Omega k_z}{k} + i\frac{\eta k^2}{2} + \sqrt{V_A^2 k_z^2 + \left(\frac{\Omega k_z}{k} - i\frac{\eta k^2}{2}\right)^2},$$

is considered. Since inertial frequency is dominant, λ_1 can be written as

$$\lambda_1 = \frac{\Omega k_z}{k} + i\frac{\eta k^2}{2} + \frac{\Omega k_z}{k}\sqrt{\left(\frac{V_A k}{\Omega}\right)^2 + \left(1 - i\frac{\eta k^3}{2\Omega k_z}\right)^2},$$

$$\lambda_1 = \frac{\Omega k_z}{k} + i\frac{\eta k^2}{2} + \frac{\Omega k_z}{k}\sqrt{\left(\frac{V_A k}{\Omega}\right)^2 + 1 - \left(\frac{\eta k^3}{2\Omega k_z}\right)^2 - i\frac{\eta k^3}{\Omega k_z}}.$$

Since $\frac{\eta k^3}{2\Omega k_z} \ll \frac{V_A k}{\Omega} \ll 1$, λ_1 approximately becomes

$$\lambda_1 \approx \frac{\Omega k_z}{k} + i\frac{\eta k^2}{2} + \frac{\Omega k_z}{k}\sqrt{1 + \left(\frac{V_A k}{\Omega}\right)^2 - i\frac{\eta k^3}{\Omega k_z}}. \tag{4.17}$$

Using Taylor series expansion, (4.17) becomes

$$\lambda_1 \approx \frac{2\Omega k_z}{k} + i\frac{\eta V_A^2 k^4}{4\Omega^2}. \tag{4.18}$$

The algebraic steps involved in obtaining (4.18) are shown in the Appendix D.1.1.

Similarly, λ_4 mode simplifies to

$$\lambda_4 \approx -\frac{2\Omega k_z}{k} + i\frac{\eta V_A^2 k^4}{4\Omega^2}. \tag{4.19}$$

$\lambda_{2,3}$ modes

The λ_3 frequency

$$\lambda_3 = -\frac{\Omega k_z}{k} + i\frac{\eta k^2}{2} + \sqrt{V_A^2 k_z^2 + \left(\frac{\Omega k_z}{k} + i\frac{\eta k^2}{2}\right)^2},$$

is considered. In the strongly rotating regime, this frequency can be written as

$$\begin{aligned}\lambda_3 &= -\frac{\Omega k_z}{k} + i\frac{\eta k^2}{2} + \frac{\Omega k_z}{k}\sqrt{\left(\frac{V_A k}{\Omega}\right)^2 + \left(1 + i\frac{\eta k^3}{2\Omega k_z}\right)^2}, \\ &= -\frac{\Omega k_z}{k} + i\frac{\eta k^2}{2} + \frac{\Omega k_z}{k}\sqrt{\left(\frac{V_A k}{\Omega}\right)^2 + 1 - \left(\frac{\eta k^3}{2\Omega k_z}\right)^2 + i\frac{\eta k^3}{\Omega k_z}}.\end{aligned}$$

Since $\frac{\eta k^3}{2\Omega k_z} \ll \frac{V_A k}{\Omega} \ll 1$, λ_3 becomes

$$\lambda_3 \approx -\frac{\Omega k_z}{k} + i\frac{\eta k^2}{2} + \frac{\Omega k_z}{k}\sqrt{1 + \left(\frac{V_A k}{\Omega}\right)^2 + i\frac{\eta k^3}{\Omega k_z}}. \tag{4.20}$$

Using Taylor series expansion, (4.20) becomes

$$\lambda_3 \approx \frac{V_A^2 k_z k}{2\Omega} + i\eta k^2. \tag{4.21}$$

The algebraic steps involved in obtaining (4.20) are shown in Appendix D.1.1. Using a similar approach, the λ_2 mode becomes

$$\lambda_2 \approx -\frac{V_A^2 k_z k}{2\Omega} + i\eta k^2. \tag{4.22}$$

From (4.18),(4.19),(4.21),(4.22), the frequencies $\lambda_1 - \lambda_4$ in the strongly rotating, wave-dominated regime are:

$$\lambda_{1,4} \approx \pm\frac{2\Omega k_z}{k} + i\frac{\eta V_A^2 k^4}{4\Omega^2}, \quad \lambda_{3,2} \approx \pm\frac{V_A^2 k_z k}{2\Omega} + i\eta k^2. \tag{4.23}$$

4.3.2 Strongly rotating, diffusion-dominated regime

Using the inequality $\frac{\eta k^2}{2} \gg \frac{\Omega k_z}{k} \gg V_A k_z$, the approximate form of $\lambda_1 - \lambda_4$ are obtained.

$\lambda_{1,4}$ modes

The λ_1 frequency

$$\lambda_1 = \frac{\Omega k_z}{k} + i\frac{\eta k^2}{2} + \sqrt{V_A^2 k_z^2 + \left(\frac{\Omega k_z}{k} - i\frac{\eta k^2}{2}\right)^2},$$

is considered. Since $\eta k^2/2$ is the dominant frequency, λ_1 can be written as

$$\lambda_1 = \frac{\Omega k_z}{k} + i\frac{\eta k^2}{2} + \frac{\eta k^2}{2}\sqrt{\left(\frac{2V_A k_z}{\eta k^2}\right)^2 + \left(\frac{2\Omega k_z}{\eta k^3} - i\right)^2}. \tag{4.24}$$

Using Taylor series expansion, (4.24) becomes

$$\lambda_1 \approx \frac{2\Omega k_z}{k} + i\frac{k_z^2}{\tau k^2}. \tag{4.25}$$

The algebraic steps involved in obtaining (4.25) are shown in Appendix D.1.2. Similarly, the frequency λ_4 takes the following form

$$\lambda_4 \approx -\frac{2\Omega k_z}{k} + i\frac{k_z^2}{\tau k^2}. \tag{4.26}$$

$\lambda_{2,3}$ modes

The λ_3 frequency

$$\lambda_3 = -\frac{\Omega k_z}{k} + i\frac{\eta k^2}{2} + \sqrt{V_A^2 k_z^2 + \left(\frac{\Omega k_z}{k} + i\frac{\eta k^2}{2}\right)^2},$$

is considered. Since $\eta k^2/2$ is the dominant frequency, λ_3 can be written as

$$\lambda_3 = -\frac{\Omega k_z}{k} + i\frac{\eta k^2}{2} + \frac{\eta k^2}{2}\sqrt{\left(\frac{2V_A k_z}{\eta k^2}\right)^2 + \left(\frac{2\Omega k_z}{\eta k^3} + i\right)^2}. \tag{4.27}$$

Using Taylor series expansion, (4.27) becomes

$$\lambda_3 \approx \frac{2\Omega V_A^2 k_z^3}{\eta^2 k^5} + i\eta k^2. \tag{4.28}$$

The algebraic steps involved in obtaining (4.28) are given in the Appendix D.1.2. Similarly, λ_2 becomes

$$\lambda_2 \approx -\frac{2\Omega V_A^2 k_z^3}{\eta^2 k^5} + i\eta k^2. \tag{4.29}$$

Therefore, the approximate frequencies in the diffusion-dominated regime are

$$\begin{aligned} \lambda_{1,4} &\approx \pm\frac{2\Omega k_z}{k} + i\frac{k_z^2}{\tau k^2}, \\ \lambda_{3,2} &\approx \pm\frac{2\Omega V_A^2 k_z^3}{\eta^2 k^5} + i\eta k^2. \end{aligned} \tag{4.30}$$

4.3.3 Weakly rotating, wave-dominated regime

Using the inequality $V_A k_z \gg \frac{\Omega k_z}{k} \gg \frac{\eta k^2}{2}$, the approximate form of $\lambda_1 - \lambda_4$ is obtained.

$\lambda_{1,4}$ modes

The λ_1 frequency

$$\lambda_1 = \frac{\Omega k_z}{k} + i\frac{\eta k^2}{2} + \sqrt{V_A^2 k_z^2 + \left(\frac{\Omega k_z}{k} - i\frac{\eta k^2}{2}\right)^2},$$

is considered. This frequency can be written as

$$\lambda_1 = \frac{\Omega k_z}{k} + i\frac{\eta k^2}{2} + V_A k_z \sqrt{1 + \left(\frac{\Omega}{V_A k} - i\frac{\eta k^2}{2V_A k_z}\right)^2}. \tag{4.31}$$

Using Taylor series expansion, (4.31) becomes

$$\lambda_1 \approx V_A k_z + \frac{\Omega k_z}{k} + i\left(\frac{\eta k^2}{2} - \frac{\Omega \eta k}{2V_A}\right). \tag{4.32}$$

The algebraic steps involved in the obtaining (4.32) are given in the Appendix D.2.1.

Similarly, λ_4 mode becomes

$$\lambda_4 \approx -\left(V_A k_z + \frac{\Omega k_z}{k}\right) + i\left(\frac{\eta k^2}{2} - \frac{\Omega \eta k}{2V_A}\right). \tag{4.33}$$

$\lambda_{2,3}$ modes

The λ_3 frequency

$$\lambda_3 = -\frac{\Omega k_z}{k} + i\frac{\eta k^2}{2} + \sqrt{V_A^2 k_z^2 + \left(\frac{\Omega k_z}{k} + i\frac{\eta k^2}{2}\right)^2},$$

is considered. This frequency can be written as

$$\lambda_3 = -\frac{\Omega k_z}{k} + i\frac{\eta k^2}{2} + V_A k_z \sqrt{1 + \left(\frac{\Omega}{V_A k} + i\frac{\eta k^2}{2V_A k_z}\right)^2}. \tag{4.34}$$

Using Taylor series expansion, (4.34) becomes

$$\lambda_3 \approx \left(V_A k_z - \frac{\Omega k_z}{k}\right) + i\left(\frac{\eta k^2}{2} + \frac{\Omega \eta k}{2V_A}\right). \tag{4.35}$$

The algebraic steps involved in obtaining (4.35) are given in Appendix D.2.1. Similarly λ_2 would satisfy

$$\lambda_2 \approx -\left(V_A k_z - \frac{\Omega k_z}{k}\right) + i\left(\frac{\eta k^2}{2} + \frac{\Omega \eta k}{2V_A}\right). \tag{4.36}$$

Therefore, in this weakly rotating, wave-dominated regime, the frequencies are of the form:

$$\begin{aligned} \lambda_{1,4} &\approx \pm\left(V_A k_z + \frac{\Omega k_z}{k}\right) + i\left(\frac{\eta k^2}{2} - \frac{\Omega \eta k}{2V_A}\right), \\ \lambda_{3,2} &\approx \pm\left(V_A k_z - \frac{\Omega k_z}{k}\right) + i\left(\frac{\eta k^2}{2} + \frac{\Omega \eta k}{2V_A}\right). \end{aligned} \tag{4.37}$$

4.3.4 Weakly rotating, diffusion-dominated regime

Using the inequality $\frac{\eta k^2}{2} \gg V_A k_z \gg \frac{\Omega k_z}{k}$, the approximate form of $\lambda_1 - \lambda_4$ are obtained.

$\lambda_{1,4}$ modes

The λ_1 frequency

$$\lambda_1 = \frac{\Omega k_z}{k} + i\frac{\eta k^2}{2} + \sqrt{V_A^2 k_z^2 + \left(\frac{\Omega k_z}{k} - i\frac{\eta k^2}{2}\right)^2},$$

is considered. This frequency can be written as

$$\lambda_1 = \frac{\Omega k_z}{k} + i\frac{\eta k^2}{2} + \frac{\eta k^2}{2}\sqrt{\left(\frac{2V_A k_z}{\eta k^2}\right)^2 + \left(\frac{2\Omega k_z}{\eta k^3} - i\right)^2}. \tag{4.38}$$

Using Taylor series expansion, λ_1 becomes

$$\lambda_1 \approx \frac{2\Omega k_z}{k} + i\frac{k_z^2}{\tau k^2}. \tag{4.39}$$

The algebraic steps involved in obtaining (4.39) are given in the Appendix D.2.2. Similarly, λ_4 becomes

$$\lambda_4 \approx -\frac{2\Omega k_z}{k} + i\frac{k_z^2}{\tau k^2}. \tag{4.40}$$

$\lambda_{2,3}$ modes

The λ_3 frequency

$$\lambda_3 = -\frac{\Omega k_z}{k} + i\frac{\eta k^2}{2} + \sqrt{V_A^2 k_z^2 + \left(\frac{\Omega k_z}{k} + i\frac{\eta k^2}{2}\right)^2},$$

is considered. This frequency can be written as

$$\lambda_3 = -\frac{\Omega k_z}{k} + i\frac{\eta k^2}{2} + \frac{\eta k^2}{2}\sqrt{\left(\frac{2V_A k_z}{\eta k^2}\right)^2 + \left(\frac{2\Omega k_z}{\eta k^3} + i\right)^2}. \tag{4.41}$$

Using Taylor series expansion, λ_3 becomes

$$\lambda_3 \approx \frac{2\Omega V_A^2 k_z^3}{\eta^2 k^5} + i\eta k^2. \tag{4.42}$$

The algebraic steps for obtaining (4.42) are shown in Appendix D.2.2. Similarly, λ_2 becomes

$$\lambda_2 \approx -\frac{2\Omega V_A^2 k_z^3}{\eta^2 k^5} + i\eta k^2. \tag{4.43}$$

Therefore, the frequencies in this weakly rotating, diffusion-dominated regime are:

$$\lambda_{1,4} \approx \pm\frac{2\Omega k_z}{k} + i\frac{k_z^2}{\tau k^2},\ \lambda_{3,2} \approx \pm\frac{2\Omega V_A^2 k_z^3}{\eta^2 k^5} + i\eta k^2. \tag{4.44}$$

Frequencies in (4.44) suggest that the modes $\lambda_{1,4}$ are the *qs* modes obtained in (4.15). In section 4.3.2, it was shown that the frequencies $\lambda_{1,4}$ in the diffusion-dominated strongly rotating regime also simplified to the *qs* form. This suggests that the *qs* phase is common to both the strongly and weakly rotating regimes. Since only two modes can physically exist in the *qs* phase, the slow wave modes $\lambda_{2,3}$ are not relevant in this regime.

4.4 Problem definition and governing equations

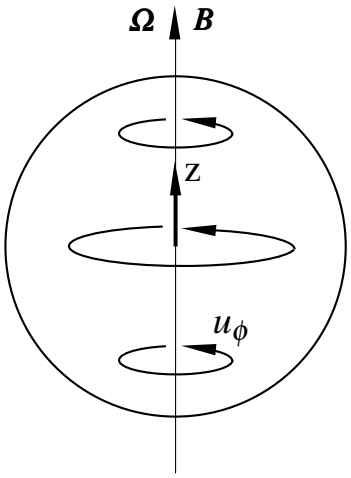

Fig. 4.1 A localized flow perturbation of the initial form given in (3.9) in an otherwise quiescent electrically conducting fluid permeated by an axial (z) magnetic field in presence of background rotation.

Similar to the non-rotating case, an axisymmetric swirling vortex blob (3.9) in the presence of an axial magnetic field is considered along with co-axial rotation. The scenario is

illustrated in the schematic figure 4.1. The initial conditions of this problem are

$$\boldsymbol{B} = (0,0,B_0),\ \boldsymbol{\Omega} = (0,0,\Omega),\ \boldsymbol{u}_0 = (0,u_{\phi 0},0), \tag{4.45}$$

where the expression for $\hat{u}_{\phi 0}$ is given by (3.9).

The scalar momentum equations in (s,ϕ,z) cylindrical polar coordinates governing the evolution of the vortex are:

$$\frac{\partial u_s}{\partial t} = -\frac{1}{\rho}\frac{\partial p^*}{\partial s} + \frac{B_0}{\mu\rho}\frac{\partial b_s}{\partial z} + 2\Omega u_\phi + \nu\left[\frac{1}{s}\frac{\partial}{\partial s}\left(s\frac{\partial u_s}{\partial s}\right) + \frac{\partial^2 u_s}{\partial z^2} - \frac{u_s}{s^2}\right], \tag{4.46}$$

$$\frac{\partial u_\phi}{\partial t} = \frac{B_0}{\mu\rho}\frac{\partial b_\phi}{\partial z} - 2\Omega u_s + \nu\left[\frac{1}{s}\frac{\partial}{\partial s}\left(s\frac{\partial u_\phi}{\partial s}\right) + \frac{\partial^2 u_\phi}{\partial z^2} - \frac{u_\phi}{s^2}\right], \tag{4.47}$$

$$\frac{\partial u_z}{\partial t} = -\frac{1}{\rho}\frac{\partial p^*}{\partial z} + \frac{B_0}{\mu\rho}\frac{\partial b_z}{\partial z} + \nu\left[\frac{1}{s}\frac{\partial}{\partial s}\left(s\frac{\partial u_z}{\partial s}\right) + \frac{\partial^2 u_z}{\partial z^2}\right]. \tag{4.48}$$

Similarly, the governing magnetic induction equations are:

$$\frac{\partial b_s}{\partial t} = B_0\frac{\partial u_s}{\partial z} + \eta\left[\frac{1}{s}\frac{\partial}{\partial s}\left(s\frac{\partial b_s}{\partial s}\right) + \frac{\partial^2 b_s}{\partial z^2} - \frac{b_s}{s^2}\right], \tag{4.49}$$

$$\frac{\partial b_\phi}{\partial t} = B_0\frac{\partial u_\phi}{\partial z} + \eta\left[\frac{1}{s}\frac{\partial}{\partial s}\left(s\frac{\partial b_\phi}{\partial s}\right) + \frac{\partial^2 b_\phi}{\partial z^2} - \frac{b_\phi}{s^2}\right], \tag{4.50}$$

$$\frac{\partial b_z}{\partial t} = B_0\frac{\partial u_z}{\partial z} + \eta\left[\frac{1}{s}\frac{\partial}{\partial s}\left(s\frac{\partial b_z}{\partial s}\right) + \frac{\partial^2 b_z}{\partial z^2}\right]. \tag{4.51}$$

Using the initial conditions (4.45) and governing equations (4.46-4.51), the general solutions of the toroidal velocity and magnetic fields are obtained in the following section. Using these general solutions, the toroidal kinetic and magnetic energy estimates and the wave–diffusion transitions are studied analytically.

4.5 General solution

4.5.1 Toroidal velocity ($\hat{u}_\phi$)

The solution of $\hat{u}_\phi$ can be written as a linear combination of solutions represented by the four modes (4.11)

$$\hat{u}_\phi = A_1 e^{i\lambda_1 t} + B_1 e^{i\lambda_2 t} + C_1 e^{i\lambda_3 t} + D_1 e^{i\lambda_4 t}, \tag{4.52}$$

where A_1,B_1,C_1 and D_1 are functions of wavenumbers k_s and k_z. Their corresponding expressions are estimated by solving the following system of equations:

$$\begin{aligned}
A_1 + B_1 + C_1 + D_1 &= \hat{u}_{\phi 0}, \\
i(A_1\lambda_1 + B_1\lambda_2 + C_1\lambda_3 + D_1\lambda_4) &= \left.\frac{\partial \hat{u}_\phi}{\partial t}\right|_{t=0}, \\
-(A_1\lambda_1^2 + B_1\lambda_2^2 + C_1\lambda_3^2 + D_1\lambda_4^2) &= \left.\frac{\partial^2 \hat{u}_\phi}{\partial t^2}\right|_{t=0}, \\
-i(A_1\lambda_1^3 + B_1\lambda_2^3 + C_1\lambda_3^3 + D_1\lambda_4^3) &= \left.\frac{\partial^3 \hat{u}_\phi}{\partial t^3}\right|_{t=0}.
\end{aligned} \tag{4.53}$$

The steps involved in solving the system of equations in (4.53) are shown in detail in Appendix C.1. The expressions for A_1, B_1, C_1, D_1 are:

$$\begin{aligned}
A_1 &= \frac{a_4 - a_3(\lambda_2+\lambda_3+\lambda_4) + a_2[\lambda_2(\lambda_3+\lambda_4)+\lambda_3\lambda_4] - a_1\lambda_3\lambda_4\lambda_2}{(\lambda_1-\lambda_2)(\lambda_1-\lambda_3)(\lambda_1-\lambda_4)}, \\
B_1 &= \frac{a_4 - a_3(\lambda_1+\lambda_3+\lambda_4) + a_2[\lambda_1(\lambda_3+\lambda_4)+\lambda_3\lambda_4] - a_1\lambda_3\lambda_4\lambda_1}{(\lambda_2-\lambda_1)(\lambda_2-\lambda_3)(\lambda_2-\lambda_4)}, \\
C_1 &= \frac{a_4 - a_3(\lambda_1+\lambda_2+\lambda_4) + a_2[\lambda_1(\lambda_2+\lambda_4)+\lambda_2\lambda_4] - a_1\lambda_2\lambda_4\lambda_1}{(\lambda_3-\lambda_4)(\lambda_3-\lambda_1)(\lambda_3-\lambda_2)}, \\
D_1 &= \frac{a_4 - a_3(\lambda_1+\lambda_2+\lambda_3) + a_2[\lambda_1(\lambda_2+\lambda_3)+\lambda_2\lambda_3] - a_1\lambda_2\lambda_3\lambda_1}{(\lambda_4-\lambda_3)(\lambda_4-\lambda_2)(\lambda_4-\lambda_1)},
\end{aligned}$$

where $\lambda_1 - \lambda_4$ are the four modes of the solution obtained in (4.11). The expressions for $a_1 - a_4$ are:

$$a_1 = \hat{u}_{\phi 0},\ a_2 = i\nu k^2 \hat{u}_{\phi 0},\ a_3 = \left(V_A^2 k_z^2 + \frac{4\Omega^2 k_z^2}{k^2} - \nu^2 k^4\right)\hat{u}_{\phi 0},$$

$$a_4 = i[(2\nu+\eta)V_A^2 k_z^2 k^2 + 12\Omega^2 \nu k_z^2 - \nu^3 k^6]\hat{u}_{\phi 0}.$$

4.5.2 Toroidal magnetic field ($\hat{b}_\phi$)

The general solution for $\hat{b}_\phi$ is

$$\hat{b}_\phi = A_2 e^{i\lambda_1 t} + B_2 e^{i\lambda_2 t} + C_2 e^{i\lambda_3 t} + D_2 e^{i\lambda_4 t}, \tag{4.54}$$

where A_2, B_2, C_2 and D_2 are functions of wavenumbers (k_s, k_z) which are estimated by solving the following system of equations:

$$\begin{aligned}
A_2 + B_2 + C_2 + D_2 = \hat{b}_{\phi 0} = 0,\\
i(A_2\lambda_1 + B_2\lambda_2 + C_2\lambda_3 + D_2\lambda_4) = \left.\frac{\partial \hat{b}_\phi}{\partial t}\right|_{t=0},\\
-(A_2\lambda_1^2 + B_2\lambda_2^2 + C_2\lambda_3^2 + D_2\lambda_4^2) = \left.\frac{\partial^2 \hat{b}_\phi}{\partial t^2}\right|_{t=0},\\
-i(A_2\lambda_1^3 + B_2\lambda_2^3 + C_2\lambda_3^3 + D_2\lambda_4^3) = \left.\frac{\partial^3 \hat{b}_\phi}{\partial t^3}\right|_{t=0}.
\end{aligned} \tag{4.55}$$

The steps involved in solving the system of equations in (4.55) are shown in detail in Appendix C.2. The expressions for A_2, B_2, C_2, D_2 are:

$$\begin{aligned}
A_2 &= \frac{b_4 - b_3(\lambda_2+\lambda_3+\lambda_4) + b_2[\lambda_2(\lambda_3+\lambda_4)+\lambda_3\lambda_4]}{(\lambda_1-\lambda_2)(\lambda_1-\lambda_3)(\lambda_1-\lambda_4)},\\
B_2 &= \frac{b_4 - b_3(\lambda_1+\lambda_3+\lambda_4) + b_2[\lambda_1(\lambda_3+\lambda_4)+\lambda_3\lambda_4]}{(\lambda_2-\lambda_1)(\lambda_2-\lambda_3)(\lambda_2-\lambda_4)},\\
C_2 &= \frac{b_4 - b_3(\lambda_1+\lambda_2+\lambda_4) + b_2[\lambda_1(\lambda_2+\lambda_4)+\lambda_2\lambda_4]}{(\lambda_3-\lambda_4)(\lambda_3-\lambda_1)(\lambda_3-\lambda_2)},\\
D_2 &= \frac{b_4 - b_3(\lambda_1+\lambda_2+\lambda_3) + b_2[\lambda_1(\lambda_2+\lambda_3)+\lambda_2\lambda_3]}{(\lambda_4-\lambda_3)(\lambda_4-\lambda_2)(\lambda_4-\lambda_1)}.
\end{aligned}$$

where $\lambda_1 - \lambda_4$ are the four modes of the solution obtained in (4.11). The expressions for $a_1 - a_4$ are

$$b_2 = \hat{u}_{\phi 0} B_0 k_z,\ b_3 = i(\nu+\eta) B_0 k_z k^2 \hat{u}_{\phi 0},$$

$$b_4 = B_0 k_z \left(V_A^2 k_z^2 + \frac{4\Omega^2 k_z^2}{k^2} - k^4(\nu^2 + \eta^2 + \nu\eta) \right) \hat{u}_{\phi 0}.$$

4.6 Quasi-static solutions

4.6.1 Toroidal velocity $(\hat{u}_{\phi,qs})$

The solution of $\hat{u}_{\phi,qs}$ can be written as a linear combination of solutions represented by two the qs modes (4.15),

$$\hat{u}_{\phi,qs} = P_1 e^{i\lambda_1 t} + Q_1 e^{i\lambda_2 t}. \tag{4.56}$$

The functions P_1, Q_1 are obtained by solving the following system of equations:

$$\begin{aligned} P_1 + Q_1 &= \hat{u}_{\phi 0}, \\ i(P_1\lambda_1 + Q_1\lambda_2) &= \left.\frac{\partial \hat{u}_{\phi,qs}}{\partial t}\right|_{t=0}. \end{aligned} \tag{4.57}$$

The steps involved in solving the system of equations in (4.57) are given in Appendix C.3.1. The expressions for P_1 and Q_1 are:

$$P_1 = \frac{a_2 - a_1\lambda_2}{\lambda_1 - \lambda_2}, \;\; Q_1 = \frac{a_2 - a_1\lambda_1}{\lambda_2 - \lambda_1}, \tag{4.58}$$

where $a_1 = \hat{u}_{\phi 0}$, $a_2 = i\nu k^2 \hat{u}_{\phi 0}$ and $\lambda_{1,2}$ are the qs frequencies as given in (4.16). Substituting the expressions (4.58) in (4.56) gives

$$\hat{u}_{\phi,qs} = \left(\frac{a_2 - a_1\lambda_2}{\lambda_1 - \lambda_2} \right) e^{i\lambda_1 t} - \left(\frac{a_2 - a_1\lambda_1}{\lambda_1 - \lambda_2} \right) e^{i\lambda_2 t}. \tag{4.59}$$

4.6.2 Toroidal magnetic field $(\hat{b}_{\phi,qs})$

The solution for toroidal magnetic field is obtained from

$$B_0 \frac{\partial u_\phi}{\partial z} + \eta \left[\frac{1}{s}\frac{\partial}{\partial s}\left(s\frac{\partial b_\phi}{\partial s} \right) + \frac{\partial^2 b_\phi}{\partial z^2} - \frac{b_\phi}{s^2} \right] = 0, \tag{4.60}$$

which is the *qs* b_ϕ induction equation. The Hankel-Fourier transformation of (4.60) gives

$$B_0 i k_z \hat{u}_\phi - \eta k^2 \hat{b}_\phi = 0. \tag{4.61}$$

From (4.61), the solution for $\hat{b}_{\phi,qs}$ is

$$\hat{b}_{\phi,qs} = \frac{B_0 i k_z \hat{u}_{\phi,qs}}{\eta k^2},$$

where $\hat{u}_{\phi,qs}$ is the solution obtained in (4.59). Hence, $\hat{b}_{\phi,qs}$ becomes

$$\hat{b}_{\phi,qs} = \frac{B_0 i k_z}{\eta k^2}\left[\left(\frac{a_2 - a_1\lambda_2}{\lambda_1 - \lambda_2}\right)e^{i\lambda_1 t} - \left(\frac{a_2 - a_1\lambda_1}{\lambda_1 - \lambda_2}\right)e^{i\lambda_2 t}\right], \tag{4.62}$$

where $a_1 = \hat{u}_{\phi 0}$, $a_2 = i\nu k^2 \hat{u}_{\phi 0}$ and $\lambda_{1,2}$ are the *qs* frequencies as given in (4.16).

4.7 Analytical energy estimates in strongly rotating regime

The toroidal velocity and magnetic field solutions from (4.52) and (4.54)

$$\hat{u}_\phi = A_1 e^{i\lambda_1 t} + B_1 e^{i\lambda_2 t} + C_1 e^{i\lambda_3 t} + D_1 e^{i\lambda_4 t},$$
$$\hat{b}_\phi = A_2 e^{i\lambda_1 t} + B_2 e^{i\lambda_2 t} + C_2 e^{i\lambda_3 t} + D_2 e^{i\lambda_4 t},$$

are considered. It is clear from (4.13) that in a strongly rotating regime, $\lambda_{1,4}$ and $\lambda_{2,3}$ are the fast and slow MC wave frequencies respectively. Therefore, the terms containing $e^{i\lambda_1 t}$ and $e^{i\lambda_4 t}$ represent two oppositely traveling fast MC waves. Similarly, the terms with coefficients $e^{i\lambda_2 t}$ and $e^{i\lambda_3 t}$ represent two oppositely traveling slow MC waves. The velocity and magnetic field components represented by λ_1 and λ_2 modes are considered, which are given by

$$\hat{u}_{\phi,f} = A_1 e^{i\lambda_1 t},\ \ \hat{u}_{\phi,s} = B_1 e^{i\lambda_2 t},\ \ \hat{b}_{\phi,f} = A_2 e^{i\lambda_1 t},\ \ \hat{b}_{\phi,s} = B_2 e^{i\lambda_2 t}.$$

In the following sections, the kinetic and magnetic energies associated with these solutions are obtained for both wave-dominated and diffusion-dominated regimes.

4.7.1 Wave-dominated regime ($\Omega k_z/k \gg V_A k_z \gg \eta k^2/2$)

From equation (4.23), the approximate form of modes $\lambda_1 - \lambda_4$ are:

$$\lambda_{1,4} \approx \pm\frac{2\Omega k_z}{k} + i\frac{\eta V_A^2 k^4}{4\Omega^2}, \;\; \lambda_{3,2} \approx \pm\frac{V_A^2 k_z k}{2\Omega} + i\eta k^2.$$

All the frequencies are complex entities. The real part physically represent the wave propagation frequency while the imaginary part indicates that the waves are damped by magnetic diffusion. When $\eta = 0$, $\lambda_{1,4} \approx 2\Omega k_z/k$ and $\lambda_{3,2} \approx \pm V_A^2 k_z k/2\Omega$, which are the frequencies of undamped fast and slow MC waves respectively obtained in (4.13). With finite magnetic diffusivity, the slow wave diffuses on a magnetic diffusion timescale $t_\eta = (\eta k_0^2)^{-1}$. Similarly, the fast wave decays on a timescale t_1 given by

$$t_1 = \frac{4\Omega^2}{\eta V_A^2 k_0^4}, \tag{4.63}$$

where k_0 is the resultant wavenumber of the initial vortex blob.

When there is no magnetic field, the timescale $t_1 \to \infty$ and the modes $\lambda_{1,4} \approx \pm 2\Omega k_z/k$ which suggest that the vortex would evolve as an undamped inertial wave. In presence of the magnetic field, the timescale t_1 is finite and decreases when the strength of the magnetic field is increased. The effect of this diffusion timescale t_1 on the evolution of kinetic and magnetic energies are currently not understood which is addressed in the following sections.

Fast wave kinetic energy

The fast wave velocity field $\hat{u}_{\phi,f} = A_1 e^{i\lambda_1 t}$ is considered, where the expression for A_1 is as given in section 4.5.1. Using the frequency approximations (4.23), $\hat{u}_{\phi,f}$ simplifies to

$$\hat{u}_{\phi,f} \approx \frac{\hat{u}_{\phi 0}}{2}\exp\left(-\frac{\eta V_A^2 k^4 t}{4\Omega^2}\right)\left[\cos\left(\frac{2\Omega k_z t}{k}\right) - \frac{3\eta V_A^2 k^5}{8\Omega^3 k_z}\sin\left(\frac{2\Omega k_z t}{k}\right)\right]. \tag{4.64}$$

The steps involved in obtaining (4.64) are shown in detail in Appendix E.

The kinetic energy (E_k) associated with the velocity field (4.64) is

$$E_{k,f} = 16\pi^4 \int_0^\infty \int_0^\infty |\hat{u}_{\phi,f}|^2 \, k_s \, dk_s \, dk_z.$$

For $t \ll t_1$, $\hat{u}_{\phi,f} \approx \hat{u}_{\phi 0}/2$. Hence, E_k for $t \ll t_1$ is

$$E_{k,f} \approx 4\pi^4 \int_0^\infty \int_0^\infty |\hat{u}_{\phi 0}|^2 \, k_s \, dk_s \, dk_z \approx E_0.$$

For $t \gtrsim t_1$, $\hat{u}_{\phi,f}$ is

$$\hat{u}_{\phi,f} \approx \frac{\hat{u}_{\phi 0}}{2} \exp\left(-\frac{\eta V_A^2 k^4 t}{4\Omega^2}\right).$$

The energy associated with this $\hat{u}_{\phi,f}$ is

$$\begin{aligned} E_{k,f} &\approx 4\pi^4 \int_0^\infty \int_0^\infty |\hat{u}_{\phi 0}|^2 \exp\left(-\frac{\eta V_A^2 k^4 t}{2\Omega^2}\right) \, k_s \, dk_s \, dk_z, \\ &\approx \frac{\pi \delta^{10}}{64} \int_0^\infty \int_0^\infty k_s^3 \exp\left(-\frac{k^2\delta^2}{2} - \frac{\eta V_A^2 k^4 t}{2\Omega^2}\right) \, dk_s \, dk_z. \end{aligned}$$

Let $k_s = k\cos\theta$ and $k_z = k\sin\theta$. Using these substitutions, the integral becomes

$$\begin{aligned} E_{k,f} &\approx \frac{\pi \delta^{10}}{64} \int_0^{\pi/2} \cos^3\theta \, d\theta \int_0^\infty k^4 \exp\left(-\frac{k^2\delta^2}{2} - \frac{\eta V_A^2 k^4 t}{2\Omega^2}\right) \, dk, \\ &\approx \frac{\pi \delta^{10}}{96} \int_0^\infty k^4 \exp\left(-\frac{k^2\delta^2}{2} - \frac{\eta V_A^2 k^4 t}{2\Omega^2}\right) \, dk. \end{aligned}$$

Now, let $a = \delta^2/2$ and $b = \dfrac{\eta V_A^2 t}{2\Omega^2}$. Hence, the integral becomes

$$E_{k,f} \approx \frac{\pi \delta^{10}}{96} \int_0^\infty k^4 \exp\left(-ak^2 - bk^4\right) \, dk.$$

From Appendix A.2, the following integral (I_A) has the solution

$$\begin{aligned} I_A &= \int_0^\infty k^4 \exp\left(-ak^2 - bk^4\right) \, dk, \\ I_A &= \frac{\sqrt{a}\exp\left(\dfrac{a^2}{8b}\right)}{32b^{5/2}} \left[(a^2+2b)K_{1/4}\left(\frac{a^2}{8b}\right) - a^2 K_{3/4}\left(\frac{a^2}{8b}\right)\right], \end{aligned} \tag{4.65}$$

where $K_n(x)$ is the modified Bessel function of second kind. For $t \gg t_1$, assuming $b \to \infty$, the integral I_A from Appendix (A.15) becomes

$$I_A \approx \frac{\Gamma(1/4)b^{-5/4}}{16} + O(b^{-7/4}).$$

Hence, the kinetic energy (E_k) becomes

$$\begin{aligned} E_{k,f} &\approx \frac{\pi\delta^{10}}{96} \times \frac{\Gamma(1/4)b^{-5/4}}{16}, \\ &\approx \frac{\pi\delta^{10}\Gamma(1/4)}{1536}\left(\frac{2t}{k_0^4 t_1}\right)^{-5/4}, \\ &\approx \frac{\pi\delta^{10}\Gamma(1/4)k_0^5}{2^{1/4}3072}\left(\frac{t}{t_1}\right)^{-5/4}, \\ &\approx \frac{25\sqrt{5}\pi\Gamma(1/4)\delta^5}{2^{1/4}3072}\left(\frac{t}{t_1}\right)^{-5/4}, \\ E_{k,f} &\approx c_1\left(\frac{t}{t_1}\right)^{-5/4}, \end{aligned} \tag{4.66}$$

where $c_1 = (25\sqrt{5}\pi\Gamma(1/4)\delta^5)/(2^{1/4}3072)$. Hence, from the energy estimate (4.66), for $t \gg t_1$, the kinetic energy of the fast wave would decay as $(t/t_1)^{-5/4}$.

Fast wave magnetic energy

The fast wave component of the toroidal magnetic field $\hat{b}_{\phi,f} = A_2\, e^{i\lambda_1 t}$ is considered. Following a similar procedure as in Appendix E, the approximate form of $\hat{b}_{\phi,f}$ is

$$\hat{b}_{\phi,f} \approx i\sqrt{\mu\rho}\,\hat{u}_{\phi 0}\frac{V_A k}{4\Omega}\exp\left(-\frac{\eta V_A^2 k^4 t}{4\Omega^2}\right)\left[\sin\left(\frac{2\Omega k_z t}{k}\right) + \frac{\eta k^3}{2\Omega k_z}\cos\left(\frac{2\Omega k_z t}{k}\right)\right]. \tag{4.67}$$

The associated magnetic energy (E_m) is given by

$$E_{m,f} = \frac{16\pi^4}{\mu\rho}\int_0^\infty\int_0^\infty |\hat{b}_{\phi,f}|^2\, k_s\, dk_s\, dk_z.$$

For $t_\Omega \ll t \ll t_1$, the magnetic energy is

$$E_{m,f} \approx \frac{\pi^4 V_A^2}{\Omega^2}\int_0^\infty\int_0^\infty k^2|\hat{u}_{\phi 0}|^2\, k_s\, dk_s\, dk_z,$$

$$E_{m,f} \approx \frac{\pi V_A^2 \delta^{10}}{256\Omega^2} \int_0^\infty \int_0^\infty k^2 k_s^3 \exp\left(-\frac{\delta^2 k^2}{2}\right)\, dk_s\, dk_z.$$

Using $k_s = k\cos\theta$ and $k_z = k\sin\theta$, the integral becomes

$$\begin{aligned} E_{m,f} &\approx \frac{\pi V_A^2 \delta^{10}}{256\Omega^2} \int_0^{\pi/2} \cos^3\theta\, d\theta \int_0^\infty k^6 \exp\left(-\frac{\delta^2 k^2}{2}\right)\, dk, \\ &\approx \frac{\pi V_A^2 \delta^{10}}{384\Omega^2} \int_0^\infty k^6 \exp\left(-\frac{\delta^2 k^2}{2}\right)\, dk, \end{aligned}$$

Using $I_6(a) = \dfrac{15\sqrt{\pi}}{16a^{7/2}}$ from Appendix $(A.1)$, the energy becomes

$$\begin{aligned} &\approx \frac{15\sqrt{2}\pi^{3/2}\delta^5}{192} Le^2, \\ E_{m,f} &\approx c_2 Le^2, \end{aligned} \tag{4.68}$$

where the constant $c_2 = 15\sqrt{2}\pi^{3/2}\delta^5/192$. This is the estimate for fast wave magnetic energy for times between $t_\Omega \ll t \ll t_1$.

For $t \gtrsim t_1$, the magnetic energy is

$$\begin{aligned} E_{m,f} &\approx \frac{\pi^4 V_A^2}{\Omega^2} \int_0^\infty \int_0^\infty k^2 |\hat{u}_{\phi 0}|^2 \exp\left(-\frac{\eta V_A^2 k^4 t}{2\Omega^2}\right)\, k_s\, dk_s\, dk_z, \\ &\approx \frac{\pi V_A^2 \delta^{10}}{256\Omega^2} \int_0^\infty \int_0^\infty k^2 k_s^3 \exp\left(-\frac{\delta^2 k^2}{2} - \frac{\eta V_A^2 k^4 t}{2\Omega^2}\right)\, dk_s\, dk_z. \end{aligned}$$

Using $k_s = k\cos\theta$ and $k_z = k\sin\theta$, the integral becomes

$$\begin{aligned} E_{m,f} &\approx \frac{\pi V_A^2 \delta^{10}}{256\Omega^2} \int_0^{\pi/2} \cos^3\theta\, d\theta \int_0^\infty k^6 \exp\left(-\frac{\delta^2 k^2}{2} - \frac{\eta V_A^2 k^4 t}{2\Omega^2}\right)\, dk, \\ &\approx \frac{\pi V_A^2 \delta^{10}}{384\Omega^2} \int_0^\infty k^6 \exp\left(-\frac{\delta^2 k^2}{2} - \frac{\eta V_A^2 k^4 t}{2\Omega^2}\right)\, dk. \end{aligned}$$

Let $a = \delta^2/2$ and $b = \eta V_A^2 t/2\Omega^2$. Hence, the integral becomes

$$E_{m,f} \approx \frac{\pi V_A^2 \delta^{10}}{384\Omega^2} \int_0^\infty k^6 \exp\left(-ak^2 - bk^4\right)\, dk.$$

From Appendix (A.12), the following integral is considered.

$$I_B = \int_0^\infty k^6 \exp\left(-ak^2 - bk^4\right)\, dk,$$

$$= \frac{a^{3/2}e^{a^2/8b}}{64b^{7/2}}\left[\left(a^2+3b\right)K_{3/4}\left(\frac{a^2}{8b}\right) - (a^2+5b)K_{1/4}\left(\frac{a^2}{8b}\right)\right].$$

From Appendix (A.16), for $t \gg t_1$, assuming $b \to \infty$, I_B becomes

$$I_B \approx \frac{3\Gamma(3/4)}{16}b^{-7/4} + O(b^{-9/4}). \tag{4.69}$$

Therefore, the magnetic energy is

$$\begin{aligned} E_{m,f} &\approx \frac{\pi V_A^2\delta^{10}}{384\Omega^2} \times \frac{3\Gamma(3/4)}{16}b^{-7/4}, \\ &\approx \frac{\pi V_A^2\delta^{10}}{384\Omega^2} \times \frac{3\Gamma(3/4)}{16}\left(\frac{2t}{k_0^4 t_1}\right)^{-7/4}, \\ &\approx \frac{5^{7/2}2^{-7/4}\pi\delta^5}{512}\Gamma(3/4)Le^2\left(\frac{t}{t_1}\right)^{-7/4}, \\ E_{m,f} &\approx c_3\, Le^2\left(\frac{t}{t_1}\right)^{-7/4}, \end{aligned} \tag{4.70}$$

where the constant is $c_3 = (5^{7/2}2^{-7/4}\pi\delta^5\Gamma(3/4))/512$. This estimate for fast wave magnetic energy suggests that the energy decays as $(t/t_1)^{-7/4}$ which is much rapid than the fast wave kinetic energy.

Slow wave kinetic energy

The slow wave component of the toroidal velocity field $\hat{u}_{\phi,s} = B_1 e^{i\lambda_2 t}$ is considered. The approximate form of B_1 is found by a similar procedure that was used to obtain A_1 in Appendix E. The $\hat{u}_{\phi,s}$ solution simplifies to

$$\hat{u}_{\phi,s} \approx -\frac{\hat{u}_{\phi 0}V_A^2k^2}{8\Omega^2}\exp\left(-\eta k^2 t\right)\left[\cos\left(\frac{V_A^2k_z kt}{2\Omega}\right) + \frac{4\eta k\Omega}{V_A^2k_z}\sin\left(\frac{V_A^2k_z kt}{2\Omega}\right)\right]. \tag{4.71}$$

The factor $V_A^2k^2/(2\Omega)^2$ can be written as

$$\frac{V_A^2k^2}{4\Omega^2} = \frac{V_A^2}{4\Omega^2\delta^2} \times \delta^2k^2 = \left(\frac{\Lambda}{S_0}\right)^2\delta^2k^2 = Le^2\delta^2k^2. \tag{4.72}$$

Using (4.72), the solution (4.71) becomes

$$\hat{u}_{\phi,s} \approx -\frac{\hat{u}_{\phi 0}}{2} Le^2 \delta^2 k^2 \exp\left(-\eta k^2 t\right) \left[\cos\left(\frac{V_A^2 k_z k t}{2\Omega}\right) + \frac{4\eta k \Omega}{V_A^2 k_z} \sin\left(\frac{V_A^2 k_z k t}{2\Omega}\right)\right].$$

The kinetic energy (E_k) associated with this slow wave is

$$E_{k,s} = 16\pi^4 \int_0^\infty \int_0^\infty |\hat{u}_{\phi,s}|^2 \, k_s \, dk_s \, dk_z.$$

The characteristic decay timescale for this $\hat{u}_{\phi,s}$ is the magnetic diffusion time $t_\eta = \delta^2/\eta \approx (\eta k_0^2)^{-1}$. For $t \ll t_\eta$, the slow wave solution is of the form

$$\hat{u}_{\phi,s} \approx -\frac{\hat{u}_{\phi 0}}{2} Le^2 \delta^2 k^2.$$

Therefore, the kinetic energy for $t \ll t_\eta$ is

$$\begin{aligned} E_{k,s} &\approx 4\pi^4 \int_0^\infty \int_0^\infty |\hat{u}_{\phi 0}|^2 Le^4 \delta^4 k^4 \, k_s \, dk_s \, dk_z, \\ &\approx \frac{\pi \delta^{14} Le^4}{64} \int_0^\infty \int_0^\infty k_s^3 k^4 \exp\left(-\frac{\delta^2 k^2}{2}\right) \, dk_s \, dk_z. \end{aligned}$$

Using $k_s = k\cos\theta$ and $k_z = k\sin\theta$, the integral becomes

$$\begin{aligned} E_{k,s} &\approx \frac{\pi \delta^{14} Le^4}{64} \int_0^{\pi/2} \cos^3\theta \, d\theta \int_0^\infty k^8 \exp\left(-\frac{\delta^2 k^2}{2}\right) \, dk, \\ &\approx \frac{\pi \delta^{14} Le^4}{96} \int_0^\infty k^8 \exp\left(-\frac{\delta^2 k^2}{2}\right) \, dk, \end{aligned}$$

Using $I_8(a) = \dfrac{105}{32a^{9/2}}$ from Appendix $(A.1)$, the energy becomes

$$\begin{aligned} &\approx \frac{\pi \delta^5 105\sqrt{2}}{192} \, Le^4, \\ E_{k,s} &\approx c_4 \, Le^4, \end{aligned} \tag{4.73}$$

where the constant $c_4 = \pi\delta^5 105\sqrt{2}/192$. From (4.73), it is clear that for $t \ll t_\eta$, the kinetic energy of the slow wave is proportional to the fourth power of Lehnert number.

For $t \gtrsim t_\eta$, the slow wave solution takes the form

$$\hat{u}_{\phi,s} \approx -\frac{\hat{u}_{\phi 0}}{2} Le^2 \delta^2 k^2 \exp\left(-\eta k^2 t\right).$$

The kinetic energy associated with this of slow wave velocity field is

$$E_{k,s} \approx 4\pi^4 \int_0^\infty \int_0^\infty |\hat{u}_{\phi 0}|^2 Le^4 \delta^4 k^4 \exp\left(-2\eta k^2 t\right)\ k_s\, dk_s\, dk_z,$$
$$\approx \frac{Le^4 \pi \delta^{14}}{64} \int_0^\infty \int_0^\infty k^4 k_s^3 \exp\left(-\frac{k^2\delta^2}{2} - 2\eta k^2 t\right)\ dk_s\, dk_z.$$

Using $k_s = k\cos\theta$ and $k_z = k\sin\theta$, the integral becomes

$$E_{k,s} \approx \frac{Le^4 \pi \delta^{14}}{64} \int_0^{\pi/2} \cos^3\theta\, d\theta \int_0^\infty k^8 \exp\left[-k^2\left(\frac{\delta^2}{2} + 2\eta t\right)\right] dk,$$
$$\approx \frac{Le^4 \pi \delta^{14}}{96} \times \int_0^\infty k^8 \exp\left[-k^2\left(\frac{\delta^2}{2} + 2\eta t\right)\right] dk,$$

Using $I_8(a) = \dfrac{105}{32a^{9/2}}$ from Appendix $(A.1)$, the energy becomes

$$\approx \frac{105 Le^4 \pi \delta^{14}}{3072} \times \left(\frac{\delta^2}{2} + 2\eta t\right)^{-9/2},$$
$$\approx \frac{105 Le^4 \pi \delta^{14}}{3072} \times \left[\frac{5}{2k_0^2}\left(1 + \frac{4}{5}\eta k_0^2 t\right)\right]^{-9/2},$$
$$\approx \frac{105 Le^4 \pi \delta^{14} k_0^9}{3072}\left(\frac{5}{2}\right)^{-9/2} \times \left(1 + \frac{4}{5}\frac{t}{t_\eta}\right)^{-9/2},$$

For $t \gg t_\eta$, the energy becomes

$$\approx \frac{105 Le^4 \pi \delta^{14} k_0^9}{2^{9/2} 3072} \times \left(\frac{t}{t_\eta}\right)^{-9/2},$$
$$\approx \frac{65625\sqrt{5}\pi\delta^5}{49152\sqrt{2}} Le^4 \left(\frac{t}{t_\eta}\right)^{-9/2},$$
$$E_{k,s} \approx c_5\, Le^4 \left(\frac{t}{t_\eta}\right)^{-9/2}, \tag{4.74}$$

where the constant $c_5 = 65625\sqrt{5}\pi\delta^5/(49152\sqrt{2})$. From (4.74), it is clear that the slow wave kinetic energy for $t \gg t_\eta$ decays as $(t/t_\eta)^{-9/2}$.

Slow wave magnetic energy

The slow wave component of the toroidal magnetic field $\hat{b}_{\phi,s} = B_2\, e^{i\lambda_2 t}$ is considered. Following a similar procedure in Appendix E, the simplified form of $\hat{b}_{\phi,s}$ is

$$\hat{b}_{\phi,s} \approx -i\frac{\hat{u}_{\phi 0} B_0 k}{4\Omega}\exp\left(-\eta k^2 t\right)\left[\sin\left(\frac{V_A^2 k_z k t}{2\Omega}\right) + \frac{\eta k^3}{2\Omega k_z}\cos\left(\frac{V_A^2 k_z k t}{2\Omega}\right)\right]. \tag{4.75}$$

The magnetic energy (E_m) associated with (4.75) is given by

$$E_{m,s} = \frac{16\pi^4}{\mu\rho}\int_0^\infty\int_0^\infty |\hat{b}_{\phi,s}|^2\, k_s\, dk_s\, dk_z.$$

From (4.75), the slow wave propagation timescale (t_s) is given by

$$t_s = \frac{2\Omega}{V_A^2 k_{z0} k_0} = \frac{t_A^2}{t_\Omega},$$

where $t_A = (V_A k_{z0})^{-1}$ is the Alfvén travel timescale and $t_\Omega = k_0/2\Omega k_{z0}$ is the inertial timescale. The slow wave magnetic field also decays on the magnetic diffusion timescale (t_η). The ratio of the timescales t_η and t_s is

$$\frac{t_\eta}{t_s} = \frac{t_\eta t_\Omega}{t_A^2} = \frac{t_\Omega}{\tau} = \Lambda,$$

where Λ is the Elsasser number. Since $\Lambda \ll 1$ in a strongly rotating regime, $t_\eta \ll t_s$. Therefore, for $t \ll t_\eta$, the evolution of slow wave magnetic energy is in a transient phase where there exists no scaling for the magnetic energy.

For $t \gtrsim t_\eta$, the slow wave magnetic energy is

$$E_{m,s} \approx \frac{\pi^4 V_A^2}{\Omega^2}\int_0^\infty\int_0^\infty k^2 |\hat{u}_{\phi 0}|^2 \exp\left(-2\eta k^2 t\right)\, k_s\, dk_s\, dk_z,$$
$$E_{m,s} \approx \frac{\pi \delta^{10} V_A^2}{16^2\Omega^2}\int_0^\infty\int_0^\infty k^2 k_s^3 \exp\left[-\left(\frac{\delta^2}{2} + 2\eta t\right)k^2\right] dk_s\, dk_z.$$

Using $k_s = k\cos\theta$ and $k_z = k\sin\theta$, the integral becomes

$$E_{m,s} \approx \frac{\pi \delta^{10} V_A^2}{16^2\Omega^2}\int_0^{\pi/2}\cos^3\theta\, d\theta \int_0^\infty k^6 \exp\left[-\left(\frac{\delta^2}{2} + 2\eta t\right)k^2\right] dk,$$

$$\approx \frac{\pi\delta^{10}V_A^2}{384\Omega^2}\int_0^\infty k^6 \exp\left[-\left(\frac{\delta^2}{2}+2\eta t\right)k^2\right]\,dk,$$

Using $I_6(a)=\dfrac{15\sqrt{\pi}}{16a^{7/2}}$ from Appendix $(A.1)$, the energy becomes

$$\approx \frac{\pi\delta^{10}V_A^2}{384\Omega^2}\times\frac{15\sqrt{\pi}}{16}\times\left(\frac{\delta^2}{2}+2\eta t\right)^{-7/2},$$

$$\approx \frac{15\pi^{3/2}\delta^{12}}{1536}\times\frac{V_A^2}{4\Omega^2\delta^2}\times\left[\frac{5}{2k_0^2}\left(1+\frac{4}{5}\eta k_0^2 t\right)\right]^{-7/2},$$

$$\approx \frac{15\pi^{3/2}\delta^{12}k_0^7Le^2}{1536}\left(\frac{5}{2}\right)^{-7/2}\left[\left(1+\frac{4}{5}\frac{t}{t_\eta}\right)\right]^{-7/2},$$

For $t \gg t_\eta$, the energy becomes

$$\approx \frac{15\pi^{3/2}\delta^{12}k_0^7}{2^{7/2}1536}Le^2\left(\frac{t}{t_\eta}\right)^{-7/2},$$

$$\approx \frac{1875\sqrt{5}\pi^{3/2}\delta^5}{12288\sqrt{2}}Le^2\left(\frac{t}{t_\eta}\right)^{-7/2},$$

$$E_{m,s}\approx c_6 Le^2\left(\frac{t}{t_\eta}\right)^{-7/2}, \tag{4.76}$$

where the constant $c_6=(1875\sqrt{5}\pi^{3/2}\delta^5)/(12288\sqrt{2})$. The estimate (4.76) suggests that the slow wave magnetic energy decays as $(t/t_\eta)^{-7/2}$.

4.7.2 Diffusion-dominated regime $(\eta k^2/2 \gg \Omega k_z/k \gg V_A k_z)$

From (4.30), the approximate form of frequencies in this diffusion-dominated phase is

$$\lambda_{1,4}\approx\pm\frac{2\Omega k_z}{k}+i\frac{k_z^2}{\tau k^2},$$

$$\lambda_{3,2}\approx\pm\frac{2\Omega V_A^2 k_z^3}{\eta^2 k^5}+i\eta k^2.$$

Kinetic energy

The fast wave component of the toroidal velocity field $\hat{u}_{\phi,f} = A_1\ e^{i\lambda_1 t}$ is considered. Following a similar procedure as in Appendix E, the approximate form of $\hat{u}_{\phi,f}$ is

$$\hat{u}_{\phi,f} \approx \frac{\hat{u}_{\phi 0}}{2}\exp\left(-\frac{k_z^2 t}{\tau k^2}\right)\left[\cos\left(\frac{2\Omega k_z t}{k}\right) - \frac{2\Omega V_A^2 k_z^3}{\eta^3 k^7}\sin\left(\frac{2\Omega k_z t}{k}\right)\right]. \tag{4.77}$$

For large times $t \gg \tau$, $k_z \ll k_s$ (so that $k \approx k_s$). Hence, (4.77) becomes

$$\hat{u}_{\phi,f} \approx \frac{\hat{u}_{\phi 0}}{2}\exp\left(-\frac{k_z^2 t}{\tau k^2}\right)\cos\left(\frac{2\Omega k_z t}{k}\right).$$

Now, the *qs* toroidal velocity field solution from (4.59)

$$\hat{u}_{\phi,qs} = \left(\frac{a_2 - a_1\lambda_2}{\lambda_1 - \lambda_2}\right)e^{i\lambda_1 t} - \left(\frac{a_2 - a_1\lambda_1}{\lambda_1 - \lambda_2}\right)e^{i\lambda_2 t},$$

is considered, where $a_1 = \hat{u}_{\phi 0},\ \ a_2 = i\nu k^2 \hat{u}_{\phi 0}$ and $\lambda_{1,2}$ are the *qs* frequencies obtained in (4.16). In the inviscid limit, (4.59) simplifies to

$$\hat{u}_{\phi,qs} = \hat{u}_{\phi 0}\exp\left(-\frac{k_z^2 t}{\tau k^2}\right)\left[\cos\left(\frac{2\Omega k_z t}{k}\right) + \frac{k_z}{2\Omega\tau k}\sin\left(\frac{2\Omega k_z t}{k}\right)\right]. \tag{4.78}$$

Since $k_z \ll k$, (4.78) approximately becomes

$$\hat{u}_{\phi,qs} \approx \hat{u}_{\phi 0}\exp\left(-\frac{k_z^2 t}{\tau k^2}\right)\cos\left(\frac{2\Omega k_z t}{k}\right).$$

This shows that the $\hat{u}_{\phi,f}$ is same as the $\hat{u}_{\phi,qs}$ solution. The kinetic energy $E_{k,qs}$ associated with this velocity field is

$$E_{k,qs} = 16\pi^4 \int_0^\infty \int_0^\infty |\hat{u}_{\phi,f}|^2\ k_s\ dk_s\ dk_z.$$

This integration is same as the one performed in section 3.4.1. Following a similar procedure, the *qs* kinetic energy is

$$\begin{aligned} E_{k,qs} &\approx \frac{3\delta^5\pi^2}{256}\left(\frac{t}{\tau}\right)^{-1/2}, \\ E_{k,qs} &\approx c_8\left(\frac{t}{\tau}\right)^{-1/2}, \end{aligned} \tag{4.79}$$

where the constant $c_8 = 3\delta^5\pi^2/256$.

Magnetic energy

The fast wave component of the toroidal magnetic field $\hat{b}_{\phi,f} = A_2\, e^{i\lambda_1 t}$ is considered. Following a similar procedure as in Appendix E, the approximate form of $\hat{b}_{\phi,f}$ is

$$\hat{b}_{\phi,f} \approx i\frac{\hat{u}_{\phi 0}B_0k_z}{2\eta k^2}\exp\left(-\frac{k_z^2t}{\tau k^2}\right)\left[\cos\left(\frac{2\Omega k_zt}{k}\right)+\frac{2\Omega k_z}{\eta k^3}\sin\left(\frac{2\Omega k_zt}{k}\right)\right]. \tag{4.80}$$

Since $k_z \ll k$, (4.80) becomes

$$\hat{b}_{\phi,f} \approx i\frac{\hat{u}_{\phi 0}B_0k_z}{2\eta k^2}\exp\left(-\frac{k_z^2t}{\tau k^2}\right)\cos\left(\frac{2\Omega k_zt}{k}\right).$$

The *qs* toroidal magnetic field solution from (4.62)

$$\hat{b}_{\phi,qs} = i\frac{B_0k_z}{\eta k^2}\left[\left(\frac{a_2-a_1\lambda_2}{\lambda_1-\lambda_2}\right)e^{i\lambda_1 t}-\left(\frac{a_2-a_1\lambda_1}{\lambda_1-\lambda_2}\right)e^{i\lambda_2 t}\right],$$

is considered, where $a_1 = \hat{u}_{\phi 0}$, $a_2 = i\nu k^2\hat{u}_{\phi 0}$ and λ_1, λ_2 are the *qs* frequencies as given in (4.16). Using (4.78), $\hat{b}_{\phi,qs}$ becomes

$$\hat{b}_{\phi,qs} = \frac{B_0ik_z\hat{u}_{\phi 0}}{\eta k^2}\exp\left(-\frac{k_z^2t}{\tau k^2}\right)\left[\cos\left(\frac{2\Omega k_zt}{k}\right)+\frac{k_z}{2\Omega\tau k}\sin\left(\frac{2\Omega k_zt}{k}\right)\right].$$

For $t \gg \tau$, $\hat{b}_{\phi,qs}$ approximately becomes

$$\hat{b}_{\phi,qs} \approx i\frac{B_0k_z\hat{u}_{\phi 0}}{\eta k^2}\exp\left(-\frac{k_z^2t}{\tau k^2}\right)\cos\left(\frac{2\Omega k_zt}{k}\right).$$

This shows that the $\hat{b}_{\phi,f}$ is same as the $\hat{b}_{\phi,qs}$ solution. The magnetic energy associated with $\hat{b}_{\phi,f}$ field is

$$E_{m,qs} = \frac{16\pi^4}{\mu\rho}\int_0^\infty\int_0^\infty |\hat{b}_{\phi,f}|^2\, k_s\, dk_s\, dk_z.$$

This integration is same as the one performed in section 3.4.2. Following a similar procedure, the *qs* kinetic energy is

$$\begin{aligned} E_{m,qs} &\approx \frac{\pi^2\delta^5}{1024} S_0^2 \left(\frac{t}{\tau}\right)^{-3/2}, \\ E_{m,qs} &\approx c_9 S_0^2 \left(\frac{t}{\tau}\right)^{-3/2}, \end{aligned} \tag{4.81}$$

where the constant $c_9 = \pi^2\delta^5/1024$. From (4.81), it is clear that the *qs* magnetic energy for the rotating case also decays as $S_0^2(t/\tau)^{-3/2}$.

4.7.3 Transition timescales

Kinetic energy's transition time to *qs* regime

The fast wave's kinetic energy in the wave-dominated regime (4.66) and *qs* regime (4.79) are:

$$E_{k,f} \sim \left(\frac{t}{t_1}\right)^{-5/4}, \; E_{k,qs} \sim \left(\frac{t}{\tau}\right)^{-1/2}.$$

These energy estimates are of same order at

$$\begin{aligned} \left(\frac{t}{t_1}\right)^{-5/4} &\sim \left(\frac{t}{\tau}\right)^{-1/2}, \\ \frac{t}{t_1} &\sim \left(\frac{t_1}{\tau}\right)^{2/3}, \\ \frac{t}{t_1} &\sim \left(\frac{4\Omega^2\delta^4}{\eta^2}\right)^{2/3}, \\ \frac{t}{t_1} &\sim E_\eta^{-4/3}, \end{aligned} \tag{4.82}$$

where E_η is the magnetic Ekman number defined as the ratio of inertial time (t_Ω) and magnetic diffusion time (t_η).

$$E_\eta = \frac{\eta}{2\Omega\delta^2}. \tag{4.83}$$

Magnetic Ekman number (E_η) is related to Lehnert number (Le) and Lundquist number (S_0) by

$$E_\eta = \frac{Le}{S_0}. \tag{4.84}$$

The timescale (4.82) is the time at which the kinetic energy undergoes transition to *qs* phase. Let this time be denoted as

$$t_k \sim E_\eta^{-4/3} t_1. \tag{4.85}$$

Magnetic energy's transition time to *qs* regime

The fast wave's magnetic energy in wave-dominated regime (4.70) and *qs* phase (4.81) are:

$$E_{m,f} \sim Le^2 \left(\frac{t}{t_1}\right)^{-7/4}, \quad E_{m,qs} \sim S_0^2 \left(\frac{t}{\tau}\right)^{-3/2}.$$

These energy estimates are of same order at

$$\begin{aligned} Le^2 \left(\frac{t}{t_1}\right)^{-7/4} &\sim S_0^2 \left(\frac{t}{\tau}\right)^{-3/2}, \\ \frac{t}{t_1} &\sim \left(\frac{Le}{S_0}\right)^8 \frac{t_1^6}{\tau^6}, \\ \frac{t}{t_1} &\sim E_\eta^8 \left(\frac{1}{E_\eta^2}\right)^6, \\ \frac{t}{t_1} &\sim E_\eta^{-4}. \end{aligned} \tag{4.86}$$

The estimate (4.86) is the time at which the magnetic energy undergoes transition to *qs* phase. Let this time be denoted as

$$t_m \sim E_\eta^{-4} t_1. \tag{4.87}$$

The energy estimates in the strongly rotating regime discussed in this section are summarized below:

1. Fast wave kinetic energy

$$\frac{E_{k,f}(t)}{E_0} \approx \begin{cases} 1 & (t \ll t_1), \\ (t/t_1)^{-5/4} & (t_1 \ll t \ll t_k), \\ (t/\tau)^{-1/2} & (t \gg t_k), \end{cases} \tag{4.88}$$

2. Fast wave magnetic energy

$$\frac{E_{m,f}(t)}{E_0} \approx \begin{cases} Le^2 & (t_\Omega \ll t \ll t_1), \\ Le^2(t/t_1)^{-7/4} & (t_1 \ll t \ll t_m), \\ S_0^2(t/\tau)^{-3/2} & (t \gg t_m), \end{cases} \tag{4.89}$$

3. Slow wave kinetic energy

$$\frac{E_{k,s}(t)}{E_0} \approx \begin{cases} Le^4 & (t \ll t_\eta), \\ Le^4(t/t_\eta)^{-9/2} & (t \gg t_\eta), \end{cases} \tag{4.90}$$

4. Slow wave magnetic energy

$$\frac{E_{m,s}(t)}{E_0} \approx Le^2(t/t_\eta)^{-7/2} \quad (t \gg t_\eta), \tag{4.91}$$

These energy transitions in the strongly rotating regime are shown in the figure 4.2. The fast wave kinetic energy (solid blue) remains of same order as the initial kinetic energy E_0 for times $t \ll t_1$, where $t_1 = 4\Omega^2/\eta V_A^2 k_0^4$. It then decays as $t^{-5/4}$ for times $t_1 \ll t \ll t_k$, where $t_k \sim E_\eta^{-4/3} t_1$ is the *qs* transition timescale after which the energy decays as $t^{-1/2}$. Similarly, the fast wave magnetic energy (solid red) is of order $Le^2 E_0$ for $t_\Omega \ll t \ll t_1$. It decays as $t^{-7/4}$ for $t_1 \ll t \ll t_m$, where $t_m \sim E_\eta^{-4} t_1$ is the *qs* transition timescale after which the energy decays as $t^{-3/2}$.

The slow wave kinetic energy (magenta) is of order Le^4E_0 for $t \ll t_\eta$ and it decays rapidly at a rate $t^{-9/2}$ for $t \gg t_\eta$. The slow wave magnetic energy is in a transient phase for $t \ll t_s$ (dashed black). Therefore, there exists no scaling for this energy during this time period. For $t \gg t_s$, the magnetic energy decays as $t^{-7/2}$. The timescale t_1 can be written as

$$t_1 = \frac{4\Omega^2\delta^2}{V_A^2} \times \frac{\delta^2 k_0^2}{\eta k_0^2} = \frac{5t_\eta}{Le^2}. \tag{4.92}$$

Since Le is always less than one for a strongly rotating regime, from (4.92), it is clear that the timescale t_1 will always be greater than diffusion timescale t_η. Hence, the slow wave energies decay earlier than the corresponding fast wave energies.

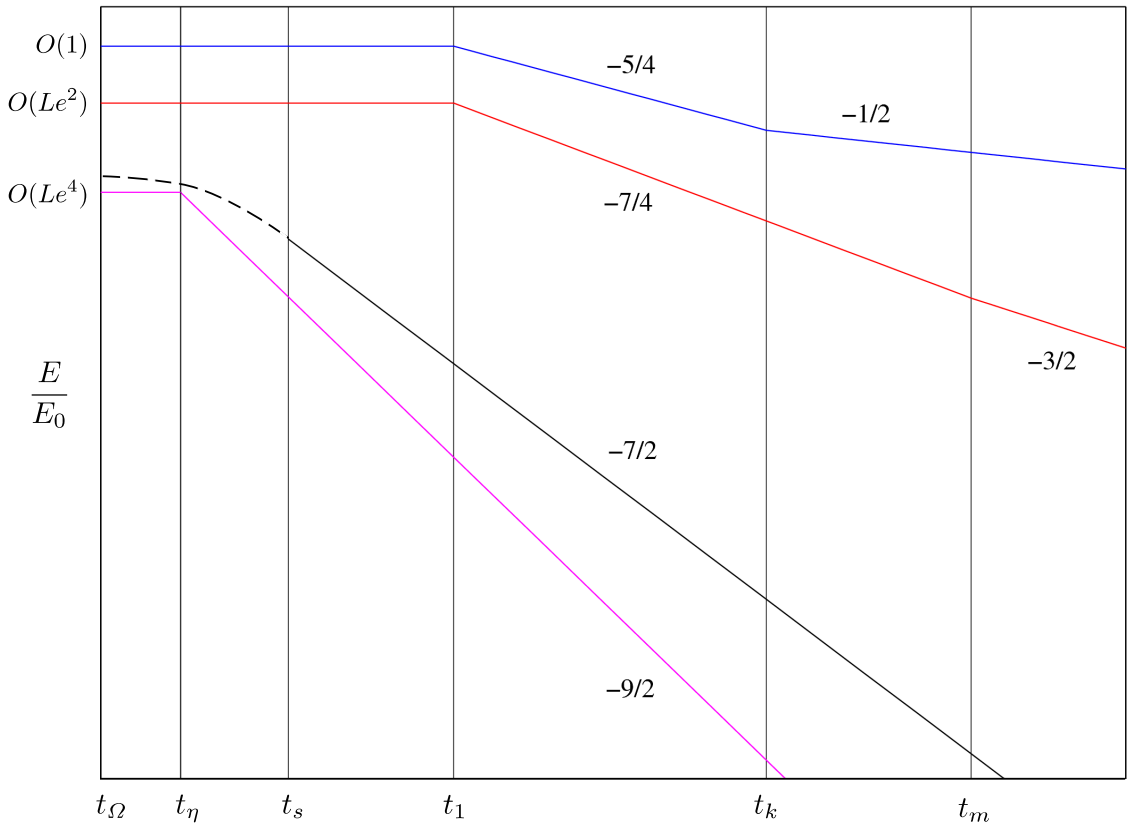

Fig. 4.2 Decay of fast wave kinetic (blue) and magnetic (red) energies, slow wave kinetic (magenta) and magnetic (black) energies. t_s is the slow wave propagation timescale. $t_k \sim E_\eta^{-4/3} t_1$ and $t_m \sim E_\eta^{-4} t_1$ are the *qs* transition timescales of fast wave's kinetic and magnetic energies respectively, where $t_1 = 4\Omega^2/\eta V_A^2 k_0^4$ and $E_\eta = \eta/2\Omega\delta^2$.

4.8 Analytical energy estimates in weakly rotating regime

The general solutions of toroidal velocity and magnetic fields are

$$\hat{u}_\phi = A_1 e^{i\lambda_1 t} + B_1 e^{i\lambda_2 t} + C_1 e^{i\lambda_3 t} + D_1 e^{i\lambda_4 t},$$
$$\hat{b}_\phi = A_2 e^{i\lambda_1 t} + B_2 e^{i\lambda_2 t} + C_2 e^{i\lambda_3 t} + D_2 e^{i\lambda_4 t}.$$

From these general solutions, the components of velocity and magnetic fields from modes λ_1 and λ_2 are considered. These solutions are defined as:

$$\hat{u}_{\phi,1} = A_1 e^{i\lambda_1 t},\ \ \hat{b}_{\phi,1} = A_2 e^{i\lambda_1 t},\ \ \hat{u}_{\phi,2} = B_1 e^{i\lambda_2 t},\ \ \hat{b}_{\phi,2} = B_2 e^{i\lambda_2 t}.$$

The approximate form of these solutions are obtained using which the kinetic and magnetic energies in this weakly rotating are estimated. In the following section, the wave-dominated regime is considered.

4.8.1 Wave-dominated regime $(V_A k_z \gg \Omega k_z/k \gg \eta k^2/2)$

From (4.37), the approximate form of frequencies $\lambda_1 - \lambda_4$ in this wave-dominated regime are:

$$\lambda_{1,4} \approx \pm\left(V_A k_z + \frac{\Omega k_z}{k}\right) + i\left(\frac{\eta k^2}{2} - \frac{\Omega \eta k}{2V_A}\right),$$
$$\lambda_{3,2} \approx \pm\left(V_A k_z - \frac{\Omega k_z}{k}\right) + i\left(\frac{\eta k^2}{2} + \frac{\Omega \eta k}{2V_A}\right).$$

Following a similar approach in Appendix E, the simplified form of $\hat{u}_{\phi,1}$, $\hat{b}_{\phi,1}$, $\hat{u}_{\phi,2}$ and $\hat{b}_{\phi,2}$ are:

$$\hat{u}_{\phi,1} \approx \frac{\hat{u}_{\phi 0}}{4}\exp\left[-\left(\frac{\eta k^2}{2} - \frac{\Omega \eta k}{2V_A}\right)t\right]\left(\cos\left[\left(V_A k_z + \frac{\Omega k_z}{k}\right)t\right]\right.$$
$$\left. + \left(\frac{\eta k^2}{2V_A k_z} - \frac{9\Omega \eta k}{4V_A^2 k_z}\right)\sin\left[\left(V_A k_z + \frac{\Omega k_z}{k}\right)t\right]\right), \tag{4.93}$$

$$\hat{u}_{\phi,2} \approx \frac{\hat{u}_{\phi 0}}{4}\exp\left[-\left(\frac{\eta k^2}{2}+\frac{\Omega\eta k}{2V_A}\right)t\right]\left(\cos\left[\left(V_A k_z-\frac{\Omega k_z}{k}\right)t\right]\right.$$
$$\left.+\left(\frac{\eta k^2}{2V_A k_z}+\frac{9\Omega\eta k}{4V_A^2 k_z}\right)\sin\left[\left(V_A k_z-\frac{\Omega k_z}{k}\right)t\right]\right), \tag{4.94}$$

$$\hat{b}_{\phi,1} \approx i\sqrt{\mu\rho}\frac{\hat{u}_{\phi 0}}{4}\exp\left[-\left(\frac{\eta k^2}{2}-\frac{\Omega\eta k}{2V_A}\right)t\right]\left(\sin\left[\left(V_A k_z+\frac{\Omega k_z}{k}\right)t\right]\right.$$
$$\left.+\left(\frac{3\eta\Omega k}{4V_A^2 k_z}\right)\cos\left[\left(V_A k_z+\frac{\Omega k_z}{k}\right)t\right]\right), \tag{4.95}$$

$$\hat{b}_{\phi,2} \approx i\sqrt{\mu\rho}\frac{\hat{u}_{\phi 0}}{4}\exp\left[-\left(\frac{\eta k^2}{2}+\frac{\Omega\eta k}{2V_A}\right)t\right]\left(\sin\left[\left(V_A k_z-\frac{\Omega k_z}{k}\right)t\right]\right.$$
$$\left.+\left(\frac{3\eta\Omega k}{4V_A^2 k_z}\right)\cos\left[\left(V_A k_z-\frac{\Omega k_z}{k}\right)t\right]\right). \tag{4.96}$$

For $V_A k/\Omega \to \infty$, the solutions (4.93), (4.94) become

$$\hat{u}_{\phi,1} \approx \hat{u}_{\phi,2} \approx \frac{\hat{u}_{\phi 0}}{4}\exp\left(-\frac{\eta k^2}{2}t\right)\left[\cos\left(V_A k_z t\right)+\left(\frac{\eta k^2}{2V_A k_z}\right)\sin\left(V_A k_z t\right)\right], \tag{4.97}$$

which is similar to the non-rotating damped Alfvén wave solution (3.25). Similarly, the solutions (4.95), (4.96) become

$$\hat{b}_{\phi,1} \approx \hat{b}_{\phi,2} \approx \frac{i\sqrt{\mu\rho}}{4}\hat{u}_{\phi 0}\exp\left(-\frac{\eta k^2 t}{2}\right)\sin\left(V_A k_z t\right), \tag{4.98}$$

which is similar to the non-rotating magnetic field solution obtained in (3.32).

From (4.97) and (4.98), it is evident that the velocity and magnetic fields propagate as damped Alfvén waves in this wave-dominated regime. Hence, the kinetic and magnetic energies follow similar decay laws as obtained in equations (3.34),(3.28) of the non-rotating section 3.4:

$$E_k \approx E_m \approx \frac{25\sqrt{5}\pi^{3/2}\delta^5}{1024}\left(\frac{t}{t_\eta}\right)^{-5/2}.$$

4.8.2 Diffusion-dominated regime $(\eta k^2/2 \gg V_A k_z \gg \Omega k_z/k)$

From the approximate form of $\lambda_{1,4}$ in the weakly rotating, diffusion-dominated regime (4.44), it is evident that these frequencies are same as the *qs* modes obtained in (4.16). Even the strongly rotating, diffusion-dominated regime is a *qs* phase. Therefore, the kinetic and magnetic energy estimates in this regime would be same as that derived in section 4.7.2 which are:

$$E_{k,qs} \approx \frac{3\delta^5\pi^2}{256}\left(\frac{t}{\tau}\right)^{-1/2}, \quad E_{m,qs} \approx \frac{\pi^2\delta^5 S_0^2}{1024}\left(\frac{t}{\tau}\right)^{-3/2}.$$

The fact that the weakly rotating regime tends to the non-rotating limit would eventually give the same transition times as obtained in section 3.4 which are $\sqrt{S_0}t_\eta$ for kinetic energy and $S_0 t_\eta$ for the magnetic energy.

The Earth's core is a rapidly rotating system. A small-scale structure of 10 km under a magnetic field of strength 2 mT will undergo transition to *qs* state at timescales $t_k \sim 10^9$ years and $t_m \sim 10^{20}$ years, which are significantly longer than the core travel times of fast and slow MC waves.

4.9 Summary

The case of evolution of vortex in presence of rotation and magnetic field is studied in this chapter. The dispersion relation shows that the blob would evolve as fast and slow MC waves. The general expressions for the toroidal velocity and magnetic fields are derived. From these solutions, the approximate form of the fast and slow wave components are obtained using which the energy transitions are evaluated analytically.

The analytical energy estimates show that in the strongly rotating regime, the fast wave kinetic and magnetic energies decay on a timescale $t_1 = 4\Omega^2/\eta V_A^2 k_0^4$. For $t \gg t_1$, the kinetic and magnetic energies decay as $t^{-5/4}$ and $t^{-7/4}$ respectively. The transition to *qs* phase occurs at $t_k \sim E_\eta^{-4/3} t_1$ and $t_m \sim E_\eta^{-4} t_1$ for the fast wave kinetic and magnetic energies

respectively. In the *qs* phase, the kinetic and magnetic energies decay as $t^{-1/2}$ and $t^{-3/2}$ respectively. For $t \ll t_\eta$, the slow wave kinetic energy is of order Le^4E_0 and for $t \gg t_\eta$, the energy decays as $t^{-9/2}$. For $t \gg t_s$, magnetic energy decays as $t^{-7/2}$. This rapid decay causes the slow wave to have very small energy content at large times.

The weakly rotating regime tends to a non-rotating situation where the vortex would evolve as a damped Alfvén wave. The kinetic and magnetic energies have similar transition characteristics as obtained in Chapter 3.

Chapter 5

Conclusion

Rapid rotation of the Earth's core gives rise to small-scale convection columns for which the magnetic Reynolds number R_m is small. While the smallest lengthscale that can survive in the core against magnetic diffusion is not well constrained, it is clear from rapidly rotating geodynamo simulations that the self-generated magnetic field does not significantly change the lengthscale of convection so as to render small scales unimportant. Convective scales of $R_m \sim 1$ are likely to exist, for which the low R_m approximation gives a good qualitative description. Studies on small-scale turbulence in the core have largely followed the quasi-static (qs) approximation where the growth rate of the induced field is considered small in comparison with the diffusion frequency in the limit of $R_m \ll 1$. Because the qs model predicts pseudo-diffusion of momentum along the magnetic field lines, MHD waves generated by small-scale flow perturbations have not received adequate attention in the treatment of turbulence of the Earth's core. This thesis investigates the dynamics of damped MHD waves with and without background rotation.

The simplified model of an isolated axisymmetric vortex in a mean magnetic field has the advantage that viscous effects can be kept small by the choice of a low, Earth-like magnetic Prandtl number. Furthermore, for Lundquist numbers $S_0 \sim 100$, the nonlinear inertial force is very small compared to the Lorentz force (and by extension, the Coriolis force) on the

core travel timescale of Alfvén waves. Therefore, it is likely that these waves are generated from small-scale convection columns that exist in an approximate magnetostrophic balance.

Under background rotation and a uniform magnetic field acting in the same (z) direction, an isolated vortex evolves into damped fast and slow MC waves. Rapid rotation delays the wave–diffusion transition of the fast wave component because the energy decays at a much slower rate than that for the non-rotating case. This result suggests that rapid rotation aids wave motion of low R_m flows in the Earth's core. Since turbulence is made up of an ensemble of isolated vortices, the results obtained for an isolated vortex are extendible without loss of generality to rotating MHD turbulence.

The case of coaxial rotation and magnetic field acting on a vortex serves as a first step in understanding MC waves in the Earth's core where the resultant magnetic field likely makes an angle with the rotation axis. The three-dimensional problem of a vortex evolving under z-rotation and an arbitrarily oriented magnetic field should be the subject of future work.

References

M. Abramowitz and I. A. Stegun. *Handbook of Mathematical Functions with Formulas, Graphs, and Mathematical Tables*. U.S. Govt. Printing Office, Washington, D.C., 1964.

D. J. Acheson and R. Hide. Hydromagnetics of rotating fluids. *Rep. Prog. Phys.*, 36:159, 1973.

T. Alboussière, P. Cardin, F. Debray, P. L. Rizza, J. Masson, F. Plunian, A. Riberio, and D. Schmitt. Experimental evidence of Alfvén wave propagation in a Gallium alloy. *Phys. Fluids*, 23:096601, 2011.

A. Alemany, R. Moreau, P. L. Sulem, and U. Frisch. Influence of an external magnetic field on homogeneous MHD turbulence. *J. de Mécanique*, 18:277–312, 1979.

H. Alfvén. Existence of Electromagnetic-Hydrodynamic Waves. *Nature*, 150:405–406, 1942.

S. I. Braginsky. Magnetohydrodynamics of the Earth's core. *Geomag. Aeron. (English translation)*, 4:698–712, 1964.

S. I. Braginsky. Magnetic waves in the Earth's core. *Geomag. Aeron. (English translation)*, 7:851–859, 1967.

S. I. Braginsky. Torsional magnetohydrodynamic vibrations in the Earth's core and variations in day length. *Geomag. Aeron. (English translation)*, 10:1–8, 1970.

S. I. Braginsky. Short- period geomagnetic secular variation. *Geophys. Astrophys. Fluid Dyn.*, 30:1–78, 1984.

S. I. Braginsky and V. P. Meytlis. Local turbulence in the Earth's core. *Geophys. Astrophys. Fluid Dyn.*, 55:2:71–87, 1990.

E. C. Bullard, C. Freedman, H. Gellman, and J. Nixon. The westward drift of the earth's magnetic field. *Philos. Trans. R. Soc. London, Ser. A*, 243:67–92, 1950.

F. H. Busse. Thermal instabilities in rapidly rotating systems. *J. Fluid Mech.*, 44:441–460, 1970.

S. Chandrasekhar. *Hydrodynamic and Hydromagnetic Stability*. Dover publications, New York, 1961.

P. A. Davidson. Magnetic damping of jets and vortices. *J. Fluid Mech.*, 299:153–186, 1995.

P. A. Davidson. *An introduction to Magnetohydrodynamics*. Cambridge University Press, New York, 2001.

P. A. Davidson and F. Siso-Nadal. On the structure of small-scale motion in the core of the Earth. *Geophys. Astrophys. Fluid Dyn.*, 96:1:49–76, 2002.

P. A. Davidson, P. J. Staplehurst, and S. B. Dalziel. On the evolution of eddies in a rapidly rotating system. *J. Fluid Mech.*, 557:135–144, 2006.

O. U. V. Fuentes. Kelvin's discovery of Taylor columns. *European Journal of Mechanics B/Fluids*, 28:469–472, 2009.

N. Gillet, D. Jault, E. Canet, and A. Fournier. Fast torsional waves and strong magnetic field within the Earth's core. *Nature*, 465:74–77, 2010.

I. S. Gradshteyn and I. M. Ryzhik. *Table of integrals, series and products*. Academic Press, Russia, 2007.

H. P. Greenspan. *The theory of rotating fluids*. Cambridge University Press, London, 1968.

R. Hide. Free hydromagnetic oscillations of the Earth's core and the theory of the geomagnetic secular variation. *Philos. Trans. R. Soc. London, Ser. A*, 259:615–647, 1966.

R. Holme and K. A. Whaler. Steady core flow in an azimuthally drifting reference frame. *Geophys. J. Int.*, 145:560–569, 2001.

K. Hori, C. A. Jones, and R. J. Teed. Slow magnetic Rossby waves in the Earth's core. *Geophys. Res. Lett.*, 42:6622–6629, 2015.

S. S. Hough. On the application of harmonic analysis to the dynamical theory of the tides. part I. on Laplace's "oscillations of the first species", and on the dynamics of ocean currents. *Proc. R. Soc. Lond.*, 61:236–238, 1897.

A. Jackson. Intense equatorial flux spots on the surface of the Earth's core. *Nature*, 424: 760–763, 2003.

A. Jackson, A. R. T. Jonkers, and M. R. Walker. Four centuries of geomagnetic secular variation from historical records. *Philos. Trans. R. Soc. London, Ser. A*, 358:957–990, 2000.

A. Jameson. *Magnetohydrodynamic waves*. PhD dissertation, University of Cambridge, 1961.

D. Jault. Axial invariance of rapidly varying diffusionless motions in the Earth's core interior. *Phys. Earth Planet. Inter.*, 166:67–76, 2008.

D. Jault, C. Gire, and J. L. Le Mouel. Westward drift, core motions and exchanges of angular momentum between core and mantle. *Nature*, 333:353–356, 1988.

B. Lehnert. Magnetohydrodynamic waves under the action of the Coriolis force. *Astrophys. J.*, 119:647, 1954a.

B. Lehnert. Magnetohydrodynamic waves in liquid sodium. *The Phys. Rev.*, 94:4:815–824, 1954b.

B. Lehnert. Magnetohydrodynamic waves under the action of the Coriolis force II. *Astrophys. J.*, 121:481–490, 1955a.

B. Lehnert. The decay of magneto-turbulence in the presence of a magnetic field and Coriolis force. *Quart. Appl. Math.*, 12:321–341, 1955b.

D. E. Loper and H. Shimizu. Time and length scales of buoyancy-driven flow structures in a rotating hydromagnetic fluid. *Phys. Earth Planet. Inter.*, 104:307–329, 1997.

S. Lundquist. Experimental Investigations of Magneto-Hydrodynamic Waves. *Phys. Rev.*, 76:1805–1809, 1949.

M. Matsushima, N. Nakajima, and P. H. Roberts. The anisotropy of local turbulence in the Earth's core. *Earth Planets Space*, 51:277–286, 1999.

H. K. Moffatt. On the suppression of turbulence by a uniform magnetic field. *J. Fluid Mech*, 28:571–592, 1967.

H. K. Moffatt. *Magnetic field generation in electrically conducting fluids*. Cambridge University Press, Great Britain, 1978.

H. K. Moffatt and D. E. Loper. The magnetostrophic rise of a buoyant parcel in the Earth's core. *Geophys. J. Int.*, 117:394–402, 1994.

J. E. Mound and B. A. Buffet. Mechanisms of core-mantle angular momentum exchange and the observed spectral properties of torsional oscillations. *J. Geophys. Res.*, 110: B08103, 2005.

J. E. Mound and B. A. Buffet. Detection of a gravitational oscillation in length-of-day. *Earth Planet. Sci. Lett*, 243:383–389, 2006.

J. Proudman. On the motion of solids in a liquid possessing vorticity. *Proc. R. Soc. Lond. A*, 92:408–424, 1916.

P. H. Roberts. *An Introduction to Magnetohydrodynamics*. Longmans, Great Britain, 1967.

C. G. Rossby. Relation between variations in the intensity of the zonal circulation of the atmosphere and the displacements of the semi-permanent centres of action. *J. Mar. Res.*, 2(1):33–55, 1939.

J. Sommeria and R. Moreau. Why, how, and when, MHD turbulence becomes two-dimensional. *J. Fluid Mech.*, 118:507–518, 1982.

B. Sreenivasan. Breakdown of a magnetohydrodynamic flow structure. *Phys. Fluids*, 15: 2041–2046, 2003.

B. Sreenivasan and T. Alboussière. Evolution of a vortex in a magnetic field. *Eur. J. Mech.*, 19:403–421, 2000.

B. Sreenivasan and T. Alboussière. Experimental study of a vortex in a magnetic field. *J. Fluid Mech.*, 464:287–309, 2002.

B. Sreenivasan and C. A. Jones. The role of inertia in the evolution of spherical dynamos. *Geophys. J. Int*, 164(2):467–476, 2006.

M. G. St Pierre. On the local nature of turbulence in Earth's outer core. *Geophys. Astrophys. Fluid Dyn.*, 83:293–306, 1996.

S. Starchenko and C. A. Jones. Typical velocities and magnetic field strengths in planetary interiors. *Icarus*, 157:426–435, 2002.

G. I. Taylor. Motion of solids in fluids when the flow is not irrotational. *Proc. R. Soc. Lond. Ser. A*, 93:99–113, 1917.

R. J. Teed, C. A. Jones, and S. M. Tobias. The dynamics and excitation of torsional waves in geodynamo simulations. *Geophys. J. Int.*, 196:724–735, 2014.

R. J. Teed, C. A. Jones, and S. M. Tobias. The transition to Earth-like torsional oscillations in magnetoconvection simulations. *Earth Planet. Sci. Lett*, 419:22–31, 2015.

E.W. Weisstein. *CRC Concise Encyclopedia of Mathematics*. Chapman and Hall/CRC, Boca Raton, Florida, 2003.

J. Wicht and U. R. Christensen. Torsional oscillations in dynamo simulations. *Geophys. J. Int.*, 181:1367–1380, 2010.

Appendix A

Integrals

A.1 Gaussian integrals

The solutions for the Gaussian integrals of the form

$$I_n(a) = \int_0^\infty x^n e^{-ax^2} dx,$$

are reported in this appendix. The proofs for the following solutions are available in Weisstein (2003).

$$I_n(a) = \int_0^\infty e^{-ax^2} x^n dx = \begin{cases} \dfrac{(n-1)!!}{2^{n/2+1} a^{n/2}} \sqrt{\dfrac{\pi}{a}} & \text{n is even} \\ \\ \dfrac{[\frac{1}{2}(n-1)]!}{2a^{(n+1)/2}} & \text{n is odd} \end{cases} \tag{A.1}$$

From (A.1), a few Gaussian integrals are:

$$I_2(a) = \frac{1}{4a}\sqrt{\frac{\pi}{a}}, \quad I_3(a) = \frac{1}{2a^2}, \quad I_4(a) = \frac{3}{8a^2}\sqrt{\frac{\pi}{a}}.$$

A.2 Evaluating $I_A = \int_0^\infty x^4\, e^{(-ax^2-bx^4)}\, dx$

From 3.469 in Gradshteyn and Ryzhik (2007), the integral

$$I = \int_0^\infty e^{-\mu x^4 - 2\nu x^2}\, dx = \frac{1}{4}\sqrt{\frac{2\nu}{\mu}}\, \exp\left(\frac{\nu^2}{2\mu}\right)\, K_{1/4}\left(\frac{\nu^2}{2\mu}\right),$$

is considered, where $K_\nu(X)$ is the modified Bessel function of the second kind. Substituting $\mu = b$ and $2\nu = a$, the integral becomes

$$I = \int_0^\infty e^{-ax^2-bx^4}\, dx = \frac{1}{4}\sqrt{\frac{a}{b}}\, \exp\left(\frac{a^2}{8b}\right)\, K_{1/4}\left(\frac{a^2}{8b}\right).$$

Using the Leibniz integral rule,

$$I_A = -\frac{\partial I}{\partial b} = \int_0^\infty x^4\, e^{(-ax^2-bx^4)}\, dx. \tag{A.2}$$

The partial derivative of I with respect to b is given by

$$\frac{\partial I}{\partial b} = -\frac{\sqrt{a}\, e^{a^2/8b}}{8\, b^{3/2}}\, K_{1/4}\left(\frac{a^2}{8b}\right) - \frac{a^{5/2}\, e^{a^2/8b}}{32\, b^{5/2}}\, K_{1/4}\left(\frac{a^2}{8b}\right) + \frac{1}{4}\sqrt{\frac{a}{b}}\, e^{a^2/8b}\, \frac{\partial}{\partial b}\left[K_{1/4}\left(\frac{a^2}{8b}\right)\right]. \tag{A.3}$$

The following identity is used to evaluate the differentiation of modified Bessel function

$$\frac{dK_\nu(X)}{dX} = -\frac{1}{2}\left[K_{\nu-1}(X) + K_{\nu+1}(X)\right]. \tag{A.4}$$

Now, let $\dfrac{a^2}{8b} = Z$ such that $db = -b\dfrac{dZ}{Z}$. Using these substitutions and the identity (A.4), the derivative of $K_{1/4}(Z)$ with respect to b is given by

$$\begin{aligned}\frac{\partial}{\partial b}\left[K_{1/4}\left(\frac{a^2}{8b}\right)\right] &= -\frac{Z}{b}\frac{\partial K_{1/4}(Z)}{\partial Z}, \\ &= -\frac{a^2}{16b^2}\left[K_{-3/4}\left(\frac{a^2}{8b}\right) + K_{5/4}\left(\frac{a^2}{8b}\right)\right].\end{aligned} \tag{A.5}$$

Now, the following identities

$$K_\nu(X) = K_{\nu-2}(X) + \frac{2(\nu-1)}{X}\, K_{\nu-1}(X), \;\; K_{-\nu}(X) = K_\nu(X), \tag{A.6}$$

are considered. Using (A.6),

$$\begin{aligned} K_{5/4}(X) &= K_{3/4}(X) + \frac{1}{2X}K_{3/4}(X), \\ K_{5/4}(X) + K_{3/4}(X) &= 2K_{3/4}(X) + \frac{1}{2X}K_{3/4}(X), \\ \implies K_{-3/4}\left(\frac{a^2}{8b}\right) + K_{5/4}\left(\frac{a^2}{8b}\right) &= 2K_{3/4}\left(\frac{a^2}{8b}\right) + \frac{4b}{a^2}K_{1/4}\left(\frac{a^2}{8b}\right). \end{aligned}$$

Using this equation, the derivative (A.5) can be written as

$$\frac{\partial}{\partial b}\left[K_{1/4}\left(\frac{a^2}{8b}\right)\right] = -\frac{a^2}{16b^2}\left[2K_{3/4}\left(\frac{a^2}{8b}\right) + \frac{4b}{a^2}K_{1/4}\left(\frac{a^2}{8b}\right)\right]. \tag{A.7}$$

Using (A.7), (A.3) becomes

$$\begin{aligned} \frac{\partial I}{\partial b} &= \frac{\sqrt{a}\, e^{a^2/8b}}{32\, b^{5/2}}\left[-(a^2+4b)K_{1/4}\left(\frac{a^2}{8b}\right) + \frac{a^2}{2}\left(2K_{3/4}\left(\frac{a^2}{8b}\right) + \frac{4b}{a^2}K_{1/4}\left(\frac{a^2}{8b}\right)\right)\right], \\ &= \frac{\sqrt{a}\, e^{a^2/8b}}{32\, b^{5/2}}\left[-(a^2+2b)K_{1/4}\left(\frac{a^2}{8b}\right) + a^2K_{3/4}\left(\frac{a^2}{8b}\right)\right]. \end{aligned} \tag{A.8}$$

Using (A.8) , the integral I_A in (A.2) becomes

$$I_A = \int_0^\infty x^4\, e^{(-ax^2-bx^4)}\, dx = \frac{\sqrt{a}\, e^{a^2/8b}}{32\, b^{5/2}}\left[(a^2+2b)K_{1/4}\left(\frac{a^2}{8b}\right) - a^2K_{3/4}\left(\frac{a^2}{8b}\right)\right]. \tag{A.9}$$

A.3 Evaluating $I_B = \int_0^\infty x^6\, e^{(-ax^2-bx^4)}\, dx$

From (A.9),

$$I_A = \int_0^\infty x^4\, e^{(-ax^2-bx^4)}\, dx = \frac{\sqrt{a}\, e^{a^2/8b}}{32\, b^{5/2}}\left[(a^2+2b)K_{1/4}\left(\frac{a^2}{8b}\right) - a^2K_{3/4}\left(\frac{a^2}{8b}\right)\right].$$

Using Leibniz integral rule,

$$I_B = -\frac{\partial I_A}{\partial a} = \int_0^\infty x^6\, e^{(-ax^2-bx^4)}\, dx. \tag{A.10}$$

The partial derivative of I_A with respect to a is

$$\frac{\partial I_A}{\partial a} = \frac{e^{a^2/8b}}{256\sqrt{a}b^{7/2}}\left[8b^2K_{1/4}\left(\frac{a^2}{8b}\right) + 24a^2bK_{1/4}\left(\frac{a^2}{8b}\right) - 20a^2bK_{3/4}\left(\frac{a^2}{8b}\right) - 2a^2bK_{5/4}\left(\frac{a^2}{8b}\right) + 2a^4K_{1/4}\left(\frac{a^2}{8b}\right) - 2a^4K_{3/4}\left(\frac{a^2}{8b}\right) - a^4K_{5/4}\left(\frac{a^2}{8b}\right) + a^4K_{7/4}\left(\frac{a^2}{8b}\right) + a^4K_{-1/4}\left(\frac{a^2}{8b}\right) - \left(a^4+2a^2b\right)K_{-3/4}\left(\frac{a^2}{8b}\right)\right].$$

Using $K_{-\nu}(X) = K_\nu(X)$ identity,

$$\frac{\partial I_A}{\partial a} = \frac{e^{a^2/8b}}{256\sqrt{a}b^{7/2}}\left[(8b^2+24a^2b+3a^4)K_{1/4}\left(\frac{a^2}{8b}\right) - \left(3a^4+22a^2b\right)K_{3/4}\left(\frac{a^2}{8b}\right) - (a^4+2a^2b)K_{5/4}\left(\frac{a^2}{8b}\right) + a^4K_{7/4}\left(\frac{a^2}{8b}\right)\right].$$

Using the identity in (A.6), $K_{5/4}\left(\frac{a^2}{8b}\right)$ and $K_{7/4}\left(\frac{a^2}{8b}\right)$ can be written as

$$K_{5/4}\left(\frac{a^2}{8b}\right) = K_{3/4}\left(\frac{a^2}{8b}\right) + \frac{4b}{a^2}K_{1/4}\left(\frac{a^2}{8b}\right),$$
$$K_{7/4}\left(\frac{a^2}{8b}\right) = K_{1/4}\left(\frac{a^2}{8b}\right) + \frac{12b}{a^2}K_{3/4}\left(\frac{a^2}{8b}\right).$$

Substituting these expressions for $K_{5/4}\left(\frac{a^2}{8b}\right)$ and $K_{7/4}\left(\frac{a^2}{8b}\right)$ in $\partial I_A/\partial a$ gives

$$\frac{\partial I_A}{\partial a} = \frac{a^{3/2}e^{a^2/8b}}{64b^{7/2}}\left[(a^2+5b)K_{1/4}\left(\frac{a^2}{8b}\right) - \left(a^2+3b\right)K_{3/4}\left(\frac{a^2}{8b}\right)\right]. \tag{A.11}$$

Using (A.11), the integral I_B in (A.10) becomes

$$I_B = \int_0^\infty x^6\, e^{(-ax^2-bx^4)}\, dx = \frac{a^{3/2}e^{a^2/8b}}{64b^{7/2}}\left[\left(a^2+3b\right)K_{3/4}\left(\frac{a^2}{8b}\right) - (a^2+5b)K_{1/4}\left(\frac{a^2}{8b}\right)\right]. \tag{A.12}$$

A.4 Asymptotic form of I_A and I_B for $b \to \infty$

From (A.9) and (A.12), the following integrals

$$I_A = \frac{\sqrt{a}\, e^{a^2/8b}}{32\, b^{5/2}} \left[(a^2+2b) K_{1/4}\left(\frac{a^2}{8b}\right) - a^2 K_{3/4}\left(\frac{a^2}{8b}\right) \right],$$
$$I_B = \frac{a^{3/2} e^{a^2/8b}}{64 b^{7/2}} \left[\left(a^2+3b\right) K_{3/4}\left(\frac{a^2}{8b}\right) - (a^2+5b) K_{1/4}\left(\frac{a^2}{8b}\right) \right].$$

are considered. The asymptotic form of these integrals for $b \to \infty$ are obtained in this section.

From 9.6.9 in Abramowitz and Stegun (1964), for $\nu > 0$ and $z \to 0$,

$$K_\nu(z) \approx \frac{1}{2}\Gamma(\nu) \left(\frac{z}{2}\right)^{-\nu}. \tag{A.13}$$

For $b \to \infty$, the ratio $\dfrac{a^2}{8b} \to 0$. Hence, using (A.13),

$$K_{1/4}\left(\frac{a^2}{8b}\right) \approx \Gamma(1/4)\frac{b^{1/4}}{a^{1/2}}, \quad K_{3/4}\left(\frac{a^2}{8b}\right) \approx 4\Gamma(3/4)\frac{b^{3/4}}{a^{3/2}}, \quad e^{a^2/8b} \approx 1. \tag{A.14}$$

Using (A.14), (A.9) and (A.12) for $b \to \infty$ becomes

$$\begin{aligned} I_A &= \frac{\sqrt{a}\, e^{a^2/8b}}{32\, b^{5/2}} \left[(a^2+2b) K_{1/4}\left(\frac{a^2}{8b}\right) - a^2 K_{3/4}\left(\frac{a^2}{8b}\right) \right], \\ &\approx \frac{\sqrt{a}}{32} \left[(a^2+2b)\Gamma(1/4)\frac{b^{-9/4}}{a^{1/2}} - 4\Gamma(3/4)\sqrt{a}\, b^{-7/4} \right], \\ I_A &\approx \frac{\Gamma(1/4)}{16} b^{-5/4} + O(b^{-7/4}). \end{aligned} \tag{A.15}$$

$$\begin{aligned} I_B &= \frac{a^{3/2} e^{a^2/8b}}{64 b^{7/2}} \left[\left(a^2+3b\right) K_{3/4}\left(\frac{a^2}{8b}\right) - (a^2+5b) K_{1/4}\left(\frac{a^2}{8b}\right) \right], \\ &\approx \frac{a^{3/2}}{64 b^{7/2}} \left[\left(a^2+3b\right) 4\Gamma(3/4)\frac{b^{3/4}}{a^{3/2}} - (a^2+5b)\Gamma(1/4)\frac{b^{1/4}}{a^{1/2}} \right], \\ I_B &\approx \frac{3\Gamma(3/4)}{16} b^{-7/4} + O(b^{-9/4}). \end{aligned} \tag{A.16}$$

Appendix B

Parseval's theorem for kinetic and magnetic energies

Using cylindrical polar coordinates (s,ϕ,z), the integral

$$I = 2\pi \int_0^\infty \int_0^\infty \boldsymbol{f}(s,z)\, \boldsymbol{g}(s,z)^*\, s\, ds\, dz, \tag{B.1}$$

is considered. The inverse Hankel-Fourier transform of $\boldsymbol{f}(s,z)$ from equation (3.13) is

$$\boldsymbol{f}(s,z) = 4\pi \int_0^\infty \int_0^\infty \hat{\boldsymbol{f}}(k_s,k_z)\, J_1(k_s s)\, e^{ik_z z}\, k_s\, dk_s\, dk_z.$$

Using this inverse transform, integral (B.1) can be written as

$$\begin{aligned}
I &= 2\pi \int_0^\infty \int_0^\infty \left\{ 4\pi \int_0^\infty \int_0^\infty \hat{\boldsymbol{f}}(k_s,k_z)\, J_1(k_s s)\, e^{ik_z z}\, k_s\, dk_s\, dk_z \right\} \boldsymbol{g}(s,z)\, s\, ds\, dz, \\
I &= 16\pi^4 \int_0^\infty \int_0^\infty \left\{ \frac{1}{2\pi^2} \int_0^\infty \int_0^\infty \boldsymbol{g}(s,z)^*\, J_1(k_s s)\, e^{ik_z z}\, s\, ds\, dz \right\} \hat{\boldsymbol{f}}(k_s,k_z)\, k_s\, dk_s\, dk_z, \\
I &= 16\pi^4 \int_0^\infty \int_0^\infty \hat{\boldsymbol{g}}(k_s,k_z)^*\, \hat{\boldsymbol{f}}(k_s,k_z)\, k_s\, dk_s\, dk_z
\end{aligned}$$

Taking $\boldsymbol{f} = \boldsymbol{g}$ in (B.1), the Parseval's theorem for Hankel-Fourier transform is

$$2\pi \int_0^\infty \int_0^\infty |\boldsymbol{f}(s,z)|^2\, s\, ds\, dz = 16\pi^4 \int_0^\infty \int_0^\infty |\hat{\boldsymbol{f}}(k_s,k_z)|^2\, k_s\, dk_s\, dk_z. \tag{B.2}$$

For $z = (-\infty, \infty)$, (B.2) can be written as

$$2\pi \int_0^\infty \int_{-\infty}^\infty |\boldsymbol{f}(s,z)|^2 \, s \, ds \, dz = 32\pi^4 \int_0^\infty \int_0^\infty |\hat{\boldsymbol{f}}(k_s,k_z)|^2 \, k_s \, dk_s \, dk_z.$$

The left hand side of this equation is the energy content of $\boldsymbol{f}$ in physical (s,z) space. While the right hand side gives the energy content of $\boldsymbol{f}$ in spectral (k_s,k_z) space . Therefore, if $\boldsymbol{f}$ is either velocity field $(\boldsymbol{u})$ or magnetic field $(\boldsymbol{b})$, the associated kinetic and magnetic energy estimates are:

$$E_k = \pi \int_0^\infty \int_{-\infty}^\infty |\boldsymbol{u}(s,z)|^2 \, s \, ds \, dz = 16\pi^4 \int_0^\infty \int_0^\infty |\hat{\boldsymbol{u}}(k_s,k_z)|^2 \, k_s \, dk_s \, dk_z, \tag{B.3}$$

$$E_m = \frac{\pi}{\mu\rho} \int_0^\infty \int_{-\infty}^\infty |\boldsymbol{b}(s,z)|^2 \, s \, ds \, dz = \frac{16\pi^4}{\mu\rho} \int_0^\infty \int_0^\infty |\hat{\boldsymbol{b}}(k_s,k_z)|^2 k_s \, dk_s \, dk_z. \tag{B.4}$$

Appendix C

Solutions for evolution of the blob in the presence of both rotation and magnetic field

The general expressions for the toroidal velocity and magnetic fields are derived in this appendix.

C.1 Toroidal velocity ($\hat{u}_\phi$)

The system of equations from (4.53):

$$\begin{aligned}
A_1 + B_1 + C_1 + D_1 &= \hat{u}_{\phi 0}, \\
i(A_1\lambda_1 + B_1\lambda_2 + C_1\lambda_3 + D_1\lambda_4) &= \left.\frac{\partial \hat{u}_\phi}{\partial t}\right|_{t=0}, \\
-(A_1\lambda_1^2 + B_1\lambda_2^2 + C_1\lambda_3^2 + D_1\lambda_4^2) &= \left.\frac{\partial^2 \hat{u}_\phi}{\partial t^2}\right|_{t=0}, \\
-i(A_1\lambda_1^3 + B_1\lambda_2^3 + C_1\lambda_3^3 + D_1\lambda_4^3) &= \left.\frac{\partial^3 \hat{u}_\phi}{\partial t^3}\right|_{t=0},
\end{aligned}$$

are considered.

1. **Estimating** $\left.\frac{\partial \hat{u}_\phi}{\partial t}\right|_{t=0}$

The momentum equation along ϕ direction from (4.47):

$$\frac{\partial u_\phi}{\partial t} = \frac{B_0}{\mu\rho}\frac{\partial b_\phi}{\partial z} - 2\Omega u_s + \nu\left[\frac{1}{s}\frac{\partial}{\partial s}\left(s\frac{\partial u_\phi}{\partial s}\right) + \frac{\partial^2 u_\phi}{\partial z^2} - \frac{u_\phi}{s^2}\right],$$

is considered. The Hankel-Fourier transform of (4.47) gives

$$\frac{\partial \hat{u}_\phi}{\partial t} = \frac{B_0}{\mu\rho} ik_z \hat{b}_\phi - 2\Omega \hat{u}_s - \nu k^2 \hat{u}_\phi. \tag{C.1}$$

At $t = 0$, this transformed momentum equation (C.1) becomes

$$\left.\frac{\partial \hat{u}_\phi}{\partial t}\right|_{t=0} = \frac{B_0}{\mu\rho} ik_z \hat{b}_{\phi 0} - 2\Omega \hat{u}_{s,0} - \nu k^2 \hat{u}_{\phi 0}.$$

Since $\hat{b}_{\phi 0} = 0$ and $\hat{u}_{s,0} = 0$, this equation simplifies to

$$\left.\frac{\partial \hat{u}_\phi}{\partial t}\right|_{t=0} = -\nu k^2 \hat{u}_{\phi 0}. \tag{C.2}$$

2. **Estimating** $\left.\frac{\partial^2 \hat{u}_\phi}{\partial t^2}\right|_{t=0}$

The ϕ momentum equation (4.47):

$$\frac{\partial u_\phi}{\partial t} = \frac{B_0}{\mu\rho}\frac{\partial b_\phi}{\partial z} - 2\Omega u_s + \nu\left[\frac{1}{s}\frac{\partial}{\partial s}\left(s\frac{\partial u_\phi}{\partial s}\right) + \frac{\partial^2 u_\phi}{\partial z^2} - \frac{u_\phi}{s^2}\right],$$

is considered. The poloidal velocity $\boldsymbol{u}_p = (u_s, 0, u_z)$ can be represented by a stream function ψ as follows:

$$\boldsymbol{u}_p = \nabla \times [(\psi/s)\hat{e}_\phi] = \left(-\frac{1}{s}\frac{\partial \psi}{\partial z}, 0, \frac{1}{s}\frac{\partial \psi}{\partial s}\right). \tag{C.3}$$

Using (C.3), $\hat{u}_\phi$ momentum equation (4.47) becomes

$$\frac{\partial u_\phi}{\partial t} = \frac{B_0}{\mu\rho}\frac{\partial b_\phi}{\partial z} + \frac{2\Omega}{s}\frac{\partial \psi}{\partial z} + \nu\left[\frac{1}{s}\frac{\partial}{\partial s}\left(s\frac{\partial u_\phi}{\partial s}\right) + \frac{\partial^2 u_\phi}{\partial z^2} - \frac{u_\phi}{s^2}\right].$$

The time derivative of this momentum equation gives

$$\frac{\partial^2 u_\phi}{\partial t^2} = \frac{B_0}{\mu\rho}\frac{\partial}{\partial z}\frac{\partial b_\phi}{\partial t} + \frac{2\Omega}{s}\frac{\partial}{\partial z}\frac{\partial \psi}{\partial t} + \nu\frac{\partial}{\partial t}\left[\frac{1}{s}\frac{\partial}{\partial s}\left(s\frac{\partial u_\phi}{\partial s}\right) + \frac{\partial^2 u_\phi}{\partial z^2} - \frac{u_\phi}{s^2}\right]. \tag{C.4}$$

Multiplying equation (C.4) by 's' gives

$$\frac{\partial^2(su_\phi)}{\partial t^2} = \frac{B_0}{\mu\rho}\frac{\partial}{\partial z}\frac{\partial(sb_\phi)}{\partial t} + 2\Omega\frac{\partial}{\partial z}\frac{\partial\psi}{\partial t} + \nu\frac{\partial}{\partial t}\left(s\left[\frac{1}{s}\frac{\partial}{\partial s}\left(s\frac{\partial u_\phi}{\partial s}\right) + \frac{\partial^2 u_\phi}{\partial z^2} - \frac{u_\phi}{s^2}\right]\right). \tag{C.5}$$

Now, the Stokes Laplacian operator (∇_*^2) given by

$$\nabla_*^2 = \frac{\partial^2}{\partial z^2} + s\frac{\partial}{\partial s}\left(\frac{1}{s}\frac{\partial}{\partial s}\right), \tag{C.6}$$

is considered. The relation between Stokes Laplacian operator and the normal cylindrical Laplacian operator of a scalar field f is

$$\nabla_*^2(sf) = s\left[\frac{1}{s}\frac{\partial}{\partial s}\left(s\frac{\partial f}{\partial s}\right) + \frac{\partial^2 f}{\partial z^2} - \frac{f}{s^2}\right]. \tag{C.7}$$

Now $\nabla_*^2\cdot$(C.5) gives

$$\begin{aligned}\frac{\partial^2\nabla_*^2(su_\phi)}{\partial t^2} = \frac{B_0}{\mu\rho}\frac{\partial}{\partial z}\frac{\partial\nabla_*^2(sb_\phi)}{\partial t} + 2\Omega\frac{\partial}{\partial z}\frac{\partial\nabla_*^2\psi}{\partial t} \\ + \nu\frac{\partial}{\partial t}\nabla_*^2\left(s\left[\frac{1}{s}\frac{\partial}{\partial s}\left(s\frac{\partial u_\phi}{\partial s}\right) + \frac{\partial^2 u_\phi}{\partial z^2} - \frac{u_\phi}{s^2}\right]\right).\end{aligned} \tag{C.8}$$

Using (C.7), the following identities:

$$\nabla_*^2\left(s\left[\frac{1}{s}\frac{\partial}{\partial s}\left(s\frac{\partial u_\phi}{\partial s}\right) + \frac{\partial^2 u_\phi}{\partial z^2} - \frac{u_\phi}{s^2}\right]\right) = \nabla_*^2(\nabla_*^2(su_\phi)) = \nabla_*^4(su_\phi), \tag{C.9}$$

$$\nabla_*^2\left(s\left[\frac{1}{s}\frac{\partial}{\partial s}\left(s\frac{\partial u_\phi}{\partial s}\right) + \frac{\partial^2 u_\phi}{\partial z^2} - \frac{u_\phi}{s^2}\right]\right) = s\left[\frac{1}{s}\frac{\partial}{\partial s}\left(s\frac{\partial}{\partial s}\right) + \frac{\partial^2}{\partial z^2} - \frac{1}{s^2}\right]^2 u_\phi, \tag{C.10}$$

are considered. Using (C.9), equation (C.8) becomes

$$\frac{\partial^2\nabla_*^2(su_\phi)}{\partial t^2} = \frac{B_0}{\mu\rho}\frac{\partial}{\partial z}\frac{\partial\nabla_*^2(sb_\phi)}{\partial t} + 2\Omega\frac{\partial}{\partial z}\frac{\partial\nabla_*^2\psi}{\partial t} + \nu\frac{\partial\nabla_*^4(su_\phi)}{\partial t}. \tag{C.11}$$

The linearized poloidal component of the momentum equation from (4.46) and (4.48) can be written as

$$\frac{\partial \boldsymbol{u}_p}{\partial t} = -\frac{\nabla p^*}{\rho} + \frac{B_0}{\mu\rho}\frac{\partial \boldsymbol{b}_p}{\partial z} + 2\Omega u_\phi \hat{e}_s + \nu\nabla^2 \boldsymbol{u}_p, \tag{C.12}$$

where $\boldsymbol{u}_p = (u_s, 0, u_z)$ and $\boldsymbol{b}_p = (b_s, 0, b_z)$. Using $\nabla \times \boldsymbol{u}_p = \omega_\phi \hat{e}_\phi$ and $\nabla \times \boldsymbol{b}_p = j_\phi \hat{e}_\phi$, the azimuthal vorticity equation obtained by taking curl of equation (C.12) is

$$\frac{\partial \omega_\phi}{\partial t} = \frac{B_0}{\rho}\frac{\partial j_\phi}{\partial z} + 2\Omega\frac{\partial u_\phi}{\partial z} + \nu\left[\frac{1}{s}\frac{\partial}{\partial s}\left(s\frac{\partial \omega_\phi}{\partial s}\right) + \frac{\partial^2 \omega_\phi}{\partial z^2} - \frac{\omega_\phi}{s^2}\right]. \tag{C.13}$$

Using (C.7), equation (C.13) can be written as

$$\frac{\partial (s\omega_\phi)}{\partial t} = \frac{B_0}{\rho}\frac{\partial (sj_\phi)}{\partial z} + 2\Omega\frac{\partial (su_\phi)}{\partial z} + \nu\nabla_*^2(s\omega_\phi). \tag{C.14}$$

Now, the curl of (C.3) gives the following relation between ψ and ω_ϕ:

$$\omega_\phi = \nabla \times (\nabla \times [(\psi/s)\hat{e}_\phi]) = -\frac{\nabla_*^2 \psi}{s}. \tag{C.15}$$

Using (C.15), equation (C.14) becomes

$$\frac{\partial \nabla_*^2 \psi}{\partial t} = -\frac{B_0}{\rho}\frac{\partial (sj_\phi)}{\partial z} - 2\Omega\frac{\partial (su_\phi)}{\partial z} + \nu\nabla_*^4 \psi. \tag{C.16}$$

Using (C.16), (C.11) becomes

$$\begin{aligned}\frac{\partial^2 \nabla_*^2 (su_\phi)}{\partial t^2} = \frac{B_0}{\mu\rho}\frac{\partial}{\partial z}\frac{\partial \nabla_*^2 (sb_\phi)}{\partial t} - \frac{2\Omega B_0}{\rho}\frac{\partial^2 (sj_\phi)}{\partial z^2} - 4\Omega^2\frac{\partial^2 (su_\phi)}{\partial z^2} \\ + 2\Omega\nu\frac{\partial \nabla_*^4 \psi}{\partial z} + \nu\frac{\partial \nabla_*^4 (su_\phi)}{\partial t}.\end{aligned} \tag{C.17}$$

Multiplying the equation (C.17) by s^{-1} and using $\nabla_*^4 \psi = -\nabla_*^2 (s\omega_\phi)$, C.17 becomes

$$\begin{aligned}\frac{1}{s}\frac{\partial^2 \nabla_*^2 (su_\phi)}{\partial t^2} = \frac{B_0}{\mu\rho}\frac{1}{s}\frac{\partial}{\partial z}\frac{\partial \nabla_*^2 (sb_\phi)}{\partial t} - \frac{2\Omega B_0}{\rho}\frac{\partial^2 j_\phi}{\partial z^2} - 4\Omega^2\frac{\partial^2 u_\phi}{\partial z^2} \\ - \frac{2\Omega\nu}{s}\frac{\partial \nabla_*^2 (s\omega_\phi)}{\partial z} + \frac{\nu}{s}\frac{\partial \nabla_*^4 (su_\phi)}{\partial t}.\end{aligned} \tag{C.18}$$

The Hankel-Fourier transforms of $\nabla_*^2(sf)/s$ and $\nabla_*^4(sf)/s$ are:

$$H\left[\frac{\nabla_*^2(sf)}{s}\right] = -k^2 f, \;\; H\left[\frac{\nabla_*^4(sf)}{s}\right] = k^4 f. \tag{C.19a,b}$$

Using (C.19a,b) , the Hankel-Fourier transform of (C.18) gives

$$\frac{\partial^2 \hat{u}_\phi}{\partial t^2} = \frac{ik_z B_0}{\mu\rho}\frac{\partial \hat{b}_\phi}{\partial t} - \frac{2\Omega B_0 k_z^2 \hat{j}_\phi}{k^2\rho} - \frac{4\Omega^2 k_z^2 \hat{u}_\phi}{k^2} - 2\Omega\nu i k_z \hat{\omega}_\phi - \nu k^2 \frac{\partial \hat{u}_\phi}{\partial t}. \tag{C.20}$$

Evaluating (C.20) at $t = 0$ gives

$$\left.\frac{\partial^2 \hat{u}_\phi}{\partial t^2}\right|_{t=0} = \frac{ik_z B_0}{\mu\rho}\left.\frac{\partial \hat{b}_\phi}{\partial t}\right|_{t=0} - \frac{4\Omega^2 k_z^2 \hat{u}_{\phi 0}}{k^2} - \nu k^2 \left.\frac{\partial \hat{u}_\phi}{\partial t}\right|_{t=0}. \tag{C.21}$$

The ϕ component of induction equation from (4.50):

$$\frac{\partial b_\phi}{\partial t} = B_0 \frac{\partial u_\phi}{\partial z} + \eta\left[\frac{1}{s}\frac{\partial}{\partial s}\left(s\frac{\partial b_\phi}{\partial s}\right) + \frac{\partial^2 b_\phi}{\partial z^2} - \frac{b_\phi}{s^2}\right], \tag{C.22}$$

is considered. The Hankel-Fourier transform of (C.22) gives

$$\frac{\partial \hat{b}_\phi}{\partial t} = B_0 i k_z \hat{u}_\phi - \eta k^2 \hat{b}_\phi. \tag{C.23}$$

Evaluating equation (C.23) at $t = 0$ gives

$$\left.\frac{\partial \hat{b}_\phi}{\partial t}\right|_{t=0} = B_0 i k_z \hat{u}_{\phi 0}. \tag{C.24}$$

From (C.2),

$$\left.\frac{\partial \hat{u}_\phi}{\partial t}\right|_{t=0} = -\nu k^2 \hat{u}_{\phi 0}.$$

Using (C.2) and (C.24), (C.23) becomes

$$\left.\frac{\partial^2 \hat{u}_\phi}{\partial t^2}\right|_{t=0} = -\left(V_A^2 k_z^2 + \frac{4\Omega^2 k_z^2}{k^2} - \nu^2 k^4\right)\hat{u}_{\phi 0}. \tag{C.25}$$

3. Estimating $\left.\dfrac{\partial^3 \hat{u}_\phi}{\partial t^3}\right|_{t=0}$

Taking time derivative of (C.11) gives

$$\frac{\partial^3 \nabla_*^2(su_\phi)}{\partial t^3} = \frac{B_0}{\mu\rho}\frac{\partial}{\partial z}\frac{\partial^2 \nabla_*^2(sb_\phi)}{\partial t^2} + 2\Omega\frac{\partial}{\partial z}\frac{\partial^2 \nabla_*^2\psi}{\partial t^2} + \nu\frac{\partial^2 \nabla_*^4(su_\phi)}{\partial t^2}. \tag{C.26}$$

Using $s\omega_\phi = -\nabla_*^2\psi$ from (C.15), equation (C.26) becomes

$$\frac{\partial^3 \nabla_*^2(su_\phi)}{\partial t^3} = \frac{B_0}{\mu\rho}\frac{\partial}{\partial z}\frac{\partial^2 \nabla_*^2(sb_\phi)}{\partial t^2} - 2\Omega\frac{\partial}{\partial z}\frac{\partial^2(s\omega_\phi)}{\partial t^2} + \nu\frac{\partial^2 \nabla_*^4(su_\phi)}{\partial t^2}. \tag{C.27}$$

Multiplying the equation (C.27) by s^{-1} gives

$$\frac{\partial^3}{\partial t^3}\left(\frac{\nabla_*^2(su_\phi)}{s}\right) = \frac{B_0}{\mu\rho}\frac{\partial}{\partial z}\frac{\partial^2}{\partial t^2}\left(\frac{\nabla_*^2(sb_\phi)}{s}\right) - 2\Omega\frac{\partial}{\partial z}\frac{\partial^2\omega_\phi}{\partial t^2} + \nu\frac{\partial^2}{\partial t^2}\left(\frac{\nabla_*^4(su_\phi)}{s}\right). \tag{C.28}$$

Using (C.19a,b), the Hankel-Fourier transform of (C.28) at $t = 0$ gives

$$\left.\frac{\partial^3\hat{u}_\phi}{\partial t^3}\right|_{t=0} = \frac{ik_zB_0}{\mu\rho}\left.\frac{\partial^2\hat{b}_\phi}{\partial t^2}\right|_{t=0} + \frac{2\Omega ik_z}{k^2}\left.\frac{\partial^2\hat{\omega}_\phi}{\partial t^2}\right|_{t=0} - \nu k^2\left.\frac{\partial^2\hat{u}_\phi}{\partial t^2}\right|_{t=0}. \tag{C.29}$$

Time derivative of (C.23) at $t = 0$ gives

$$\left.\frac{\partial^2\hat{b}_\phi}{\partial t^2}\right|_{t=0} = B_0ik_z\left.\frac{\partial\hat{u}_\phi}{\partial t}\right|_{t=0} - \eta k^2\left.\frac{\partial\hat{b}_\phi}{\partial t}\right|_{t=0}. \tag{C.30}$$

From (C.2) and (C.24),

$$\left.\frac{\partial\hat{u}_\phi}{\partial t}\right|_{t=0} = -\nu k^2\hat{u}_{\phi 0}, \quad \left.\frac{\partial\hat{b}_\phi}{\partial t}\right|_{t=0} = B_0ik_z\hat{u}_{\phi 0}.$$

Substituting these estimates in (C.30) gives

$$\left.\frac{\partial^2\hat{b}_\phi}{\partial t^2}\right|_{t=0} = -(\nu+\eta)B_0ik_zk^2\hat{u}_{\phi 0}. \tag{C.31}$$

Hankel-Fourier transform of equation (C.13) gives

$$\frac{\partial\hat{\omega}_\phi}{\partial t} = \frac{B_0ik_z}{\rho}\hat{j}_\phi + 2\Omega ik_z\hat{u}_\phi - \nu k^2\hat{\omega}_\phi. \tag{C.32}$$

At $t = 0$, the equation (C.32) becomes

$$\left.\frac{\partial \hat{\omega}_\phi}{\partial t}\right|_{t=0} = 2\Omega i k_z \hat{u}_{\phi 0}. \tag{C.33}$$

Time derivative of equation (C.32) at $t = 0$ gives

$$\left.\frac{\partial^2 \hat{\omega}_\phi}{\partial t^2}\right|_{t=0} = \frac{B_0 i k_z}{\rho}\left.\frac{\partial \hat{j}_\phi}{\partial t}\right|_{t=0} + 2\Omega i k_z \left.\frac{\partial \hat{u}_\phi}{\partial t}\right|_{t=0} - \nu k^2 \left.\frac{\partial \hat{\omega}_\phi}{\partial t}\right|_{t=0}. \tag{C.34}$$

The azimuthal current equation is

$$\frac{\partial j_\phi}{\partial t} = \frac{B_0}{\mu}\frac{\partial \omega_\phi}{\partial z} + \eta\left[\frac{1}{s}\frac{\partial}{\partial s}\left(s\frac{\partial j_\phi}{\partial s}\right) + \frac{\partial^2 j_\phi}{\partial z^2} - \frac{j_\phi}{s^2}\right]. \tag{C.35}$$

The Hankel-Fourier transform of equation (C.35) at $t = 0$ gives

$$\left.\frac{\partial \hat{j}_\phi}{\partial t}\right|_{t=0} = \frac{B_0 i k_z \hat{\omega}_{\phi 0}}{\mu} - \eta k^2 \hat{j}_{\phi 0} = 0. \tag{C.36}$$

Using (C.36), (C.2) and (C.33), (C.34) becomes

$$\left.\frac{\partial^2 \hat{\omega}_\phi}{\partial t^2}\right|_{t=0} = -4\Omega \nu i k_z k^2 \hat{u}_{\phi 0}. \tag{C.37}$$

Using (C.37), (C.31) and (C.25) in (C.29) at $t = 0$ gives

$$\begin{aligned}
\left.\frac{\partial^3 \hat{u}_\phi}{\partial t^3}\right|_{t=0} &= (\nu+\eta)V_A^2 k_z^2 k^2 \hat{u}_{\phi 0} + 8\nu\Omega^2 k_z^2 \hat{u}_{\phi 0} + \nu k^2\left(V_A^2 k_z^2 + \frac{4\Omega^2 k_z^2}{k^2} - \nu^2 k^4\right)\hat{u}_{\phi 0}, \\
\left.\frac{\partial^3 \hat{u}_\phi}{\partial t^3}\right|_{t=0} &= [(2\nu+\eta)V_A^2 k_z^2 k^2 + 12\Omega^2 \nu k_z^2 - \nu^3 k^6]\hat{u}_{\phi 0}.
\end{aligned} \tag{C.38}$$

From (C.2), (C.25), (C.38), the system of equations (4.53) become

$$\begin{aligned}
A_1 + B_1 + C_1 + D_1 &= \hat{u}_{\phi 0} = a_1, \\
A_1\lambda_1 + B_1\lambda_2 + C_1\lambda_3 + D_1\lambda_4 &= i\nu k^2 \hat{u}_{\phi 0} = a_2, \\
A_1\lambda_1^2 + B_1\lambda_2^2 + C_1\lambda_3^2 + D_1\lambda_4^2 &= \left(V_A^2 k_z^2 + \frac{4\Omega^2 k_z^2}{k^2} - \nu^2 k^4\right)\hat{u}_{\phi 0} = a_3, \\
A_1\lambda_1^3 + B_1\lambda_2^3 + C_1\lambda_3^3 + D_1\lambda_4^3 &= i[(2\nu+\eta)V_A^2 k_z^2 k^2 + 12\Omega^2 \nu k_z^2 - \nu^3 k^6]\hat{u}_{\phi 0} = a_4.
\end{aligned}$$

The solutions of A_1, B_1, C_1, D_1 by solving these system of equations are :

$$A_1 = \frac{a_4 - a_3(\lambda_2+\lambda_3+\lambda_4) + a_2[\lambda_2(\lambda_3+\lambda_4)+\lambda_3\lambda_4] - a_1\lambda_3\lambda_4\lambda_2}{(\lambda_1-\lambda_2)(\lambda_1-\lambda_3)(\lambda_1-\lambda_4)},$$
$$B_1 = \frac{a_4 - a_3(\lambda_1+\lambda_3+\lambda_4) + a_2[\lambda_1(\lambda_3+\lambda_4)+\lambda_3\lambda_4] - a_1\lambda_3\lambda_4\lambda_1}{(\lambda_2-\lambda_1)(\lambda_2-\lambda_3)(\lambda_2-\lambda_4)},$$
$$C_1 = \frac{a_4 - a_3(\lambda_1+\lambda_2+\lambda_4) + a_2[\lambda_1(\lambda_2+\lambda_4)+\lambda_2\lambda_4] - a_1\lambda_2\lambda_4\lambda_1}{(\lambda_3-\lambda_4)(\lambda_3-\lambda_1)(\lambda_3-\lambda_2)},$$
$$D_1 = \frac{a_4 - a_3(\lambda_1+\lambda_2+\lambda_3) + a_2[\lambda_1(\lambda_2+\lambda_3)+\lambda_2\lambda_3] - a_1\lambda_2\lambda_3\lambda_1}{(\lambda_4-\lambda_3)(\lambda_4-\lambda_2)(\lambda_4-\lambda_1)}.$$

Substituting these expressions in (4.52), the toroidal velocity solution ($\hat{u}_\phi$) is obtained. The inverse Hankel-Fourier transform (3.13) of $\hat{u}_\phi$ would yield the solution in the physical space.

C.2 Toroidal magnetic field $(\hat{b}_\phi)$

The system of equations from (4.55):

$$\begin{aligned} A_2 + B_2 + C_2 + D_2 &= \hat{b}_{\phi 0} = 0, \\ i(A_2\lambda_1 + B_2\lambda_2 + C_2\lambda_3 + D_2\lambda_4) &= \left.\frac{\partial \hat{b}_\phi}{\partial t}\right|_{t=0}, \\ -(A_2\lambda_1^2 + B_2\lambda_2^2 + C_2\lambda_3^2 + D_2\lambda_4^2) &= \left.\frac{\partial^2 \hat{b}_\phi}{\partial t^2}\right|_{t=0}, \\ -i(A_2\lambda_1^3 + B_2\lambda_2^3 + C_2\lambda_3^3 + D_2\lambda_4^3) &= \left.\frac{\partial^3 \hat{b}_\phi}{\partial t^3}\right|_{t=0}, \end{aligned} \tag{C.39}$$

are considered. From (C.24) and (C.31),

$$\left.\frac{\partial \hat{b}_\phi}{\partial t}\right|_{t=0} = B_0 i k_z \hat{u}_{\phi 0}, \quad \left.\frac{\partial^2 \hat{b}_\phi}{\partial t^2}\right|_{t=0} = -(\nu+\eta) B_0 i k_z k^2 \hat{u}_{\phi 0},$$

were obtained. Now, the time derivative of (C.30) at $t = 0$ gives

$$\left.\frac{\partial^3 \hat{b}_\phi}{\partial t^3}\right|_{t=0} = B_0 i k_z \left.\frac{\partial^2 \hat{u}_\phi}{\partial t^2}\right|_{t=0} - \eta k^2 \left.\frac{\partial^2 \hat{b}_\phi}{\partial t^2}\right|_{t=0}. \tag{C.40}$$

From (C.31) and (C.25),

$$\left.\frac{\partial^2 \hat{b}_\phi}{\partial t^2}\right|_{t=0} = -(\nu+\eta)B_0 i k_z k^2 \hat{u}_{\phi 0}, \quad \left.\frac{\partial^2 \hat{u}_\phi}{\partial t^2}\right|_{t=0} = -\left(V_A^2 k_z^2 + \frac{4\Omega^2 k_z^2}{k^2} - \nu^2 k^4\right)\hat{u}_{\phi 0}.$$

Using these estimates, (C.40) becomes

$$\begin{aligned}
\left.\frac{\partial^3 \hat{b}_\phi}{\partial t^3}\right|_{t=0} &= -B_0 i k_z \left(V_A^2 k_z^2 + \frac{4\Omega^2 k_z^2}{k^2} - \nu^2 k^4\right)\hat{u}_{\phi 0} + \eta k^2 \left((\nu+\eta)B_0 i k_z k^2 \hat{u}_{\phi 0}\right), \\
\left.\frac{\partial^3 \hat{b}_\phi}{\partial t^3}\right|_{t=0} &= -B_0 i k_z \left(V_A^2 k_z^2 + \frac{4\Omega^2 k_z^2}{k^2} - k^4(\nu^2+\eta^2+\nu\eta)\right)\hat{u}_{\phi 0}. \qquad \text{(C.41)}
\end{aligned}$$

Using (C.24),(C.31), (C.41), the system of equations (4.55) become

$$\begin{aligned}
A_2 + B_2 + C_2 + D_2 &= 0 = b_1, \\
A_2\lambda_1 + B_2\lambda_2 + C_2\lambda_3 + D_2\lambda_4 &= B_0 k_z \hat{u}_{\phi 0} = b_2, \\
A_2\lambda_1^2 + B_2\lambda_2^2 + C_2\lambda_3^2 + D_2\lambda_4^2 &= (\nu+\eta)B_0 i k_z k^2 \hat{u}_{\phi 0} = b_3, \\
A_2\lambda_1^3 + B_2\lambda_2^3 + C_2\lambda_3^3 + D_2\lambda_4^3 &= B_0 k_z \left(V_A^2 k_z^2 + \frac{4\Omega^2 k_z^2}{k^2} - k^4(\nu^2+\eta^2+\nu\eta)\right)\hat{u}_{\phi 0} = b_4.
\end{aligned}$$

Solving these equations, the expressions for A_2, B_2, C_2, D_2 are obtained. The expressions are:

$$\begin{aligned}
A_2 &= \frac{b_4 - b_3(\lambda_2+\lambda_3+\lambda_4) + b_2[\lambda_2(\lambda_3+\lambda_4)+\lambda_3\lambda_4]}{(\lambda_1-\lambda_2)(\lambda_1-\lambda_3)(\lambda_1-\lambda_4)}, \\
B_2 &= \frac{b_4 - b_3(\lambda_1+\lambda_3+\lambda_4) + b_2[\lambda_1(\lambda_3+\lambda_4)+\lambda_3\lambda_4]}{(\lambda_2-\lambda_1)(\lambda_2-\lambda_3)(\lambda_2-\lambda_4)}, \\
C_2 &= \frac{b_4 - b_3(\lambda_1+\lambda_2+\lambda_4) + b_2[\lambda_1(\lambda_2+\lambda_4)+\lambda_2\lambda_4]}{(\lambda_3-\lambda_4)(\lambda_3-\lambda_1)(\lambda_3-\lambda_2)}, \\
D_2 &= \frac{b_4 - b_3(\lambda_1+\lambda_2+\lambda_3) + b_2[\lambda_1(\lambda_2+\lambda_3)+\lambda_2\lambda_3]}{(\lambda_4-\lambda_3)(\lambda_4-\lambda_2)(\lambda_4-\lambda_1)}.
\end{aligned}$$

Using these expressions for A_2, B_2, C_2, D_2 in (4.54), $\hat{b}_\phi$ is obtained. The corresponding physical space solution can be obtained by performing an inverse Hankel-Fourier transform.

C.3 Quasi-static solution

C.3.1 Toroidal velocity field ($\hat{u}_\phi$)

From (4.57), the system of equations

$$P_1 + Q_1 = \hat{u}_{\phi 0},$$
$$i(P_1\lambda_1 + Q_1\lambda_2) = \left.\frac{\partial \hat{u}_\phi}{\partial t}\right|_{t=0},$$

are considered. The momentum equation along ϕ direction from (4.47):

$$\frac{\partial u_\phi}{\partial t} = \frac{B_0}{\mu\rho}\frac{\partial b_\phi}{\partial z} - 2\Omega u_s + \nu\left[\frac{1}{s}\frac{\partial}{\partial s}\left(s\frac{\partial u_\phi}{\partial s}\right) + \frac{\partial^2 u_\phi}{\partial z^2} - \frac{u_\phi}{s^2}\right],$$

is considered. The Hankel-Fourier transform of equation (4.47) gives

$$\frac{\partial \hat{u}_\phi}{\partial t} = \frac{B_0}{\mu\rho} ik_z \hat{b}_\phi - 2\Omega\hat{u}_s - \nu k^2 \hat{u}_\phi. \tag{C.42}$$

Since $\hat{b}_{\phi 0} = 0$ and $\hat{u}_{s,0} = 0$, evaluating (C.42) at $t = 0$ gives

$$\left.\frac{\partial \hat{u}_\phi}{\partial t}\right|_{t=0} = -\nu k^2 \hat{u}_{\phi 0}. \tag{C.43}$$

Using (C.43), the system of equations (4.57) become

$$P_1\lambda_1 + Q_1\lambda_2 = i\nu k^2 \hat{u}_{\phi 0}.$$

The system of linear equations become

$$P_1 + Q_1 = \hat{u}_{\phi 0} = a_1,$$
$$P_1\lambda_1 + Q_1\lambda_2 = i\nu k^2 \hat{u}_{\phi 0} = a_2.$$

The solutions of P_1, Q_1 are:

$$P_1 = \frac{a_2 - a_1\lambda_2}{\lambda_1 - \lambda_2},\ \ Q_1 = \frac{a_2 - a_1\lambda_1}{\lambda_2 - \lambda_1}.$$

Appendix D

Taylor series expansions of frequencies in strongly and weakly rotating regimes

In this appendix, the Taylor series expansions of the modes in the dispersion relation (4.11) are derived for strongly and weakly rotating regimes.

D.1 Strongly rotating regime $(V_A k/\Omega \ll 1)$

D.1.1 Wave-dominated regime: $\Omega k_z/k \gg V_A k_z \gg \eta k^2/2$

λ_1 mode

From (4.17), λ_1 frequency is

$$\lambda_1 \approx \frac{\Omega k_z}{k} + i\frac{\eta k^2}{2} + \frac{\Omega k_z}{k}\sqrt{1+\left(\frac{V_A k}{\Omega}\right)^2 - i\frac{\eta k^3}{\Omega k_z}}.$$

Let $x = V_A k/\Omega$ and $y = \eta k^3/\Omega k_z$. For small values of x and y, the Taylor series expansion of $\sqrt{1+x^2-iy}$ is

$$\sqrt{1+x^2-iy} = \sqrt{1+x^2}\left[1 - i\frac{y}{1+x^2}\right]^{1/2},$$

$$\begin{aligned}
&\approx \sqrt{1+x^2}\left[1-i\frac{y}{2(1+x^2)}\right],\\
&\approx \sqrt{1+x^2}-i\frac{y}{2\sqrt{1+x^2}},\\
&\approx 1+\frac{x^2}{2}-i\frac{y}{2}\left(1-\frac{x^2}{2}\right),\\
\sqrt{1+\left(\frac{V_Ak}{\Omega}\right)^2-i\frac{\eta k^3}{\Omega k_z}} &\approx 1+\frac{V_A^2k^2}{2\Omega^2}-i\frac{\eta k^3}{2\Omega k_z}\left(1-\frac{V_A^2k^2}{2\Omega^2}\right).
\end{aligned}$$

Using this Taylor series expansion, λ_1 becomes

$$\begin{aligned}
\lambda_1 &\approx \frac{\Omega k_z}{k}+i\frac{\eta k^2}{2}+\frac{\Omega k_z}{k}\left[1+\frac{V_A^2k^2}{2\Omega^2}-i\frac{\eta k^3}{2\Omega k_z}\left(1-\frac{V_A^2k^2}{2\Omega^2}\right)\right],\\
\lambda_1 &\approx \frac{2\Omega k_z}{k}+i\frac{\eta V_A^2k^4}{4\Omega^2}.
\end{aligned}$$

λ_3 mode

From (4.20), λ_3 frequency is

$$\lambda_3 \approx -\frac{\Omega k_z}{k}+i\frac{\eta k^2}{2}+\frac{\Omega k_z}{k}\sqrt{1+\left(\frac{V_Ak}{\Omega}\right)^2+i\frac{\eta k^3}{\Omega k_z}}.$$

Let $x = V_Ak/\Omega$ and $y = \eta k^3/\Omega k_z$. The Taylor series expansion of $\sqrt{1+x^2+iy}$ for small values of x and y is

$$\begin{aligned}
\sqrt{1+x^2+iy} &= \sqrt{1+x^2}\left[1+i\frac{y}{1+x^2}\right]^{1/2},\\
&\approx \sqrt{1+x^2}+i\frac{y}{2\sqrt{1+x^2}},\\
&\approx 1+\frac{x^2}{2}+i\frac{y}{2}\left(1-\frac{x^2}{2}\right),\\
\sqrt{1+\left(\frac{V_Ak}{\Omega}\right)^2+i\frac{\eta k^3}{\Omega k_z}} &\approx 1+\frac{V_A^2k^2}{2\Omega^2}+i\frac{\eta k^3}{2\Omega k_z}\left(1-\frac{V_A^2k^2}{2\Omega^2}\right).
\end{aligned}$$

Using this Taylor series expansion, λ_3 becomes

$$\lambda_3 \approx -\frac{\Omega k_z}{k}+i\frac{\eta k^2}{2}+\frac{\Omega k_z}{k}\left[1+\frac{V_A^2k^2}{2\Omega^2}+i\frac{\eta k^3}{2\Omega k_z}\left(1-\frac{V_A^2k^2}{2\Omega^2}\right)\right],$$

$$\lambda_3 \approx \frac{V_A^2 k_z k}{2\Omega} + i\eta k^2.$$

D.1.2 Diffusion-dominated regime: $\eta k^2/2 \gg \Omega k_z/k \gg V_A k_z$

λ_1 mode

From (4.24), λ_1 frequency is

$$\lambda_1 = \frac{\Omega k_z}{k} + i\frac{\eta k^2}{2} + \frac{\eta k^2}{2}\sqrt{\left(\frac{2V_A k_z}{\eta k^2}\right)^2 + \left(\frac{2\Omega k_z}{\eta k^3} - i\right)^2}.$$

Let $x = 2V_A k_z/\eta k^2$ and $y = 2\Omega k_z/\eta k^3$. The Taylor series expansion of $\sqrt{x^2+(y-i)^2}$ for small values of x and y is

$$\begin{aligned}
\sqrt{x^2+(y-i)^2} &= \sqrt{(y-i)^2}\left[1+\frac{x^2}{(y-i)^2}\right]^{1/2}, \\
&\approx (y-i) + \frac{x^2(y+i)}{2(1+y^2)}, \\
&\approx y - i + \frac{x^2 y}{2} + i\frac{x^2}{2}, \\
&\approx y\left(1+\frac{x^2}{2}\right) - i\left(1-\frac{x^2}{2}\right), \\
\sqrt{\left(\frac{2V_A k_z}{\eta k^2}\right)^2 + \left(\frac{2\Omega k_z}{\eta k^3} - i\right)^2} &\approx \frac{2\Omega k_z}{\eta k^3}\left(1+\frac{1}{2}\left[\frac{2V_A k_z}{\eta k^2}\right]^2\right) - i\left(1-\frac{1}{2}\left[\frac{2V_A k_z}{\eta k^2}\right]^2\right).
\end{aligned}$$

Using this Taylor series expansion, λ_1 becomes

$$\begin{aligned}
\lambda_1 &\approx \frac{\Omega k_z}{k} + i\frac{\eta k^2}{2} + \frac{\eta k^2}{2}\left[\frac{2\Omega k_z}{\eta k^3}\left(1+\frac{1}{2}\left[\frac{2V_A k_z}{\eta k^2}\right]^2\right) - i\left(1-\frac{1}{2}\left[\frac{2V_A k_z}{\eta k^2}\right]^2\right)\right], \\
\lambda_1 &\approx \frac{2\Omega k_z}{k} + i\frac{k_z^2}{\tau k^2}.
\end{aligned}$$

λ_3 mode

From (4.27), λ_3 frequency is

$$\lambda_3 = -\frac{\Omega k_z}{k} + i\frac{\eta k^2}{2} + \frac{\eta k^2}{2}\sqrt{\left(\frac{2V_A k_z}{\eta k^2}\right)^2 + \left(\frac{2\Omega k_z}{\eta k^3} + i\right)^2}.$$

Let $x = 2V_A k_z/\eta k^2$ and $y = 2\Omega k_z/\eta k^3$. The Taylor series expansion of $\sqrt{x^2+(y-i)^2}$ for small values of x and y is

$$\begin{aligned}
\sqrt{x^2+(y+i)^2} &= \sqrt{(y+i)^2}\left[1+\frac{x^2}{(y+i)^2}\right]^{1/2}, \\
&\approx (y+i)\left[1+\frac{x^2}{2(y+i)^2}\right], \\
&\approx y+i+\frac{x^2 y}{2}-i\frac{x^2}{2}, \\
&\approx y\left(1+\frac{x^2}{2}\right)+i\left(1-\frac{x^2}{2}\right), \\
\sqrt{\left(\frac{2V_A k_z}{\eta k^2}\right)^2+\left(\frac{2\Omega k_z}{\eta k^3}+i\right)^2} &\approx \frac{2\Omega k_z}{\eta k^3}\left(1+\frac{1}{2}\left[\frac{2V_A k_z}{\eta k^2}\right]^2\right)+i\left(1-\frac{1}{2}\left[\frac{2V_A k_z}{\eta k^2}\right]^2\right).
\end{aligned}$$

Using this Taylor series expansion, λ_3 becomes

$$\begin{aligned}
\lambda_3 &\approx -\frac{\Omega k_z}{k}+i\frac{\eta k^2}{2}+\frac{\eta k^2}{2}\left[\frac{2\Omega k_z}{\eta k^3}\left(1+\frac{1}{2}\left[\frac{2V_A k_z}{\eta k^2}\right]^2\right)+i\left(1-\frac{1}{2}\left[\frac{2V_A k_z}{\eta k^2}\right]^2\right)\right], \\
\lambda_3 &\approx \frac{2\Omega V_A^2 k_z^3}{\eta^2 k^5}+i\eta k^2.
\end{aligned}$$

D.2 Weakly rotating regime: $V_A k/\Omega \gg 1$

D.2.1 Wave-dominated regime: $V_A k_z \gg \Omega k_z/k \gg \eta k^2/2$

λ_1 mode

From 4.31, λ_1 frequency is

$$\lambda_1 = \frac{\Omega k_z}{k}+i\frac{\eta k^2}{2}+V_A k_z\sqrt{1+\left(\frac{\Omega}{V_A k}-i\frac{\eta k^2}{2V_A k_z}\right)^2}.$$

Let $x = \Omega/V_A k$ and $y = \eta k^2/2V_A k_z$. For small values of x and y such that $x \gg y$, the Taylor series expansion of $\sqrt{1+(x-iy)^2}$ is

$$\sqrt{1+(x-iy)^2} \approx \sqrt{1+x^2-y^2-i2xy},$$

$$
\begin{aligned}
&\approx \sqrt{1+x^2}\sqrt{1-i\frac{2xy}{1+x^2}},\\
&\approx \sqrt{1+x^2}\left(1-i\frac{xy}{1+x^2}\right),\\
&\approx \sqrt{1+x^2}-i\frac{xy}{\sqrt{1+x^2}},\\
&\approx 1+\frac{x^2}{2}-ixy\left(1-\frac{x^2}{2}\right),\\
\sqrt{1+\left(\frac{\Omega}{V_A k}-i\frac{\eta k^2}{2V_A k_z}\right)^2} &\approx 1+\frac{1}{2}\left(\frac{\Omega}{V_A k}\right)^2-i\frac{\Omega\eta k}{2V_A^2 k_z}\left[1-\frac{1}{2}\left(\frac{\Omega}{V_A k}\right)^2\right].
\end{aligned}
$$

Using this Taylor series expansion, λ_1 becomes

$$
\begin{aligned}
\lambda_1 &\approx \frac{\Omega k_z}{k}+i\frac{\eta k^2}{2}+V_A k_z\left(1+\frac{1}{2}\left(\frac{\Omega}{V_A k}\right)^2-i\frac{\Omega\eta k}{2V_A^2 k_z}\left[1-\frac{1}{2}\left(\frac{\Omega}{V_A k}\right)^2\right]\right),\\
\lambda_1 &\approx \left(V_A k_z+\frac{\Omega k_z}{k}\right)+i\left(\frac{\eta k^2}{2}-\frac{\Omega\eta k}{2V_A}\right).
\end{aligned}
$$

λ_3 mode

From (4.34), λ_3 frequency is

$$
\lambda_3 = -\frac{\Omega k_z}{k}+i\frac{\eta k^2}{2}+V_A k_z\sqrt{1+\left(\frac{\Omega}{V_A k}+i\frac{\eta k^2}{2V_A k_z}\right)^2}.
$$

Let $x=\Omega/V_A k$ and $y=\eta k^2/2V_A k_z$. For small values of x and y such that $x \gg y$, the Taylor series expansion of $\sqrt{1+(x+iy)^2}$ is

$$
\begin{aligned}
\sqrt{1+(x+iy)^2} &= \sqrt{1+x^2-y^2+i2xy},\\
&\approx \sqrt{1+x^2}\sqrt{1+i\frac{2xy}{1+x^2}},\\
&\approx \sqrt{1+x^2}\left(1+i\frac{xy}{1+x^2}\right),\\
&\approx \sqrt{1+x^2}+i\frac{xy}{\sqrt{1+x^2}},\\
&\approx 1+\frac{x^2}{2}+ixy\left(1-\frac{x^2}{2}\right),
\end{aligned}
$$

$$\sqrt{1+\left(\frac{\Omega}{V_A k}+i\frac{\eta k^2}{2V_A k_z}\right)^2} \approx 1+\frac{1}{2}\left(\frac{\Omega}{V_A k}\right)^2+i\frac{\Omega\eta k}{2V_A^2 k_z}\left[1-\frac{1}{2}\left(\frac{\Omega}{V_A k}\right)^2\right].$$

Using this Taylor series expansion, λ_3 becomes

$$\lambda_3 \approx -\frac{\Omega k_z}{k}+i\frac{\eta k^2}{2}+V_A k_z\left(1+\frac{1}{2}\left(\frac{\Omega}{V_A k}\right)^2+i\frac{\Omega\eta k}{2V_A^2 k_z}\left[1-\frac{1}{2}\left(\frac{\Omega}{V_A k}\right)^2\right]\right),$$
$$\lambda_3 \approx \left(V_A k_z-\frac{\Omega k_z}{k}\right)+i\left(\frac{\eta k^2}{2}+\frac{\Omega\eta k}{2V_A}\right).$$

D.2.2 Diffusion-dominated regime: $\eta k^2/2 \gg V_A k_z \gg \Omega k_z/k$

λ_1 mode

From (4.38), λ_1 frequency is

$$\lambda_1 = \frac{\Omega k_z}{k}+i\frac{\eta k^2}{2}+\frac{\eta k^2}{2}\sqrt{\left(\frac{2V_A k_z}{\eta k^2}\right)^2+\left(\frac{2\Omega k_z}{\eta k^3}-i\right)^2}.$$

Let $x = 2V_A k_z/\eta k^2$ and $y = 2\Omega k_z/\eta k^3$. For small values of x and y such that $x \gg y$, the Taylor series expansion of $\sqrt{x^2+(y-i)^2}$ is

$$\begin{aligned}\sqrt{x^2+(y-i)^2} &= (y-i)\sqrt{1+\frac{x^2}{(y-i)^2}},\\ &\approx (y-i)\left[1+\frac{x^2}{2(y-i)^2}\right]\\ &\approx y-i+\frac{x^2}{2(y-i)},\\ &\approx y\left(1+\frac{x^2}{2}\right)-i\left(1-\frac{x^2}{2}\right),\end{aligned}$$
$$\sqrt{\left(\frac{2V_A k_z}{\eta k^2}\right)^2+\left(\frac{2\Omega k_z}{\eta k^3}-i\right)^2} \approx \frac{2\Omega k_z}{\eta k^3}\left[1+\frac{1}{2}\left(\frac{2V_A k_z}{\eta k^2}\right)^2\right]-i\left[1-\frac{1}{2}\left(\frac{2V_A k_z}{\eta k^2}\right)^2\right].$$

Using this Taylor series expansion, λ_1 becomes

$$\lambda_1 \approx \frac{\Omega k_z}{k}+i\frac{\eta k^2}{2}+\frac{\eta k^2}{2}\left(\frac{2\Omega k_z}{\eta k^3}\left[1+\frac{1}{2}\left(\frac{2V_A k_z}{\eta k^2}\right)^2\right]-i\left[1-\frac{1}{2}\left(\frac{2V_A k_z}{\eta k^2}\right)^2\right]\right),$$

$$\lambda_1 \approx \frac{2\Omega k_z}{k} + i\frac{k_z^2}{\tau k^2}.$$

λ_3 mode

From (4.41), the expression for λ_3 is

$$\lambda_3 = -\frac{\Omega k_z}{k} + i\frac{\eta k^2}{2} + \frac{\eta k^2}{2}\sqrt{\left(\frac{2V_A k_z}{\eta k^2}\right)^2 + \left(\frac{2\Omega k_z}{\eta k^3} + i\right)^2}.$$

Let $x = 2V_A k_z/\eta k^2$ and $y = 2\Omega k_z/\eta k^3$. For small values of x and y such that $x \gg y$, the Taylor series expansion of $\sqrt{x^2+(y+i)^2}$ is

$$\begin{aligned}
\sqrt{x^2+(y+i)^2} &= (y+i)\sqrt{1+\frac{x^2}{(y+i)^2}}, \\
&\approx (y+i)\left[1+\frac{x^2}{2(y+i)^2}\right], \\
&\approx y+i+\frac{x^2}{2(y+i)}, \\
&\approx y\left(1+\frac{x^2}{2}\right)+i\left(1-\frac{x^2}{2}\right), \\
\sqrt{\left(\frac{2V_A k_z}{\eta k^2}\right)^2 + \left(\frac{2\Omega k_z}{\eta k^3} - i\right)^2} &\approx \frac{2\Omega k_z}{\eta k^3}\left[1+\frac{1}{2}\left(\frac{2V_A k_z}{\eta k^2}\right)^2\right] + i\left[1-\frac{1}{2}\left(\frac{2V_A k_z}{\eta k^2}\right)^2\right].
\end{aligned}$$

Using this Taylor series expansion, λ_3 becomes

$$\begin{aligned}
\lambda_3 &\approx -\frac{\Omega k_z}{k} + i\frac{\eta k^2}{2} + \frac{\eta k^2}{2}\left(\frac{2\Omega k_z}{\eta k^3}\left[1+\frac{1}{2}\left(\frac{2V_A k_z}{\eta k^2}\right)^2\right] + i\left[1-\frac{1}{2}\left(\frac{2V_A k_z}{\eta k^2}\right)^2\right]\right), \\
\lambda_3 &\approx \frac{2\Omega V_A^2 k_z^3}{\eta^2 k^5} + i\eta k^2.
\end{aligned}$$

Appendix E

Fast wave approximate solution

In this appendix, the approximate solution for the fast wave component of $\hat{u}_\phi$ is obtained for strongly rotating regime. The following notations are used for deriving the solution.

$$\omega_\Omega = \frac{2\Omega k_z}{k},\ \omega_1 = \frac{\eta V_A^2 k^4}{4\Omega^2},\ \omega_{\Omega V} = \frac{\Omega \eta k}{2V_A},\ \omega_\eta = \eta k^2,\ \omega_V = V_A k_z,\ \omega_A = \frac{V_A^2 k_z k}{2\Omega}. \quad \text{(E.1)}$$

From the $\hat{u}_\phi$ general solution (4.52), the fast wave component $\hat{u}_{\phi,f} = A_1 e^{i\lambda_1 t}$ is considered, where A_1 is given by

$$A_1 = \frac{a_4 - a_3(\lambda_2+\lambda_3+\lambda_4) + a_2[\lambda_2(\lambda_3+\lambda_4)+\lambda_3\lambda_4] - a_1\lambda_3\lambda_4\lambda_2}{(\lambda_1-\lambda_2)(\lambda_1-\lambda_3)(\lambda_1-\lambda_4)}.$$

The expressions for $a_1 - a_4$ are

$$a_1 = \hat{u}_{\phi 0},\ a_2 = i\nu k^2 \hat{u}_{\phi 0},\ a_3 = \left(V_A^2 k_z^2 + \frac{4\Omega^2 k_z^2}{k^2} - \nu^2 k^4\right)\hat{u}_{\phi 0},$$

$$a_4 = i[(2\nu+\eta)V_A^2 k_z^2 k^2 + 12\Omega^2 \nu k_z^2 - \nu^3 k^6]\hat{u}_{\phi 0}.$$

From (4.23), the frequencies $(\lambda_1 - \lambda_4)$ in the strongly rotating regime are:

$$\lambda_{1,4} \approx \pm\frac{2\Omega k_z}{k} + i\frac{\eta V_A^2 k^4}{4\Omega^2},\ \ \lambda_{3,2} \approx \pm\frac{V_A^2 k_z k}{2\Omega} + i\eta k^2.$$

In the inviscid limit and using the notations (E.1), the expressions for $a_1 - a_4$ become

$$a_1 = \hat{u}_{\phi 0},\ a_2 = 0,\ a_3 = \hat{u}_{\phi 0}(\omega_V^2 + \omega_\Omega^2),\ a_4 = i\hat{u}_{\phi 0}{\omega_V}^2\omega_\eta.$$

Let N and D be defined such that $A_1 = N/D$. This gives

$$\begin{aligned} N &= a_4 - a_3(\lambda_2 + \lambda_3 + \lambda_4) + a_2[\lambda_2(\lambda_3 + \lambda_4) + \lambda_3\lambda_4] - a_1\lambda_3\lambda_4\lambda_2, \\ D &= (\lambda_1 - \lambda_2)(\lambda_1 - \lambda_3)(\lambda_1 - \lambda_4). \end{aligned}$$

Using the expressions for $a_1 - a_4$ and $\lambda_1 - \lambda_4$, N can be written as

$$\begin{aligned} N = &\left(\omega_1\,{\omega_A}^2 - 2\,{\omega_\Omega}^2\,\omega_\eta - \omega_1\,{\omega_\Omega}^2 - {\omega_V}^2\,\omega_\eta - \omega_1\,{\omega_V}^2 + \omega_1\,{\omega_\eta}^2\right) i\,\hat{u}_{\phi 0} \\ &(-{\omega_A}^2\,\omega_\Omega + {\omega_\Omega}^3 + \omega_\Omega\,{\omega_V}^2 - \omega_\Omega\,{\omega_\eta}^2)\,\hat{u}_{\phi 0}. \end{aligned}$$

Similarly, D can be written as

$$\begin{aligned} D &= (\lambda_1 - \lambda_2)(\lambda_1 - \lambda_3)(\lambda_1 - \lambda_4), \\ D &= \left(4\,{\omega_\Omega}^2\,\omega_1 - 4\,{\omega_\Omega}^2\,\omega_\eta\right) i - 2\,{\omega_A}^2\,\omega_\Omega + 2\,{\omega_\Omega}^3 - 2\,\omega_\Omega\,{\omega_\eta}^2 \\ &\quad + 4\,\omega_\Omega\,\omega_\eta\,\omega_1 - 2\,\omega_\Omega\,{\omega_1}^2. \end{aligned}$$

Let $\overline{D}$ be the conjugate of D. The corresponding expression for $\overline{D}$ is

$$\begin{aligned} \overline{D} = &-\left(4\,{\omega_\Omega}^2\,\omega_1 - 4\,{\omega_\Omega}^2\,\omega_\eta\right) i - 2\,{\omega_A}^2\,\omega_\Omega + 2\,{\omega_\Omega}^3 - 2\,\omega_\Omega\,{\omega_\eta}^2 \\ &+ 4\,\omega_\Omega\,\omega_\eta\,\omega_1 - 2\,\omega_\Omega\,{\omega_1}^2. \end{aligned}$$

Now, a simplified expression for A_1 is obtained by evaluating

$$A_1 = \frac{N\overline{D}}{D\overline{D}}. \tag{E.2}$$

The expression for $D\overline{D}$ is

$$D\overline{D} = {\omega_\Omega}^6\left(4 + \frac{4\,{\omega_A}^4}{{\omega_\Omega}^4} - \frac{8\,{\omega_A}^2}{{\omega_\Omega}^2} + \frac{8\,{\omega_\eta}^2}{{\omega_\Omega}^2} + \frac{4\,{\omega_\eta}^4}{{\omega_\Omega}^4} + \frac{8\,{\omega_1}^2}{{\omega_\Omega}^2} + \frac{4\,{\omega_1}^4}{{\omega_\Omega}^4} - \frac{16\,\omega_\eta\,\omega_1}{{\omega_\Omega}^2}\right.$$

$$
\begin{aligned}
&- \frac{16\,\omega_\eta\,{\omega_1}^3}{{\omega_\Omega}^4} - \frac{16\,{\omega_\eta}^3\,\omega_1}{{\omega_\Omega}^4} + \frac{8\,{\omega_A}^2\,{\omega_\eta}^2}{{\omega_\Omega}^4} + \frac{8\,{\omega_A}^2\,{\omega_1}^2}{{\omega_\Omega}^4} \\
&+ \frac{24\,{\omega_\eta}^2\,{\omega_1}^2}{{\omega_\Omega}^4} - \frac{16\,{\omega_A}^2\,\omega_\eta\,\omega_1}{{\omega_\Omega}^4}\Bigg).
\end{aligned}
$$

Since ω_Ω is the dominant frequency in this regime, the magnitude of the fractions in this expression is much less than 1. Therefore, considering only the leading order terms, $D\overline{D}$ becomes

$$
D\overline{D} \approx 4\omega_\Omega^6 \tag{E.3}
$$

Similarly, the expression for $N\overline{D}$ is

$$
\begin{aligned}
N\overline{D} = -i\,\hat{u}_{\phi 0}\,{\omega_\Omega}^6 \Bigg(&\frac{2\,{\omega_1}^3}{{\omega_\Omega}^3} - \frac{6\,\omega_1}{\omega_\Omega} + \frac{8\,{\omega_A}^2\,\omega_1}{{\omega_\Omega}^3} - \frac{2\,{\omega_A}^4\,\omega_1}{{\omega_\Omega}^5} + \frac{2\,{\omega_V}^2\,\omega_\eta}{{\omega_\Omega}^3} - \frac{6\,{\omega_V}^2\,\omega_1}{{\omega_\Omega}^3} \\
&- \frac{2\,{\omega_\eta}^4\,\omega_1}{{\omega_\Omega}^5} - \frac{2\,{\omega_A}^2\,{\omega_1}^3}{{\omega_\Omega}^5} + \frac{2\,{\omega_V}^2\,{\omega_\eta}^3}{{\omega_\Omega}^5} + \frac{2\,{\omega_V}^2\,{\omega_1}^3}{{\omega_\Omega}^5} - \frac{2\,{\omega_\eta}^2\,{\omega_1}^3}{{\omega_\Omega}^5} + \frac{4\,{\omega_\eta}^3\,{\omega_1}^2}{{\omega_\Omega}^5} \\
&+ \frac{2\,{\omega_A}^2\,{\omega_V}^2\,\omega_\eta}{{\omega_\Omega}^5} + \frac{2\,{\omega_A}^2\,{\omega_V}^2\,\omega_1}{{\omega_\Omega}^5} + \frac{4\,{\omega_A}^2\,\omega_\eta\,{\omega_1}^2}{{\omega_\Omega}^5} - \frac{4\,{\omega_A}^2\,{\omega_\eta}^2\,\omega_1}{{\omega_\Omega}^5} \\
&- \frac{2\,{\omega_V}^2\,\omega_\eta\,{\omega_1}^2}{{\omega_\Omega}^5} - \frac{2\,{\omega_V}^2\,{\omega_\eta}^2\,\omega_1}{{\omega_\Omega}^5}\Bigg) + \hat{u}_{\phi 0}\,{\omega_\Omega}^6 \Bigg(2 + \frac{2\,{\omega_A}^4}{{\omega_\Omega}^4} - \frac{4\,{\omega_A}^2}{{\omega_\Omega}^2} + \frac{2\,{\omega_V}^2}{{\omega_\Omega}^2} \\
&+ \frac{4\,{\omega_\eta}^2}{{\omega_\Omega}^2} + \frac{2\,{\omega_\eta}^4}{{\omega_\Omega}^4} - \frac{6\,{\omega_1}^2}{{\omega_\Omega}^2} - \frac{8\,{\omega_\eta}^3\,\omega_1}{{\omega_\Omega}^4} - \frac{2\,{\omega_A}^2\,{\omega_V}^2}{{\omega_\Omega}^4} + \frac{4\,{\omega_A}^2\,{\omega_\eta}^2}{{\omega_\Omega}^4} + \frac{6\,{\omega_A}^2\,{\omega_1}^2}{{\omega_\Omega}^4} \\
&+ \frac{2\,{\omega_V}^2\,{\omega_\eta}^2}{{\omega_\Omega}^4} - \frac{6\,{\omega_V}^2\,{\omega_1}^2}{{\omega_\Omega}^4} + \frac{6\,{\omega_\eta}^2\,{\omega_1}^2}{{\omega_\Omega}^4} - \frac{8\,{\omega_A}^2\,\omega_\eta\,\omega_1}{{\omega_\Omega}^4} + \frac{4\,{\omega_V}^2\,\omega_\eta\,\omega_1}{{\omega_\Omega}^4}\Bigg)
\end{aligned}
$$

Considering the leading order terms, $N\overline{D}$ simplifies to

$$
N\overline{D} \approx \hat{u}_{\phi 0}\omega_\Omega^6 \left(2 + i\,\frac{6\omega_1}{\omega_\Omega}\right). \tag{E.4}
$$

Using (E.4) and (E.3) in (E.2), A_1 becomes

$$
A_1 = \frac{N\overline{D}}{D\overline{D}} \approx \hat{u}_{\phi 0}\left(\frac{1}{2} + i\,\frac{3\omega_1}{2\omega_\Omega}\right).
$$

Using this simplified expression for A_1, the $\hat{u}_{\phi,f} = A_1 e^{i\lambda_1 t}$ becomes

$$
\hat{u}_{\phi,f} \approx \hat{u}_{\phi 0}\left(\frac{1}{2} + i\,\frac{3\omega_1}{2\omega_\Omega}\right)\exp(-\omega_1 t)\left[\cos(\omega_\Omega\, t) + i\sin(\omega_\Omega\, t)\right].
$$

The real part of this expression is the required $\hat{u}_{\phi,f}$ solution which is given by

$$\hat{u}_{\phi,f} \approx \frac{\hat{u}_{\phi 0}}{2} \exp(-\omega_1 t)\left[\cos(\omega_\Omega t) - \frac{3\omega_1}{\omega_\Omega}\sin(\omega_\Omega t)\right],$$
$$\hat{u}_{\phi,f} \approx \frac{\hat{u}_{\phi 0}}{2} \exp\left(-\frac{\eta V_A^2 k^4 t}{4\Omega^2}\right)\left[\cos\left(\frac{2\Omega k_z t}{k}\right) - \frac{3\eta V_A^2 k^5}{8\Omega^3 k_z}\sin\left(\frac{2\Omega k_z t}{k}\right)\right].$$

This expression for $\hat{u}_{\phi,f}$ is the approximate solution of fast wave toroidal velocity in the strongly rotating regime.